An ultra scale-down study to understand and predict *E. coli* cell recovery from high-speed discharge centrifuges

A thesis submitted to the University of London
for the degree of Engineering Doctorate

by

Gerard Hoi Toh Chan

Sept 2006

The Advanced Centre for Biochemical Engineering,

Department of Biochemical Engineering,

University College London,

Torrington Place,

London,

WC1E 7JE,

UK.

UMI Number: U592707

UMI

Dissertation Publishing

ProQuest

ACKNOWLEDGMENTS

ABSTRACT

The ability to recover cells from a fermentation broth in an intact form can be an important criterion for determining the overall performance of a recovery and purification sequence. Disruption of the cells can lead to undesired contamination of an extracellular product with intracellular components and vice versa loss of intracellular products may occur. In particular, the value of directed location of a product in the periplasmic space of say *Escherichia coli* would be diminished by such premature non-selective cell disruption. Several options exist for cell recovery or removal; namely centrifugation, in a batch or a continuous configuration, filtration or membrane operations, and in selected cases expanded beds. The choice of operation is dependant on many variables including the impact on the overall process sequence. In all cases the cells are exposed to shear stresses of varying levels and times and additionally such environments exist in ancillary operations such as pumping, pipe flow and control valves.

In this thesis an ultra scale-down device has been designed to expose cells to controlled levels of shear, time and impact in a way that seeks to mimic those effects that may occur during full-scale processes using continuous or intermittent discharge disc stack centrifuges. Results demonstrate that the extent of cell breakage was found to be proportional to shear stress. An additional level of breakage occurred due to the jet impacting on the collecting surface. Here it was possible to correlate the additional breakage with the impact velocity, which is a function of the distance that the jet travels before impacting on the collection surface, and the initial jet velocity.

The accuracy of the ultra scale-down predictions has been tested using two scales of intermittent discharge disc-stack centrifuges. After the calibration of the ultra scale-down device using cells of a standard preparation the mimic gave a similar trend of cell breakage to that observed at large-scale. However the error margins for the mimic was up to +/-20% and hence further work is required to refine the mimic and further understanding of the calibration factor is necessary. In addition, an initial understanding of the effect of change of centrifuge geometry and method of operation

on the level of cell damage was gained. Finally, the extent of damage as represented by protein release is shown to be indicative of even greater extents of damage with studies using flow cytometry showing significant changes in cell wall structure.

CONTENTS

5

LIST OF TABLES

LIST OF FIGURES

14

1 INTRODUCTION

1.1 Project significance

A new generation of therapeutic products are emerging (Aunins et al., 2000), together with increasing interest in plasmids (Curly and Smiley, 2003; Teeters et al., 2003) and antibody fragment vectors (Neal et al., 2004; Roque et al., 2004), all of which are low-volume, high-value biopharmaceuticals expressed inside bacterial cells. Downstream processing (DSP) is critical for the successful purification of such products, with the aim of satisfying regulatory requirements in terms of purity and efficacy, and represents a major proportion of the manufacturing costs involved (Lightfoot et al., 2003). In addition, the rising cost of health-care places increasing strain on biopharmaceutical companies to improve production yield and control manufacturing costs.

Large volumes of cell broth produced by fermentation are traditionally concentrated as a first step in primary recovery. Solids and liquids can be separated by several methods of which the most common include flocculation, filtration and centrifugation (Lightfoot et al., 2004). This thesis will focus on the use of centrifugation for early product purification, specifically the use of a disc-stack centrifuge for solids recovery where the product is expressed intracellularly. With the increasing demand for therapeutic production, centrifuges are becoming mainstream for rapid concentration of high density fermentations. This is because of their ability to separate continuously cells from liquor over long periods of time in a contained environment. However, many issues arise when using centrifugal separators, including the concern with cell damage and subsequent product loss caused by the shear environment within the feed zone of the separator. A number of publications have investigated the damaging effects during centrifuge recovery of extracellular products (Maybury et al., 2000; Byrne et al., 2002; Neal et al., 2003) but few have yet addressed the effects of solids discharge on cell and intracellular product viability (Gray et al., 1972).

The aim of this thesis will, in the first instance, be to study those operating factors that potentially influence the integrity of *E. coli* cells, and hence recovery yields, during

centrifuge discharge. The thesis then explores and evaluates a new ultra scale-down methodology to predict centrifuge discharge performance using a number of different *E. coli* strains. Based on the findings, operating and equipment design strategies are recommended to improve solids recovery in large-scale centrifuges. The results will hopefully prove valuable to a process engineer faced with the challenge of designing an efficient process line under strict time constraints, where the use of the ultra scale-down technology described in this thesis could quickly and effectively optimise centrifuge performance.

1.2 Primary purification of intracellular products

Following a typical fermentation the intracellular product requires concentrating before continuing with further downstream purification. The objective of any separation technique is to remove the very large volumes of liquor as well as extracellular contaminates such as antifoam from the intracellular product. The type of separation step employed depends on many factors including fermentation and product characteristics, machine capability and cost, which will be further elaborated in section 1.3.

1.2.1 Comparison of crossflow filtration and centrifuge recovery of intracellular products

Crossflow filters are presently the main competitors of centrifuges and separate on the basis of size exclusion. They are characterised as easily scalable and disposable; their stress conditions (i.e. across the membrane surface) are an order of magnitude less than their centrifuge counterparts (Virkar et al., 1981) although care has to be taken in pump and valve design in the recycle loop. Crossflow filtration offers the versatile tool of diafiltration for buffer exchange and cell washing, while in the case of centrifugation cells have to be washed by repeated centrifugation and redilution steps. Also, since the membrane physically retains the cells, recovery is essentially 100% with crossflow filtration. Crossflow filters do however have a tendency to foul when heavily contaminated or high cell density feeds are processed (Bell et al., 1983) and

hence are often associated with high membrane costs since the membranes have to be replaced on a regular basis. Under normal circumstances where the product resides in the permeate, filter aids can be used to maintain flux and reduce fouling. However, with the same practice applied to the recovery of intracellular products several additional stages would be necessary to completely remove the filter aid that can complicate/compromise the process and FDA approval. Crossflow filters often have long operating times with the potential of reduced biological product activity and have difficulty in achieving very high concentrations.

In most cases intracellular products can be easily separated from a fermentation broth using centrifugation (Belter et al., 1988). The recovery of viable cells will however depend on the type of centrifuge employed and method of operation. For example, with the presence of a high shear field during entry into a semi-hermetic centrifuge cells are potentially damaged and reduced in size. This can cascade on to affect recovery performance, cost and quality of material (Byrne et al., 2002; Boychyn et al., 2001; Maybury et al., 2000; Neal et al., 2003). However, the use of a hydro-hermetic feed has been proven to dampen the shear rate and hence improve cell viability during initial entry into the centrifuge (Boychyn et al., 2001). Centrifuges operating in continuous mode will recover concentrated cells via high speed discharge from the centrifuge bowl and depending on the discharge conditions can contribute to cell damage (Gray et al., 1972). Alternatively, batch operations give optimum separation, characterised by intact and compact cell paste. Batch operations do however suffer from long downtimes and are not practical for separation of high volume, high density fermentation broths.

1.2.2 Types of centrifugation

The application and design of centrifuge separators has been reviewed by Axelsson (1985) and Brunner et al. (1988). There are four main types of centrifuges, which are used for different process environments. The efficiency of solid and liquid separation is greatly dependant upon particle size, solid-liquid density difference, liquid viscosity, residence time and the relative centrifugation forces (RCF). The following

sections summaries the different types of centrifuges currently available on the market with their individual advantages and disadvantages (Leung 1998).

1.2.2.1 Tubular bowl centrifuge

The tubular bowl centrifuge has the simplest configuration of all the centrifuges considered here, consisting of a vertically mounted cylindrical bowl suspended by an overhead motor. During operation the liquid moves up through the base of the centrifuge before progressing along the sides of the bowl during which solids are spun out and accumulated at the wall surface. As the flowrate is increased the liquid layer ascending the wall of the centrifuge moves faster thus reducing the centrifuge performance by shortening the residence time available for cell sedimentation. The system operates in a batch mode; thus over time solid deposition increases and reduces the overall performance. On reaching a full bowl volume the centrifuge is brought to rest before emptying the sediment. Some tubular bowl centrifuges do this with the aid of an internal scraper, e.g. CARR Powerfuge, avoiding the need to dismantle the centrifuge and allowing cell recovery in a contained fashion. Solids removal by this means is time consuming and for this reason the tubular bowl centrifuge is commonly used either when high G-forces are necessary for achieving satisfactory separation and dryness, or when separating a low cell density feed suspension. These centrifuges are typically found towards the end of process lines as a polishing step.

1.2.2.2 Multichamber bowl centrifuge

The internal design of the multichamber consists of a series of concentric chambers mounted within the larger outer chamber. The centrifuge is driven from the bottom and feed enters via an inlet situated at the top of the bowl. The centrifuge works in batch mode. The feed takes a circuitous route through the chambers, where larger particles are deposited closer to the centre and smaller particles are collected in the outer chambers where they are subjected to greater centrifugal forces. Its high

efficiency is achieved by long residence times but often result in unacceptable temperature rises. However, this can be minimised by direct cooling of the bowl top.

1.2.2.3 Scrolling decanter centrifuge

The scrolling decanter is a continuous centrifuge, consisting of two main parts, an Archimedean screw encapsulated by an outer cylindrical component. Both rotate in the same direction but at different speeds. The suspension enters through the spindle of the Archimedean screw and is released into the bowl where separation begins. The suspension flows towards the weir whilst the solids deposit on the wall and build up into a cake. The clarified liquid is discharged at the weir. The screw scrapes the solids towards the conical end of the bowl and the slope of the cone allows drainage to increase liquid removal from the solids before discharge. Although the centrifugal force is low the design allows for separation of very high solids load and can often be found in the treatment of wastewater.

1.2.2.4 Disc-stack centrifuge

Separation in a disc-stack centrifuge begins by pumping material in through the feed inlet positioned at the top of the bowl. The material descends into the distributor and proceeds into the stack of active discs where solid/liquid separation occurs. Separation is based on a density difference existing between two or more phases with the heavy components of the feed directed towards the periphery of the bowl under the influence of centrifugal forces as lighter liquid is displaced towards the centre of the bowl. The liquid component is discharged through a centripetal pump positioned at the top of the centrifuge. Disc-stack centrifuge designs include batch and continuously operated machines. In batch operation solids must be removed manually. Some centrifuges are equipped with peripheral nozzles for continuous solids removal; others have valves i.e. sliding piston for intermittent discharge. The nature of these continuous centrifuges make them ideal for primary separation of high cell density broths (Higgins et al., 1978; Datar and Rosen, 1987).

1.3 Factors influencing the selection of centrifuge separation method

Correct specification of the type of centrifuge to be used in a process line is central to achieving optimum separation and recovery of product. In this section we review the effect of different process scenarios on centrifuge selection.

1.3.1 Solids feed density

With high cell density fermentations the best process options are either continuous discharge centrifuges such as the disc-stack and scrolling decanter or intermittent disc-stack centrifuges. Both types of centrifuge are capable of handling high solids concentration feed streams. However, solids must remain sufficiently wet to flow through the discharge nozzles in order to avoid blockage. For the recovery of intracellular products the performance is also determined by the discharge conditions with more intensive discharge leading to lower yields of viable product. Under these circumstances intermittent discharge centrifuges provide more precise control over solids dryness and discharge conditions than continuous centrifuges.

Batch machines may be used successfully when dealing with a low concentration of solids and with the correct solids holding capacity the bowl will not require emptying until all material has been processed. Choosing the correct size and capacity are vital for achieving good clarification. Figure 1.1 illustrates the type of centrifuge best suited to different solids load.

1.3.2 Feed sensitivity

Intense shear forces are often found in centrifuges during initial entry into the feed zone and during discharge in continuous/intermittent machines. In the case of shear sensitive materials, e.g. mammalian cells, optimum recovery can be achieved through the use of a batch operation with the installation of a hydro-hermetic feed zone that floods the inlet and dissipates the energy generated upon entry into the centrifuge.

1.3.3 Separation efficiency

Separation requirements will also influence the choice of centrifuge. In many cases, the driving force may be to achieve good clarification, dewatering and solids recovery. It is useful to know the particle size and size distribution in the feed suspension as this will help determine the equivalent settling area and G-force necessary to accomplish any defined separation goals. A typical scenario where performance is paramount is the removal of fine cell debris after releasing intracellular products by homogenisation of whole cells. Jin et al. (1994) demonstrated that the recovery efficiency of inclusion bodies in a disc-stack centrifuge is dependant on the feed flow rate. Maximum recovery was achieved at a flow rate of 460 L.h^{-1} with 100% removal of cell debris and 92% recovery of product. The performance was observed to deteriorate as the flow rate increased. The cell debris becomes increasingly difficult to remove with small sizes and broad size distributions (Bonnerjea, 1988). A subsequent step may involve high-resolution chromatography of which poor centrifugal separation performance will lead to fouling of the column, a problem that could incur costly time delays. Figure 1.2 illustrates the type of centrifuges most suited to separating particles of different sizes.

1.3.4 Three phase feed suspensions

When dealing with separation of three phase mixtures, for example an oil/water/solids mixture, the only machines currently available for this type of procedure branch from the family of disc-stack centrifuges and scrolling decanters.

1.3.5 Cost of centrifuges

During process specification, in addition to the technical decisions, the cost of centrifuges will also need to be considered, especially if the process design is restricted to a tight budget as is the case with many small biotechnology companies. The overall cost of installing and maintaining a centrifuge will vary depending on the size and capability of the centrifuge, the ancillaries and whether it has to be explosion resistant or bio-contained.

1.4 Host cell selection

Many factors play a key role in evaluating an expression system for production of therapeutics including productivity, process economics, product quality and safety, lead time, scalability, regulatory acceptance and biomechanical properties. The most common host cells for biopharmaceutical products are *E. coli*, yeast, and mammalian cells. Recombinant technology was first introduced in *E. coli* with the technology later extended to higher, more complex organisms such as mammalian cells (Demain 2000). Considerable efforts have been made to optimise these host cells. For example, Bowering (2000) enhanced *E. coli* antibody fragment titres from 200 $mg.L^{-1}$ to 680 $mg.L^{-1}$ and significantly improved product retained inside the periplasm from 50% to 80-90%. In addition, Garcia et al. (2005) compared two feeding strategies i.e. repeated batch and pH-stat fermentation in terms of product yield and cell stability. The pH-stat method proved superior with a two-fold increase in antibody fragment titre and a dry cell weight of 33 $g.L^{-1}$ compared to 17 $g.L^{-1}$ for the repeated batch after 50 h. This difference was due to substrate oscillation in the repeated batch, which has previously been reported to influence cell and product stability due to imbalances in carbon uptake rate and the switch from oxidative to fermentative metabolism (Johnston et al., 2002). Shown in Figure 1.3 is a simplistic illustration of how these organisms compare in terms of biomechanical properties under shear stresses. The data was compiled based on the minimum stress at which damage is first detected (Yim et al., 2000).

Solids concentration (vol%)	0	20	40	60	80	100
Multi-chamber centrifuge	■					
Tubular bowl centrifuge	■					
Self-cleaning centrifuge	■■					
Disc stack centrifuge		■■■■				
Scrolling decanter centrifuge		■■■■■■■■■■■				

Figure 1.1   Classifying centrifuges by feed solids concentration (vol %) (Brumner and Hemfort, 1988).
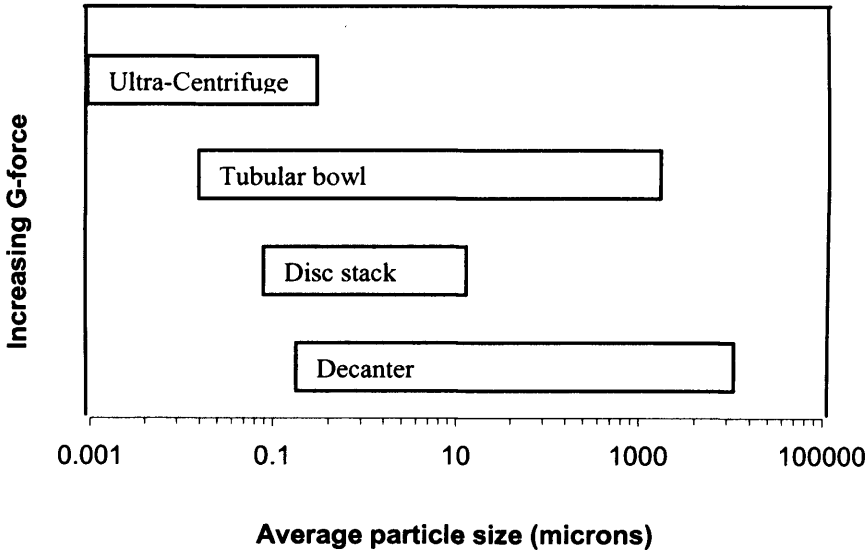
Figure 1.2   Classifying centrifuges by feed particles (Leung, 1998).

Strength (N.m^{-1})

10^5 — Plant cells

10^3 — Yeast cells

10^1

10^{-1} — *E.coli* cells

10^{-3}

Mammalian cells

10^{-5}
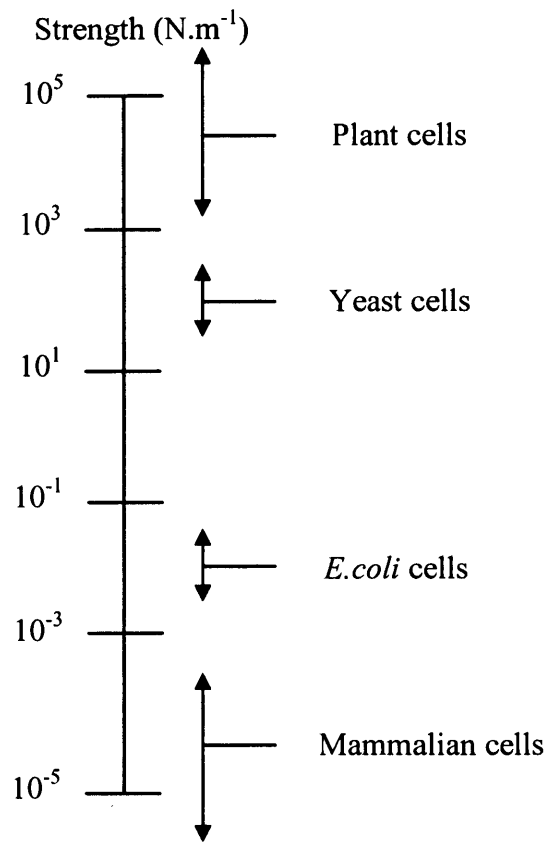
Figure 1.3   Estimation of the minimum stress required to cause irreversible cell damage for a range of biological materials (Yim et al., 2000).

1.4.1 *E. coli* host cell

1.4.1.1 Advantages of *E. coli*

The Gram-negative bacterium *E. coli* was chosen as the cell type for all experiments in this thesis for the following reasons:

- It is a simple prokaryotic organism.

- It has been extensively researched and is well characterised (Bowering 2000; Garcia 2005).

- *E. coli* is a rapidly growing organism, capable of reaching very high cell densities.

- Fermentation protocols for *E. coli* are well established at UCL and relatively straightforward and inexpensive to run.

- The introduction of foreign genes can be easily achieved.

- The organism is used in the biopharmaceutical industry for the production of therapeutics such as DNA vaccines and antibody fragment for cancer therapy.

1.4.1.2 Disadvantages of *E. coli*

Acetate production, caused by either anaerobic growth conditions or cultures in the presence of excess glucose, can reduce *E. coli* growth rate, biomass yield and cell density (Lee 1996). Furthermore, acetate accumulation has been reported to be more detrimental to recombinant cells than non-recombinant cells (Lee 1996). High levels of carbon dioxide can also affect cell growth by stimulating acetate production.

1.4.2 *E. coli* cell morphology

E. coli is a member of the Gram negative (-ve) bacteria. These procaryotic organisms display properties that are relatively simple compared to eucaryotes. A typical *E. coli* cell consists of four basis structures: the outer membrane, the peptidoglycan layer, the inner membrane and the cytoplasm that houses the genomic DNA and ribosomes. The cells are typically rod shaped with dimensions of 1.5 to 5.5 μm in length by 0.5 to 1 μm in width (Nanninga. 1998). In the following section the morphological structure of *E. coli* cells will be discussed with reference to the outer and inner membranes.

1.4.2.1 Cell envelope

The cell envelope of Gram +ve and -ve bacteria is distinctly different as shown in Figure 1.4. The purpose of the envelope is primarily to prevent damage to the underlying cytoplasm molecules by toxic compounds (Nikaido et al., 1985). Gram +ve bacteria exhibit a thick peptidoglycan layer (~250Å) positioned above the inner membrane. However, Gram –ve bacterial envelopes appear as thin multi-layered structures with only a thin sheet of peptidoglycan (~30Å) positioned between the outer and inner membranes. In some cases, a polysaccharide capsule or glycocalyx may surround the cell wall of bacteria which can serve the purpose of aiding cell adhesion to surfaces, act as a carbohydrate reserve for metabolism and protect cells from attach e.g. phagocytosis. The *E. coli* capsule mainly comprises of polysaccharides such as glucose, galactose and fructose glucuronic acid.

1.4.2.2 Outer membrane

The outer membrane structure of *E. coli* comprises of a lipid bilayer very similar to that of the inner membrane. The inner half of this outer membrane layer is composed of phospholipids while the outer face is dominated by lipopolysaccharides (LPS). The LPS consist of three main regions, a toxic lipid A region that is attached to a

hydrophilic polysaccharide region made up of a core polysaccharide and O-specific polysaccharide. The tail is understood to aid defence against phagocytes and also contribute to bacterial adhesion. Shown in Figure 1.5 is a schematic representation of an outer membrane lipopolysaccharide.

A number of proteins are found to traverse the outer membrane to form attachments with the underlying peptidoglycan layer. Of these the most commonly found are Braun lipoproteins positioned in the hydrophobic region of the outer membrane and covalently attached to the peptidoglycan layer as shown in Figure 1.6. Braun (1975) suggested that a possible function of these lipoprotein molecules could be to act as spacers between the outer membrane and peptidoglycan layer. Another common group of proteins that traverse the outer membrane are porins (Nikaido and Vuara 1985). Porins form channels through the membrane that allow passage of molecules up to 750 daltons through i.e. mainly nutrients. Large molecules and harmful compounds are excluded from entry. Omp A, Omp C and Omp F are amongst the most common porins found in *E. coli* (Murrell 1998).

1.4.2.3 Peptidoglycan layer (cell wall)

Between the outer and inner membrane of Gram –ve *E. coli* is a thin sheet of peptidoglycan made up of alternating units of N-acetylglucosamine (G) and N-acetylmuramic acid (M) connected by beta 1-4 glycoside bonds as shown in Figure 1.7. Attached to N-acetylmuramic acid (M) is a tetrapeptide chain consisting of L-alanine (L-ala), D-glutamate (D-glu), Diaminopimelic acid (DAP) and D-alanine (D-ala). Neighbouring tetrapeptide chains have the ability to bond the carboxyl group of D-ala on one chain to the amino group of DAP on an adjacent chain. The cell wall gives cells their characteristic shapes and permits them to live in hypotonic (less than intracellular salt concentration) environments that would otherwise cause them to swell osmotically until they burst.

1.4.2.4 Inner membrane

The inner membrane is by far the most dynamic and complex part of the cell envelope. It functions as a selective barrier only permitting entry of specific molecules into the cytoplasm. Molecules such as H_2O and those with molecular weight < 100 daltons can move through passively but larger molecules can only enter via membrane transport systems. The membrane acts as an energy generator i.e. the respiratory chain and ATP synthase, providing energy to drive cellular processes that include biosynthesis and active transport systems. The membrane contains enzymes involved with synthesis of murein, membrane lipids and DNA replication.

Figure 1.8 shows the importance of H^+ ions in the transport of molecules across the inner membrane. Molecules are transported through the cell membrane by three different mechanisms: a uniport process where solute travel is unidirectional, a symport process where two solutes travel in the same direction at the same time, and an antiport process where two solutes travel in opposite directions. In many instances movement of solutes is against a concentration gradient and therefore in order to facilitate transport of these solutes active transport systems are employed of which there are three types: ion driven transport (IDT), binding-protein dependant transport (BPDT) and group translocation transport (GTT) all of which usually exist as symport or antiport processes. IDT is associated with the movement of ions and amino acids across the membrane. The active membrane protein requires H^+ ions i.e. proton motive force (pmf) to operate. In the case of BPDT the transport of molecules, e.g. sugars and amino acids, involves four transmembrane proteins and is driven by energy released from the hydrolysis of adenosine triphosphate (ATP) to adenosine diphosphate (ADP). Finally GTT is involved with the transport of sugars e.g. glucose. The system derives its energy from phosphoenol pyruvate (PEP). During entry of molecules such as glucose, PEP is hydrolysed to pyruvate and glucose is phosphorylated to form glucose phosphate.

Lodged in the inner membrane are ATP synthase molecules that are analogous to mitochondria in eukaryotes. In aerobic bacteria free H^+ ions allow the ATP synthase molecules to establish a pmf across the cell membrane by flowing down an

electrochemical gradient through the ATP synthase. The free energy released drives the ATP synthase to make ATP. Glycolysis also contributes to ATP production in the cell. In anaerobic conditions the lack of an electrochemical gradient causes a shift in mode of operation in order to maintain a pmf across the membrane. Under these circumstances the ATP synthase works in reverse using ATP produced by glycolysis to form ADP, phosphate and H^+ ions. The H^+ ions are pumped out of the cell to stabilise the pmf and hence maintain the active transport systems. The active transport processes are diminished in injured cells and do not become fully functional in repaired organisms (Hurst et al., 1976).

1.4.2.5 Cytoplasm

The cytoplasm constitutes the inner portion of a prokaryotic cell and is characterised as the holding chamber for chromosomes, ribosomes and intracellular products e.g. plasmid vaccine vectors that multiply and accumulate in this space.

1.4.3 *E. coli* expression techniques

There is a variety of expression techniques possible with *E. coli* such as secretion into the cytoplasm, periplasm and exterior environment, all of which are governed by the type of leader sequence used. Each expression strategy possesses its own unique advantages and disadvantages.

1.4.3.1 Cytoplasmic expression

Cytoplasmic expression is a very straightforward procedure but this method requires a very high level of expression to overcome protease degradation that may otherwise lead to the product accumulating in the form of insoluble inclusion bodies. This often results in the need for re-solubilisation-renaturation processes that consequently give low yield (Buchner and Rudolf 1991). Carlson et al. (1995) gives an extensive insight into the problems associated with the recovery of cytoplasmic products such as

plasmid DNA from *E. coli* cells. Non-selective recovery methods such as sonication, homogenisation, microfluidization, bead milling and nebulization were evaluated for the extraction of the cytoplasmic product. Carlson et al. (1995) reported severe loss of product i.e. almost complete degradation in all methods except microfluidization and bead milling which gave acceptable recovery levels. In the majority of cases product damage was due to high shear rates and cavitation. Besides product damage the formation of fine debris and contaminants of similar size to the product, e.g. genomic DNA fragments, place a heavy burden on subsequent separation and purification steps, e.g. fouling of chromatography columns (Hearle et al., 1994) and filters (Gray et al., 1973). The best processing method was bead milling with over 90% of plasmid remaining intact. The report demonstrates the negative aspects of cytoplasmic expression. However in recent years chemical lysis, often associated with lower shear rates, has proven to be more desirable for cytoplasmic product recovery (Levy et al., 1999).

1.4.3.2 Periplasmic expression

A large numbers of products have been successfully secreted into the periplasm with the help of a variety of leader sequences. The majority of products are correctly folded at this point (Little et al., 1989). Murrell (1998) illustrates the effectiveness of periplasmic expression by using a MalE protein synthesised in the cytoplasm as a precursor protein. Its amino acid leader sequence directed the molecule to the periplasm and upon entry the signal sequence was cleaved by signal peptidase. Very little quantity of generic molecules are found in this space hence the expressed product can be contained as a relatively pure component. The product can later be extracted by means of selective disruption such as selective chemical lysis, where disruption is only targeted to the outer membrane while the inner membrane remains intact.

There are a number of concerns regarding periplasmic expression. The periplasmic space is limited in capacity and therefore over-expression of a product may render the outer membrane leaky and consequently loss of product through the release into the

surrounding media. Bowering (2000) reported periplasmic antibody fragment leakage of up to 50%. Accumulation of product signal sequences in the periplasmic space can lead to a heat-shock stress response and increase proteolysis (Wild et al., 1993). Finally, it is not always possible to identify a leader sequence that will transport a product to the required destination.

1.4.3.3 Extracellular expression

A product which is directly secreted into the extracellular media can be easily purified from unwanted whole cells through a range of separation steps. However, a "fusion" protein with a sequence targeting the product to the media must often be used and hence generates the need for extra purification steps in order to fully remove this fusion protein. In addition, products expressed extracellularly are not protected from external stress conditions found in unit operations such as centrifuges (Neal et al., 2003).

1.4.4 Product review

This thesis focuses on Fab' antibody fragments expressed in the periplasmic space of W3110 *E. coli* and 20 kb supercoiled plasmids expressed in the cytoplasm of DH5α *E. coli* cells.

1.4.4.1 Antibodies

1.4.4.1.1 The use of antibodies

Antibodies are commonly referred to as immunoglobulins and are produced naturally by the body with the sole purpose of combating infection and disease. However, there is much pressure to generate pharmaceutical grade antibodies with unique specificity and affinity in order to treat a growing number of diseases. The use of mice

hybridoma technology for antibody production was the first of its kind and they now constitute a 20% share of the biopharmaceuticals currently in development (Roque et al., 2004). In some cases the nature of antibody binding may be all that is needed to render the antigen inactive. However, this is rare and in most cases the specific binding must be complemented with either molecules that stimulate the recruitment of the patient's own immune cells or conjugating it with selected drugs. Examples of antibody use include fusion of antibody fragments to radiolabels (Hudson 1999; Segal et al., 1999) and enzymes (Chester and Hawkes 1995) for cancer imaging/therapy and prodrug therapy (i.e. the enzyme activates the drug at the tumour site) respectively. Whatever the approach, the success rate of a potential antibody candidate will depend on the nature of the conjugate linker used, the potency of the drug and the ease of manufacture.

1.4.4.1.2 Structure of antibodies and antibody fragments

A typical antibody consists of two polypeptide light chains linked by disulfide bonds to two heavy chains in the form of a Y-shape. Each chain is divided into sub-domains with each light chain consisting of one variable and one constant domain and each heavy chain consisting of one variable and three constant domains. The variable domain of both chains combine to form the specific antigen-binding site often referred to as the complementary determining region (CDR). The efficiency of CDRs is greatly improved with the existence of the flexible hinge region that allows for change in distance between the two binding sites.

Antibody fragments, such as Fab' molecules, contain the variable and constant domains of the light chain and the corresponding heavy chain domains. They have been reported to have the same affinity as whole antibodies (Shibui et al., 1993). In recent years a number of scientists have enhanced the affinity of Fab' fragments by linking of two fragments (Carter et al., 1992; Rodrigues et al., 1993) thus improving the probability of antibody-antigen binding.

1.4.4.1.3 Antibody production and purification

Antibody development typically takes in excess of 10 years before market release (Brekke et al., 2003). The first step in antibody development is to select the source and to screen antibodies for affinity and specificity to a target antigen. The chosen antibody/antibody fragment can then be modified in format and expressed in an organism of choice, usually mammalian cells (Willems et al., 2003) or bacterial cells such as *E. coli* (Humphreys et al., 2003). To achieve correct product folding in *E. coli* the antibody fragments are directed into the periplasmic space where the oxidation of cysteine thiols to disulfides occur (Humphrey et al., 2004). Expression into either the cytoplasm or extracellular matrix of *E. coli* leads to incorrect folding and formation of inclusion bodies thus rendering them unfit for antigen affinity. The main disadvantage with using mammalian and bacterial host cells is the associated costs of production and purification. An alternative method of producing antibodies is to now use transgenic plants which act as bioreactors to cultivate the product. Plants possess a number of advantages such as low production cost, easy to handle, and are free from human pathogens. However, this form of production is still in early development with much research needed to prove its efficacy and potency.

Upon completion of the fermentation the antibody product is recovered and purified to a high level. As a rule of thumb downstream processing accounts for 50-80% of the overall process manufacturing cost (Roque et al., 2004) and as such the challenge facing industry is to increase efficiency and reduce cost of operation. During downstream processing there is considerable effort to reduce flow stresses as this could lead to damage or contamination of product e.g. incorporation of a hydro-hermetic feed to reduce the shear stresses at the feed inlet of large scale centrifuges.

1.4.4.2 Plasmids

1.4.4.2.1 The use of plasmids

The use of plasmid DNA for gene therapy and vaccination has gained considerable attention over the last decade (Wang et al., 2004). A recent report estimated the number of DNA products in clinical trials to be in excess of 600 (Prather et al., 2003).

Plasmids are double stranded DNA molecules which carry genetic information. Apart from their helical structure, they occur in a range of shapes, namely the linear form, open circular (OC) and supercoiled (SC) of which the SC plasmid DNA are the most common form for product delivery (Prazeres et al., 2004). These macromolecules are used for gene therapy and DNA vaccination (Wang et al., 2004) where they can express molecules that mimic intracellular pathogenic infections and trigger both humoral B-cell and cellular T-cell responses (Prather et al., 2003). This feature makes plasmid DNA vaccines more attractive than protein based vaccines that generally only elicit humoral responses. However the process of plasmid development and manufacture pose a difficult challenge whereby the focus is to produce a consistency in purity, potency, efficiency and safety which is compliant with the Food and Drugs Administration (FDA) and European Medicines Evaluation Agency (EMEA) regulations. The following section gives an overview of plasmid DNA vaccines from forming the construct through to patient delivery.

1.4.4.2.2 Plasmid construction

When constructing a DNA plasmid for therapeutic applications, a number of key features need to be addressed including the nature of the antigenic protein, size of plasmid, copy number and molecular stability.

Stage one involves specifying the antigen and its use in treatment of disease. The code for this antigen is then inserted into the appropriate plasmid vector usually supercoiled circular DNA (Levy et al., 2000). Positioned on the plasmid are a number of functional groups which dictate the behaviour of the plasmid. Of these, the

replication origin governs the plasmid copy number i.e. the rate of plasmid multiplication. High copy numbers are desirable as it gives a higher yield of plasmid per unit cell (Durland et al., 1998). Another critical element of plasmids is a selective marker such as an antibiotic resistance gene. The function of the marker is to suppress growth of plasmid free bacteria during fermentation. This is achieved by addition of the antibiotic to the growth media which kills bacteria absent of the resistant gene but allows the continuous growth of those possessing the plasmid resistant genes. In addition, high copy number characteristics frequently reduce the growth rate of plasmid containing cells and as a result without the resistant gene plasmid free cells would quickly outgrow the target cell. Although this method of selectivity is simple and effective, there are concerns that the antibiotic added to the initial fermentation may contaminate downstream purification steps and the final plasmid product (Durland et al., 1998).

Once the plasmid construct has been established, a suitable host organism must be selected. Desirable cell phenotypes include the ability to reach high cell densities during fermentation, easy to handle, minimal potential for genetic mutation and compatible with subsequent downstream purification steps.

1.4.4.2.3 Plasmid recovery

One of the main challenges with plasmid recovery during downstream processing is to design a process that enables the release of the plasmid product for the host cell and removal of the numerous sources of impurities including RNA, genomic DNA, proteins, and endotoxins without damage to the product, until the desired specification is achieved. Many of these contaminants possess very similar physical and chemical characteristics to the plasmid and therefore careful consideration of the unit operation sequence should be made. It is mandatory that high purity specifications are obtained when the manufactured product is intended for therapeutic applications. Ideally the overall process should consist of a limited number of steps with the aim of reducing processing costs, operating time and labour charges without a compromise in product quality.

A typical process example for manufacturing and recovery of DNA vaccines starts with a fermentation of recombinant *E. coli* cells followed by centrifuge harvesting and chemical lysis (Ciccolini et al., 2002; Levy et al., 2000). During chemical lysis all forms of DNA are denatured but providing conditions are controlled the denaturation of plasmids is reversible. The plasmid may then be recovered by filtration and purified by chromatograph before formulation. Throughout all these procedures the shear sensitivity of DNA must not be ignored.

E. coli chromosomal DNA is significantly larger than plasmid DNA (i.e. 4500kbp and <50kbp respectively) and therefore theoretically speaking the separation of these two DNA forms should be straight forward. However because of their delicate nature any shear effects encountered will shred the molecules into fine fragments; the sensitivity of which is critically dependant on plasmid size and ionic strength of the environment. Shear effects can convert the desired SC form of the plasmid to an OC or linear form rendering it useless. Levy et al. (1999) has previously shown that plasmid size > 20 kbp are sensitive to shear rates in excess of $1 \times 10^6 \, s^{-1}$. In many process situations the genomic DNA is fragmented into molecular sizes comparable to plasmid DNA and hence adversely affects the performance and recovery from subsequent unit operations.

1.4.4.2.4 Therapeutic application

The following section explains how DNA vaccines can be used for therapeutic applications. The purified and formulated plasmid encoding the antigen protein is injected into intramuscular tissue via a gene gun, after which the plasmid begins to produce the antigenic protein. The proteins are presented on the MHC I receptors of the antigen presenting cells (APC) which subsequently activate a cascade of immune responses. DNA vaccines offer a number of advantages over protein vaccines. The encoded protein is expressed in its natural form exactly as it would do by the pathogen and they induce both humoral and cell mediated responses making them superior to protein based vaccines which generally only stimulate the humoral immune pathway (Prather et al., 2003).
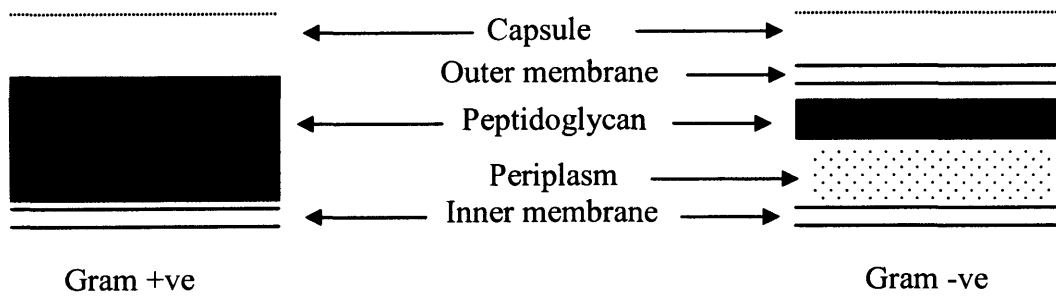
Figure 1.4   A comparison between Gram +ve and −ve bacterial cell envelopes.
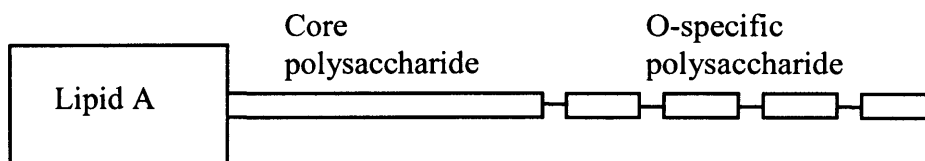
Figure 1.5   Schematic illustration of an outer membrane lipopolysaccharide consisting of a lipid A region and hydrophilic polysaccharide.
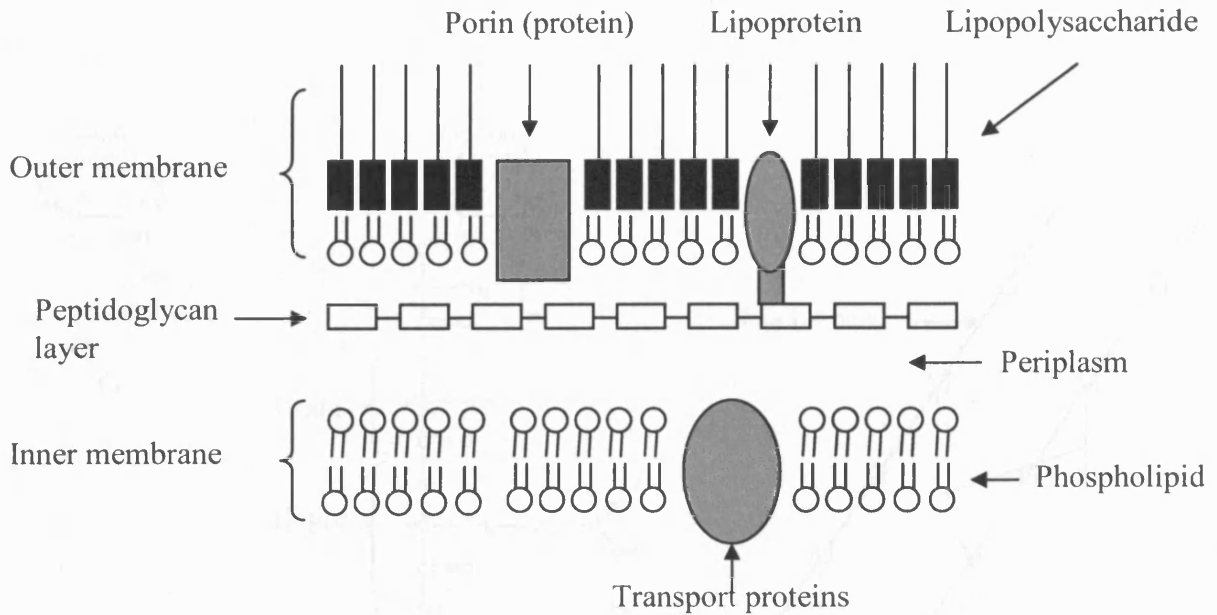
Figure 1.6   A schematic representation of a Gram –ve *E. coli* cell envelope. The outer cell membrane consists of lipopolysaccharides attached to a phospholipid foundation. Embedded between the outer and inner membrane is a peptidoglycan layer and the periplasmic space (Prescott et al., 1999).

Figure 1.7   The structure of a peptidoglycan layer. (G) represents a molecule of N-acetylglucosamine; (M) represents a N-acetylmuramic acid chain and (C) is the polymeric form of the molecules as they appear in the peptidoglycan layer.
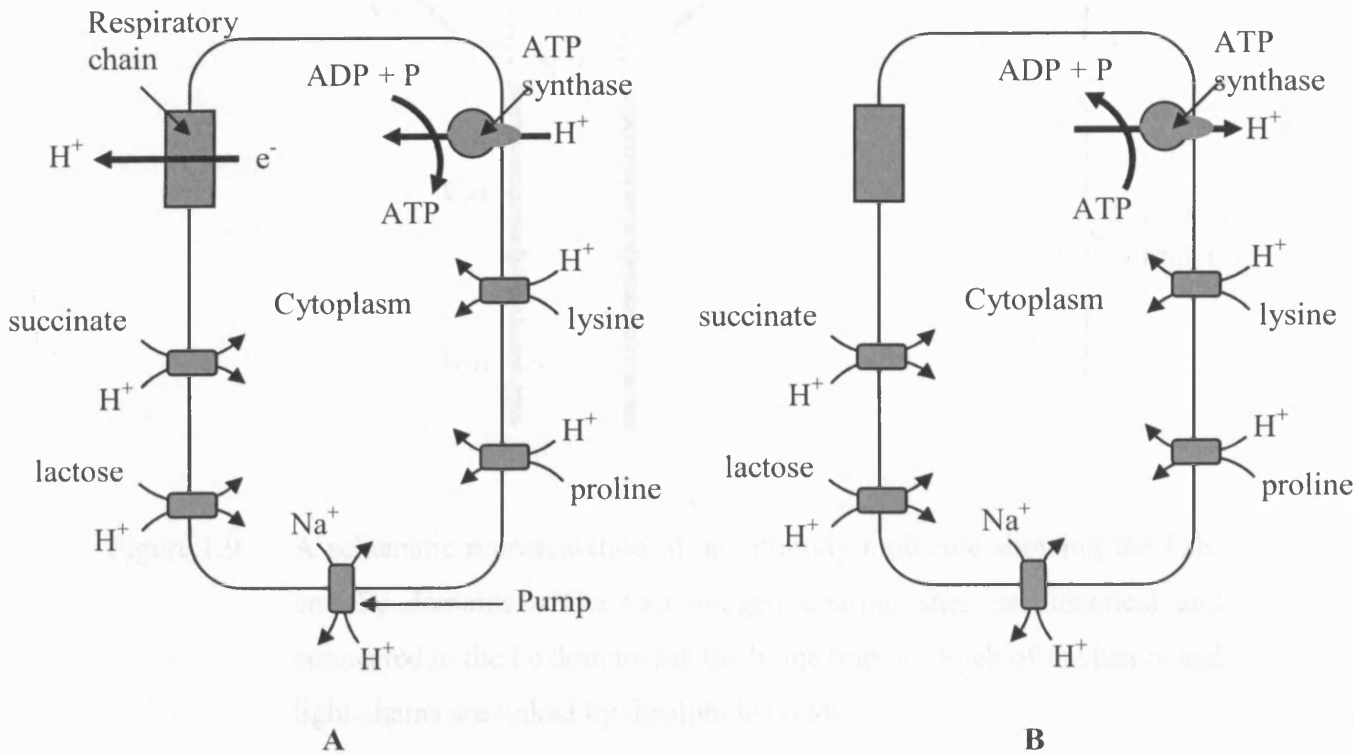
Figure 1.8   A schematic illustration showing the importance of free H^+ ions for transport of solutes in and out of a prokaryotic cell. (A) corresponds to aerobic respiration and (B) corresponds to anaerobic respiration (Alberts et al., 1994).

Figure 1.9   A schematic representation of an antibody molecule showing the Fab'
and Fc domains. The two antigen binding sites are identical and
connected to the Fc domain via the hinge region. Each of the heavy and
light chains are linked by disulphide bonds.
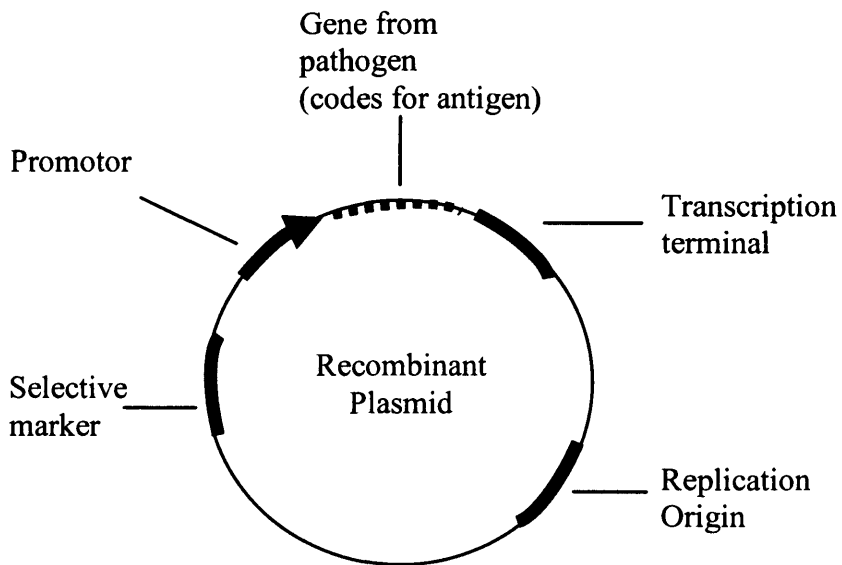
Figure 1.10   Schematic representation of a typical plasmid DNA construct.

44

1.5 Stresses in bioprocess unit operations

During bioprocess development, besides choosing the cell strain and expression system to use, an equally important consideration is the optimisation of unit operations to ensure minimum loss of integrity of labile materials. The detrimental physical and biological effects of flow stresses have been widely documented for mammalian, bacterial and plant cells (Yim et al., 2000; Doran, 1993). These effects have also been observed at large scale with bioprocess equipment such as homogenisers (Shamlou et al., 1995; Maa et al., 1996), crossflow filtration rigs (Jaouen et al. 1999), centrifuges (Dunlop et al., 1994; Papoutsakis 1991) bioreactors (Virkar et al., 1982; Hewitt et al., 1998) and pumps (Virkar et al., 1981). Figure 1.11 provides a rough estimation of the energy dissipation associated with operating different bioprocess units; the energy dissipation is notoriously difficult to define, especially in complex flow fields and with multiphase suspensions commonly faced in downstream processing.

Shear rate can influence the performance of all unit operations, from upstream fermentation to vialing, and the understanding of these effects is essential if one aims to maximise product yield. Shear rate can easily convert a sensitive cell or product into a non-desirable form. For example, Levy et al. (1999) have shown that plasmids of >20 kb are sensitive to a shear rate of 1×10^6 s^{-1}, which are commonly experienced in many unit operations. Lencki et al. (1993) demonstrated that macromolecules such as proteins, are normally stable up to a shear rate threshold but beyond this loss of viability is evident. The following section gives a brief introduction into the flow stresses experienced in downstream bioprocess operations and their effects on product stability.

Energy dissipation (W.kg^{-1})
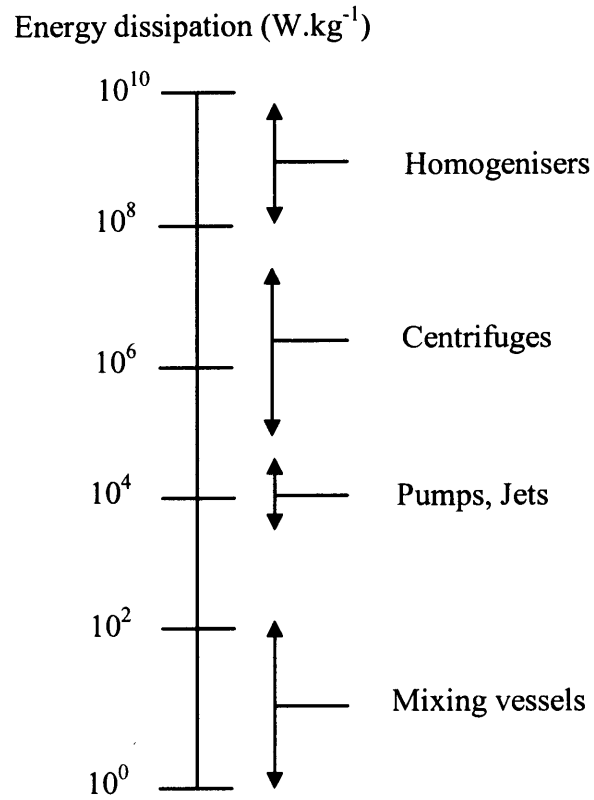
Figure 1.11   Estimation of fluid energy dissipation associated with different bioprocess units (Yim et al., 2000).

1.5.1 Centrifuge stresses

Centrifuges are renowned for their high shear at the entrance zone (Maybury et al., 1998) and although new designs are addressing this, the problem still exists for sensitive biomaterials. Particle size and strength have a major influence on the separation efficiency of a centrifuge. With the presence of a high shear field during entry into a centrifuge, cells can potentially be reduced in size. This can cascade on to affect recovery performance, cost, and quality of material. Byrne et al. (2002) demonstrated this phenomenon with protein precipitates. A positive correlation between precipitate robustness and clarification efficiency was evident. Small compact precipitates were more resilient to the high shear and hence achieved better clarification than larger fragile precipitates that fragmented and became difficult to separate.

Filter centrifuges have been used in the recovery of shear sensitive materials such as nematodes (Surrey and Davies 1996), precipitates (Shah and Kothari 1991) and cellulase (Ramamurthy et al., 1992). Limited work has been published on the effect of fluid-induced damage to biological materials during filter centrifugation. However, Boulding et al. (2002) focused on mapping the hydrodynamic conditions i.e. energy dissipation and shear rate in a pilot-scale filter centrifuge in order to assess the primary recovery of single-chain F_v antibody fragments: Computational Fluid Dynamics (CFD) simulation of the pilot-scale filter centrifuge (Figure 1.12), operating at a rotational speed of 3000 rpm, estimated the energy dissipation and shear rate occurring along the filter cloth to be in the order of 2×10^5 W.kg^{-1} and 1.88×10^4 s^{-1} respectively. These conditions were reported to lead to the recovery of only 85% of the antibody product.

Neal et al. (2003) extended the CFD simulation work to include disc stack centrifuges. The centrifuge performance was again predicted with CFD analysis in conjunction with experimental trials. It was established that the maximum shear rate of a pilot-scale disc stack, operating at 7500 rpm, was 1×10^4 s^{-1} and was concentrated around the spindle nut. This level of shear was sufficient to reduce the size of antibody precipitates from an average size of 14.5 μm to 5.3 μm. Boychyn et

al. (2004) mapped the energy dissipation for the same type centrifuge operating at a rotational speed of 9900 rpm; the maximum energy dissipation rate was estimated to be 2 x 10^5 W.kg^{-1}. Byrne et al. (2002) and Maybury et al. (2000) identified the same region of high shear in a disc stack centrifuge demonstrating particle break-up/ cell damage upon contact with the spindle nut.

Similar cell damage results were reported by Boychyn et al. (2001) for a multi-chamber centrifuge. CFD simulations of the multi-chamber bowl (Figure 1.13) running continuously with a flooded and non-flooded feed zone were carried out, with the highest energy dissipation rate concentrated around the spindle nut and along the base and exit of the inner chamber. The maximum energy dissipation experienced in the flooded and non-flooded configurations were 6 x 10^5 and 12 x 10^5 W kg^{-1} respectively. This confirmed that non-flooded conditions generate more cell damage. This was also supported by a reduction in subsequent clarification performance of precipitate suspensions.

1.5.2. Crossflow filtration stresses

Centrifuge recovery of biological species is often very efficient but cell damage is a common occurrence for fragile materials (Jaouen et al., 1999). An alternative is the use of low shear cross-flow microfiltration where suspensions are concentrated by recycling across the membrane surface. Typical industrial use of crossflow filtration includes primary concentration of material from fermentation broths, and sterile filtration as a final polishing step. Shown in Figure 1.14 is a typical layout of a cross-flow filtration rig. The separation technique is generally associated with low shear across the membrane surface (Virkar et al., 1981; Bowen et al., 1992). However, if the shear levels exceed the critical stress of the product in question shear damage will occur. Bowen et al. (1992) describes the loss of enzyme activity by shear-induced deformation from prolonged membrane interactions. The enzyme activity was observed to decrease by up to 20%.

Filtration pumps play a significant role in the performance of filters as they are central to controlling flowrate, permeate flux and membrane fouling. The effect of shear

stresses in various filtration pumps was investigated by Jaouen et al. (1999) with a number of intriguing conclusions. Fragile biological microalgae material i.e. *Tetraselmis suecica* was circulated though a cross-flow microfiltration unit with different types of pump and different pump flow rates. It was reported that the intensity of the induced shear stress was a function of pump design and flowrate, with centrifugal pumps causing the highest loss of cell viability. Similar observations were reported by Vandanjon et al. (1999), where centrifugal pumps proved most detrimental to *Skeletonema costatum* cells.

Throttling valves, often found on filtration rigs, have also been demonstrated to contribute to the cell damage process. As cells pass through throttling valves differential pressure can inflict cell damage (Schutte et al., 1990; Save et al., 1994). Vandanjon et al. (1999) compared the performance of two valves, namely a globe valve and a ball valve using the pressure drop coefficient (K_v). Under the same pressure drop coefficient a globe valve caused more damage to cells than a ball valve. Furthermore, Vogel et al. (1999) demonstrate how cell damage can speed up membrane clogging.

1.5.3 Homogenisation stresses

Following primary separation, the isolation of intracellular products such as proteins and enzymes involve the disruption of the cell envelope. Conventional cell disruption of microbial cells to release intracellular components is achieved through the use of homogenisers (Hetherington 1971; Scawen 1980) and high-speed bead milling (Schutte 1983). A commonly used device to rupture cells is the Manton Gaulin APV homogeniser (Bowering 2000; Chisti and Moo-Young 1986) (Figure 1.15). Optimum performance is characterised by maximum product release whilst limiting the exposure time in order to minimise product degradation and formation of fine cell debris that can have adverse effects on further downstream purification steps (Siddiqi et al., 1997; Mosqueira et al., 1981). For example, fine debris has previously been shown to foul chromatography columns (Hearle et al., 1994) and block filter membranes hence reducing membrane flux (Gray et al., 1973; Kula et al., 1990;

49

Virkar et al., 1982). However, with subsequent centrifugation steps performance is only compromised if the debris is of similar density to the product of interest.

A common form of homogeniser stress is fluid mechanical stress caused by turbulent flow in the core of the homogeniser valve (Doulah et al., 1975; Cherry et al. 1986; Shamlou et al. 1993). Cherry et al. (1986) and Shamlou et al. (1993) assessed the effect of fluid induced stresses in turbulent flow on cell viability and concluded that the key parameter was the size ratio of cells to eddies. Shear stresses are thought to occur when the eddy size falls below that of the cell. In situations where the eddy size exceeds the cell size, breakage is most likely due to the mechanical stresses caused by pressure fluctuations. Doulah et al. (1975) further supports the concept of turbulent flow as the main contributing factor to cell rupture. However, it was suggested that oscillation of the cell suspension, as a result of turbulent conditions, caused cell breakage. When the kinetic energy of the oscillating motion exceeds the wall strength of cells, damage is expected to occur.

In a more recent publication (Shamlou et al., 1995), a model was devised for predicting yeast cell breakage in a homogeniser. The theory, based on elongation stresses, suggests that cells flowing out of the homogeniser valve strike the impact ring before forming a plane hyperbolic flow field responsible for the extensional stresses. It was assumed that cell rupture occurs when the elongation stresses exceed the mechanical strength of the cells. Collins et al. (1996) reports on the recent commercialisation of a new homogenisation device, which relies entirely on flow of suspensions through a narrow orifice to achieve disruption and suggested that elongation stresses play a key role in the disruption process.

Kesharvez-Moore et al. (1990) carried out an extensive investigation on the effects of valve unit configuration, impact ring and impact distance on disruption of yeast cells. It was reported that impact effects played a significant role in the disruption process with higher impact stress generating more cell breakage. With increasing impact distance cell breakage was observed to drop. Varying the valve unit configuration also contributed to cell breakage with knife-edged valves causing most damage.

1.5.4 Chemical lysis stresses

Other forms of intracellular product recovery include chemical methods such as alkaline lysis used for recovery of plasmid DNA (Ciccolini et al., 2002; Durland et al., 1998). The process involves mixing whole cells containing the plasmid with lysis reagents such as sodium dodecyl sulfate in a mixing vessel with typical shear rates of 46 s^{-1} to 461 s^{-1} (Ciccolini et al., 2002; Harnby et al., 1992). Genomic and plasmid DNA released from cells during chemical lysis are fragile entities and prolonged exposure to the shear rates found in the mixing vessel can result in genomic fragments of similar physical and chemical properties to the plasmid that are difficult to separate (Durland et al., 1998).

1.5.5 Chromatography and formulation stresses

Chromatography technology is generally incorporated into the latter stages of downstream processing, e.g. for the purification of therapeutic molecules, and can be considered a gentle process with negligible shear. Lutkemeyer et al. (1999) tested the shear environment of an expanded-bed chromatography column using sensitive hybridoma cells and reported that neither the high flow rates nor the passage through the column caused any relevant cell damage or clogging of the gel. However, associated mixing tanks and peristaltic pumps generated some cell debris and therefore it is paramount that the correct hardware components are used with chromatography columns to achieve the desired performance. At the formulation stage products are usually in a concentrated and highly pure state and hence considered as high value. Any damage at this stage is particularly undesirable. Stresses resulting from injection into vials may pose a potential concern.

ENERGY DISSIPATION RATE
(W kg^{-1})

1.71x10^5 - 2.00x10^5
1.43x10^5 - 1.71x10^5
1.14x10^5 - 1.43x10^5
8.57x10^4 - 1.14x10^5
5.71x10^4 - 8.57x10^4
2.86x10^4 - 5.71x10^4
0 - 2.86x10^4

ENERGY DISSIPATION RATE
(W kg^{-1})

1.71x10^5 - 2.00x10^5
1.43x10^5 - 1.71x10^5
1.14x10^5 - 1.43x10^5
8.57x10^4 - 1.14x10^5
5.71x10^4 - 8.57x10^4
2.86x10^4 - 5.71x10^4
0 - 2.86x10^4
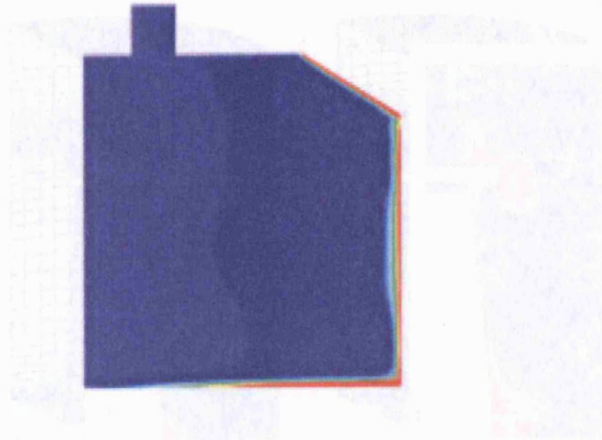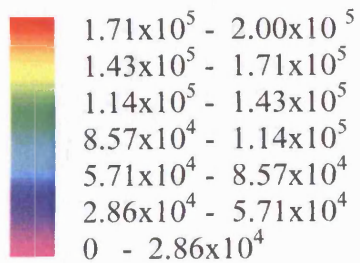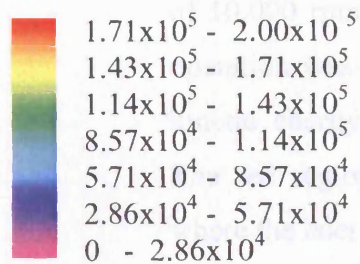
Figure 1.12   Computational Fluid Dynamics (CFD) simulation of a filter centrifuge
(Boulding et al., 2002) and the inlet of a disc-stack centrifuge (Boychyn
et al., 2004) respectively. The plots illustrate the potential and kinetic
energy involved with the centrifuge zones during operation. The red
regions represent most intense energy and in certain cases where the
energy dissipation is high cell damage has been reported.

ENERGY DISSIPATION RATE
(W kg^{-1})

$5.14 \times 10^5 - 6.00 \times 10^5$
$4.29 \times 10^5 - 5.14 \times 10^5$
$3.43 \times 10^5 - 4.29 \times 10^5$
$2.57 \times 10^5 - 3.43 \times 10^5$
$1.71 \times 10^5 - 2.57 \times 10^5$
$8.57 \times 10^4 - 1.71 \times 10^5$
$0 \ - 8.57 \times 10^4$

A   **B**
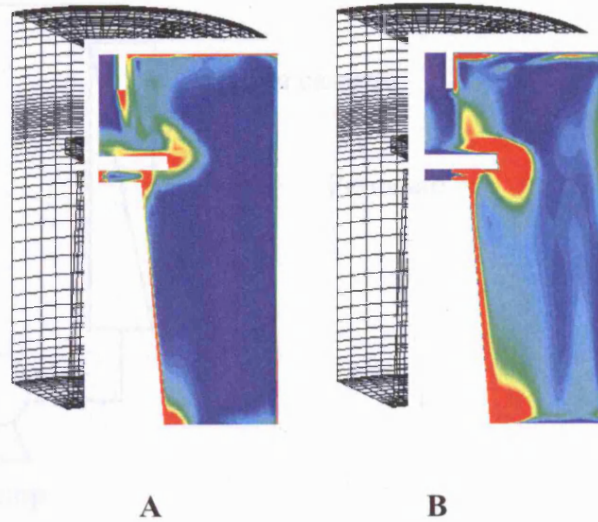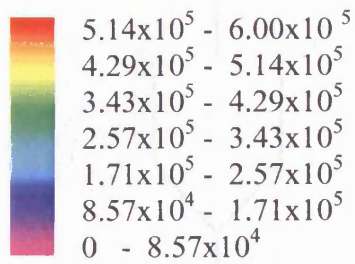
Figure 1.13   CFD analysis of a flooded (A) and non-flooded (B) inlet zone of a multi-chamber centrifuge (Boychyn et al., 2001). Both centrifuge bowls were operated with a flow rate of 22 L.h^{-1} and a rotational speed of 10,000 rpm. The maximum energy dissipation in the non-flooded operation was 12 x 10^5 W.kg^{-1}. The plots illustrate the potential and kinetic energy involved with the centrifuge zones during operation. The red regions represent most intense energy and in certain cases where the energy dissipation is high cell damage has been reported.
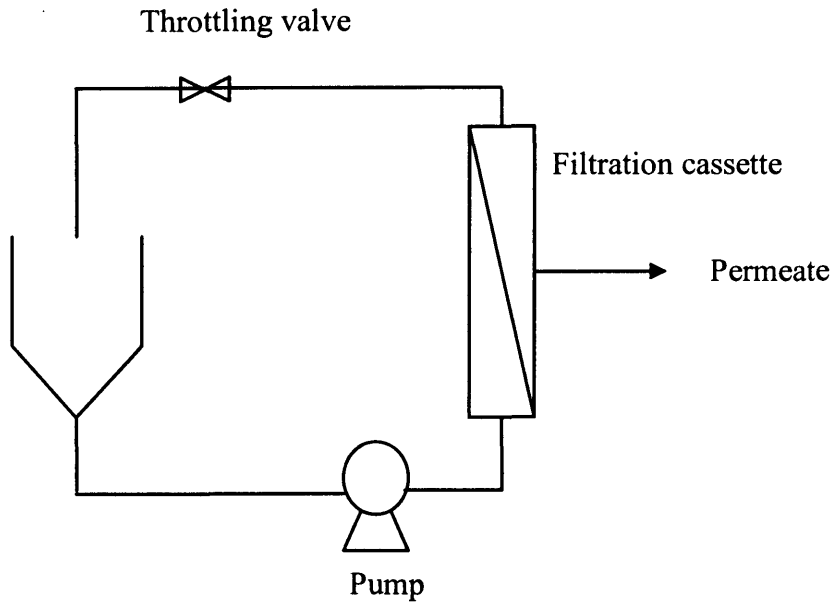
Figure 1.14   Schematic diagram of a cross-flow filtration rig: pumps and valves induce shear damage.
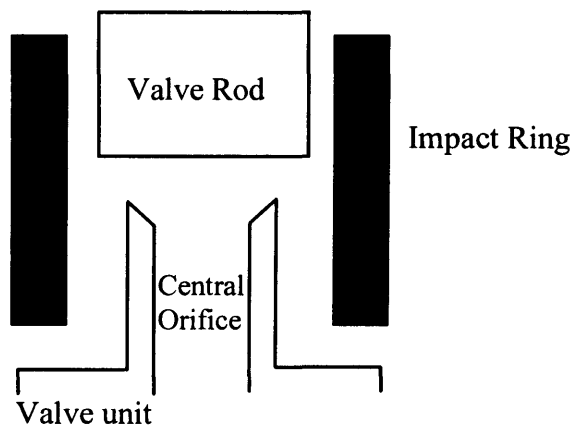
Figure 1.15   Homogeniser valve geometry. Cell damage occurs as a result of lateral movement across the orifice and impact with the impact ring.

1.6 Scale-down

Up to this point much of the emphasis has been directed at the considerable literature on breakage of materials during biomanufacturing processes. The objective of this thesis is to use the evidence and understanding of stress related cell responses to identify the primary flow stresses existent in bioprocess equipment, namely discharge in a disc stack centrifuge and to mimic closely these conditions in a purpose built small-scale device.

1.6.1 Scale-down philosophy

There is increasing pressure exerted on biopharmaceutical manufacturers to develop and deliver new products to the market in very short time frames (Varga et al., 2001). Traditionally the approach to this crisis would involve huge investment into development at the pilot-scale capacity, which is costly, labour intensive and time consuming. However, as raw materials become more expensive and world population health-care demands rise, the ability to work in this fashion soon becomes unfeasible. It has been estimated that late delivery of final products puts a figure of $1 million for each day delayed (Willoughby et al., 2004). The current work involves developing a scale-down device as a rapid tool for bioprocess optimisation and reducing development time.

The goal of any scale-down model is to simulate the conditions of its large-scale counterpart thus enabling the performance of the large-scale machine to be predicted early on in the design and development of a bioprocess manufacturing facility. This involves a detailed understanding of the large-scale flow dynamics before identifying the key parameters for scaling purposes. Scale-down is particularly advantageous when dealing with materials at the early stages of bioprocess development where only small quantities of test material are made available because fermentations are operated at small-scale during this initial phase. Furthermore, as the process development matures extensive trials are required for optimisation and if a robust small-scale methodology were available then there would be potential for significant reduction in development costs and time (Siddiqi et al., 1997). These considerations provide the

incentive for the current work in which a ultra scale-down approach will be devised to mimic large-scale centrifuge separation of *E. coli* cells.

1.6.2 Scale-down achievements

1.6.2.1 General scale-down

Scale-down is well established in the field of fermentation but less so further downstream (Siddiqi et al., 1997). In some cases, scale-down may be accomplished simply by geometrically reducing the size of the equipment as in the case of a stirred tank reactor. A typical example is the scale-down of precipitation. The properties of protein precipitates at small-scale can be kept consistent with large-scale by ensuring that the mechanical and process parameters such as tank and impeller ratios and the Camp number respectively are maintained between scales of operation (Boychyn et al., 2000; Neal et al., 2003). However this scaling technique only applies to a limited range of process units.

1.6.2.2 Scale-down of centrifuge clarification

A common method of comparing centrifuge separation performance is to use the Sigma theory (Σ), which describes the settling characteristics of a particle in a centrifuge (Ambler 1959). Based on this theory, assuming that all particles are identical throughout the separation process, then by maintaining the same flow rate to Sigma area ratio (Q/Σ) at large and small-scale the clarification performance should be comparable as demonstrated by Boychyn et al. (2000) in Figure 1.16. A correction factor is normally introduced to account for non-ideal flow conditions in large-scale equipment.

The standard Sigma concept is however, only valid for dilute suspensions. Salte et al. (2005) reports of inaccurate clarification predictions with high *E. coli* cell density broths i.e. 15% w/v where hindered settling and particle aggregation play a significant

role. At small-scale, particle aggregation lead to larger particles with higher settling velocity. On the other hand, the large-scale centrifuge separation environment was semi-turbulent and hence not permitting the formation of these aggregates. Using previously developed clarification methodology (Ambler 1959; Boychyn et al. 2001) the small-scale results significantly over predicted the actual large-scale clarification. To rectify the discrepancy in flow conditions, small-scale experimental samples were diluted beforehand; accurate large-scale predictions were achieved.

1.6.2.3 Scale-down of a centrifuge feed inlet

The accuracy of the Sigma clarification theory (Q/Σ) is also governed by cell robustness, which becomes less accurate with shear-sensitive biomaterials where damage at the feed inlet zone of a large-scale centrifuge generates fine particles with different settling characteristics to whole cells. Boychyn et al. (2000) and Mannweiler et al. (1989) demonstrate the challenge faced when mimicking centrifuge separation, illustrating the extreme difficulty in quantifying the shear stresses in a centrifuges; this is made more challenging as biological products become increasingly complex and fragile. However, with the use of CFD to analyse and quantify the flow environment, it is possible to predict and mimic the conditions in the feed inlet using a rotating disc device (Boychyn et al., 2001).

The small-scale rotating disc device, as described by Levy et al. (1998), consists of a Perspex chamber of diameter 40 mm. The chamber height can be varied from between 10 mm and 40 mm. Housed inside the chamber is a flat circular disc that is powered by an external DC motor. The mimic of the feed inlet typically involves solving the flow equations in order to map the shear rate and energy dissipation in both large and small-scale devices and to then determine the small-scale settings necessary to achieve similar hydrodynamic conditions. By using this approach in combination with the Sigma theory, much improved clarification comparisons between larger and small-scale were achieved for shear sensitive materials. This ultra scale-down approach both yields quantitative information of the effect of the process

environment on the material and also the means to translate this prediction to full scale.

The CFD analysis in Figure 1.17 illustrates the energy dissipation associated with operating the disc device at a rotational speed of 415 and 545 rps. These conditions were used to provide an estimate of how shear sensitive particles might respond to the forces prevailing in a centrifuge feed inlet such as for a multi-chamber bowl with an maximum energy dissipation rate of 12×10^5 W.kg^{-1} (Boychyn et al., 2001).

An alternative method to predict and mimic the response of suspensions to the feed inlet is to use the less laborious tip velocity approach. In this approach the velocity at the tip of the centrifuge spindle nut and the velocity in the rotating disc device are kept the same (Neal 2005).

1.6.2.4 Scale-down of a centrifuge by reducing the number of active discs

Other significant scale-down advances in the centrifuge field include work by Maybury et al. (1998) where the number of separating discs and bowl space were reduced enabling a reduction in volume of process material to be used for clarification studies. A 76% scale-down of the settling area in conjunction with a 70% reduction in bowl volume was achieved whilst still maintaining a separation performance similar to that of a full-scale machine. The settling area was reduced by replacing active discs with solid stainless steel blanks. The separation performance of the full-scale machine and scale-down version were compared using the grade efficiency concept. This concept was built on earlier work by Mannweiler et al. (1992). Mannweiler et al. (1992) highlighted the importance of correctly positioning the blanks on recovery performance. Blanking the active discs at the top of the centrifuge resulted in poor clarification because of the occurrence of turbulence as the feed was separated in the lower discs. However, by raising the position of the active discs i.e. blanking the lowest section of the separation area the recovery performance was comparable to the full-scale disc stack centrifuge. Although the work of Mannweiler et al. (1992) and Maybury et al. (1998) successfully demonstrate the scale-down of a

centrifuge, the method still required several litres of process material; a more ideal scale-down device would require only millilitres of test material.

1.6.2.5 Scale down: future work

The scale-down of a continuous/intermittent industrial centrifuge is still in its infancy. The most relevant work has been achieved in the development of models to predict feed inlet conditions and clarification efficiency (Mannweiler et al., 1992; Maybury et al., 1999; Boychyn 2000). Recent advances in computational fluid dynamics have provided an additional tool for quantifying the complex flow patterns found in centrifuges. However, there exists no comprehensive review of the effects of solids discharge on whole cell and product viability. Gray et al. (1972) does however demonstrate the undesirable damage to cells during product recovery via discharge. The scale-down approach for this thesis will be, in the first instance, to assess and understand cell response to large-scale discharge and then select a suitable small-scale tool to mimic these conditions.

To summarise the potential of scale-down practice, Figure 1.18 features some of the differences between conventional process design and the scale-down approach (personal communication with Titchener-Hooker N, Titchener-Hooker et al., 2001). As the new generation of biopharmaceutical products become more complex the FDA safety regulations follow suite by raising the margins for acceptability. As a result, over 90% of all products fail during the development phase making large-scale conventional technology unfavourable until the late stages of completion where process operations have been satisfactorily defined. The scale-down version uses millitre quantities of test material to identify critical process issues before moving to pilot-scale confirmation trials.

1.7 Project aims

The general reason for pushing towards better and more diverse scale-down technology is to have the ability to run extensive trials during early bioprocess

development using only millilitre quantities of raw material to identify desired operating conditions. To date, much success has already been accumulated in the scale-down of a centrifuge operation, namely the feed inlet and clarification. This project develops the scale-down research to include mimicking the recovery of solid paste via intermittent discharge through centrifuge nozzles. The task will involve designing a novel scale-down methodology, and reducing the quantity of test material required to predict the performance of a large-scale centrifuge. Additionally, solids recovery from different centrifuge models will be investigated and possible routes of optimisation explored.
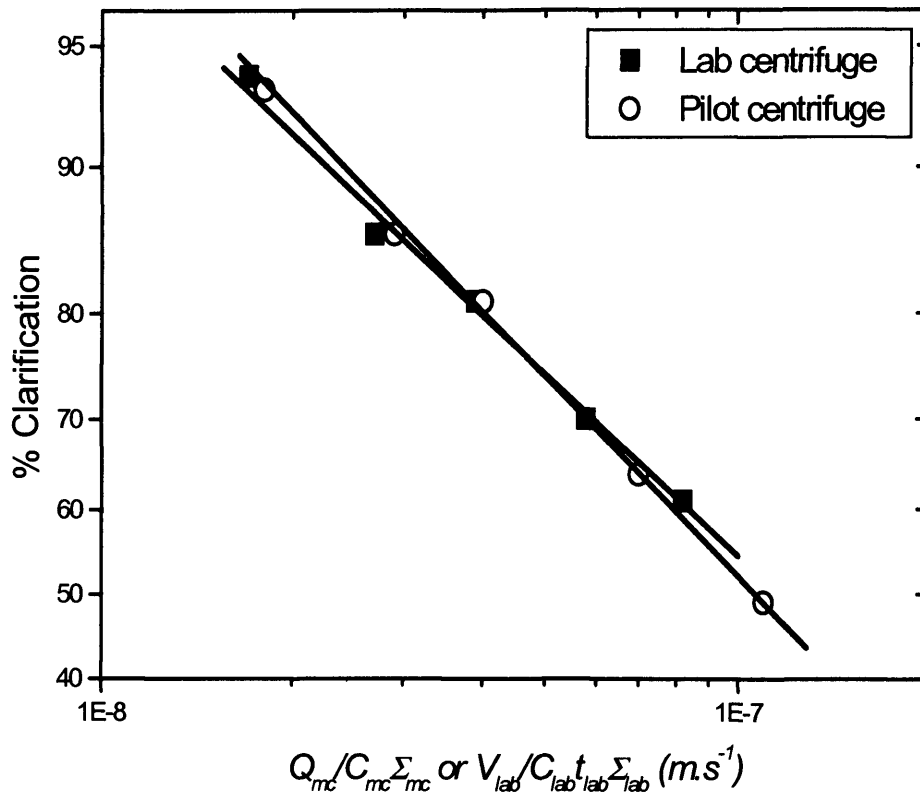
Figure 1.16   A probability-log relationship of percentage clarification and equivalent flow rate per centrifuge separation area for polyvinyl acetate particles (Boychyn et al., 2000).

Symbols: Q is the flow rate; C is a correction factor; Σ is the settling area; V is the sample volume; t is the residence time in the lab centrifuge; mc is the multichamber centrifuge and lab is the laboratory centrifuge.

ENERGY DISSIPATION RATE

(W kg^{-1})

$5.14 \times 10^5 - 6.00 \times 10^5$
$4.29 \times 10^5 - 5.14 \times 10^5$
$3.43 \times 10^5 - 4.29 \times 10^5$
$2.57 \times 10^5 - 3.43 \times 10^5$
$1.71 \times 10^5 - 2.57 \times 10^5$
$8.57 \times 10^4 - 1.71 \times 10^5$
$0 \;\; - 8.57 \times 10^4$

A

ENERGY DISSIPATION RATE
(W kg^{-1})

$5.14 \times 10^5 - 6.00 \times 10^5$
$4.29 \times 10^5 - 5.14 \times 10^5$
$3.43 \times 10^5 - 4.29 \times 10^5$
$2.57 \times 10^5 - 3.43 \times 10^5$
$1.71 \times 10^5 - 2.57 \times 10^5$
$8.57 \times 10^4 - 1.71 \times 10^5$
$0 \;\; - 8.57 \times 10^4$
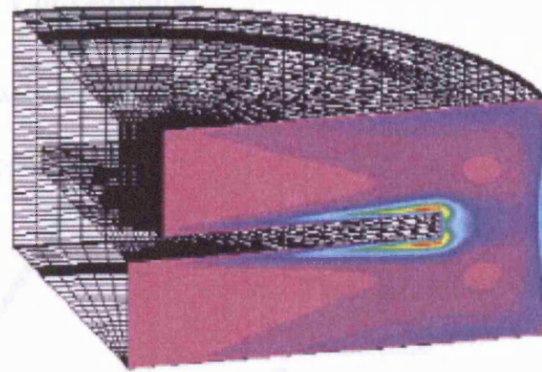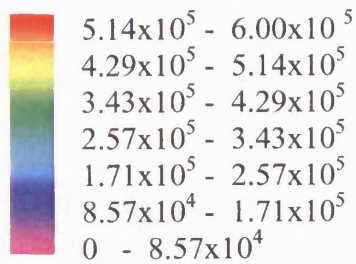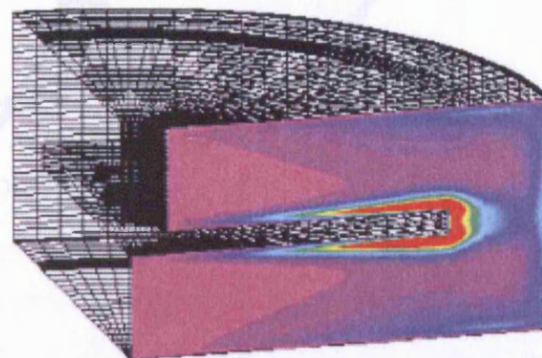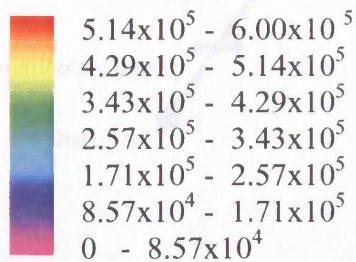
B

Figure 1.17   CFD analysis of a fully flooded shear cell operating at 415 rps (A) and 545 rps (B) to mimic a flooded and non-flooded multi-chamber bowl respectively (Boychyn et al., 2001). The maximum energy dissipation rate generated from the shear cell mimic of the non-flooded centrifuge was 6 x 10^5 W.kg^{-1}. The plots illustrate the potential and kinetic energy involved with the shear cell during operation. The red regions represent most intense energy and in certain cases where the energy dissipation is high cell damage has been reported.

Conventional
Time Scale: 10-15yrs

Manufacture

Approval

Clinical trials

Scale-down
Time Scale: 5-7yrs

Manufacture

Approval

Clinical trials

Pilot scale

Pilot scale

Bioprocess modelling

Pre-clinical

Pre-clinical

scale-down

Isolation/Synthesis

Isolation/Synthesis

Discovery

Discovery
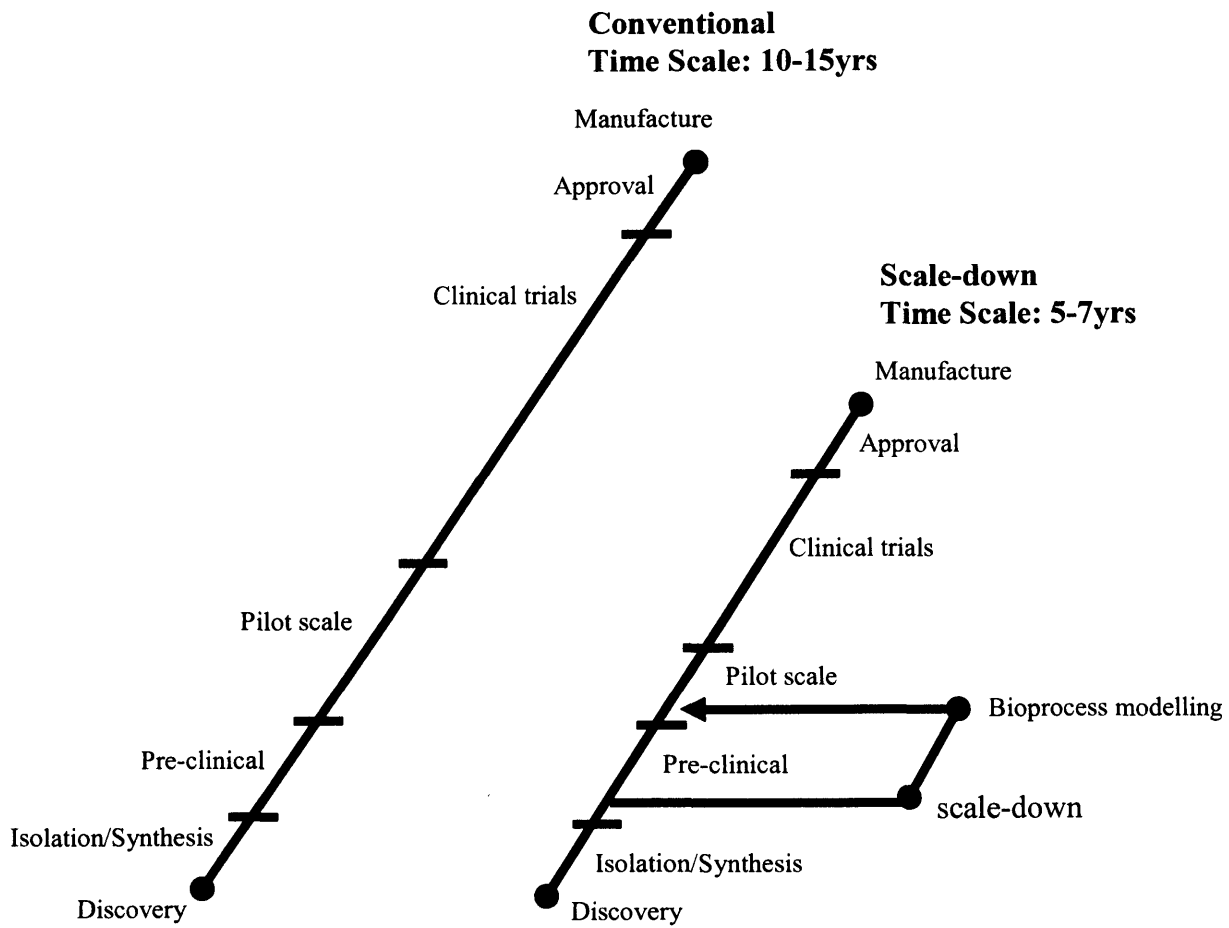
Figure 1.18   Comparison between conventional and scale-down technology in a biopharmaceutical lifecycle.

2 MATERIALS AND METHODS

2.1 Chemicals

All chemicals, unless otherwise stated, were obtained from Sigma Aldrich (Dorset, UK) and were of analytical grade.

2.2 Microorganisms

The W3110 and DH5α *E. coli* working cell banks were supplied by Celltech (Slough, UK) and GlaxoSmithKline (Kent, UK) respectively and stored at -80°C.

2.3 Fermentation of W3110 *E. coli* with expression of Fab' antibody fragments

The pH-stat fermentation strategy (Garcia-Arrazola et al., 2005) was used for producing W3110 *E. coli* cells for the work presented in this thesis.

2.3.1 Sterilisation

All ancillaries and inoculum media were steam sterilised in an autoclave (The Sterilizing Equipment Company Ltd., Leicester, UK) at 121°C for 20 min. A 20 L fermenter vessel (Applikon, Scheidam, Holland) was filled with 11.25 L defined media and sterilised at 121°C with an overhead pressure of 1.2 bar for 20 min.

2.3.2 Inoculum preparation

Tetracycline (10 mg.mL^{-1}) was added to five sterilised 2 L baffled shake flasks containing 0.25 L complex media (Table 2.1) through a sterile 0.2 μm filter in a laminar flow hood. Each flask was then inoculated with a vial (250 μL) from the

working cell bank and left to incubate in a G25 shaker (New Brunswick Scientific Ltd, UK) at 200 rpm and 30°C. The optical density (OD) was monitored at an absorbance of 600 nm using the DU-spectrophotometer (Beckman Instruments Ltd., High Wycombe, UK). On reaching an OD of 3.0, 25 mL from each flask was transferred into flasks containing 0.25 L defined media and left to incubate in the G25 shaker at 200 rpm and 30°C until an OD of 3.0 was achieved. The defined media composition can be found in Table 2.2 and 2.3.

2.3.3 Production at the 20 L scale

The fermentation of W3110 *E. coli* was carried out in a 20 L fermenter vessel (Applikon, Scheidam, Holland) (Figure 2.1) and computer controlled using the BioXpert software (Applikon, Scheidam, Holland). All data was logged using the MTX PROPACK software (Acquisition Systems, Berkshire, UK). The working volume of the 20 L fermenter was 12.5 L of which 10% (v/v) was defined media inoculum. The agitation rate and airflow rate were set at 500 rpm and 2.5 L.min^{-1} respectively. Dissolved oxygen tension (DOT) was measured using a DOT probe (Broadley Technologies, UK) and maintained at 30%. Foaming was controlled by the addition of sterile polypropylene glycol antifoam (2000 grade) (Fisher Scientific, UK). The initial working temperature was fixed at 30°C. The pH was set at 6.95 +/- 0.5 and monitored using a pH probe (Broadley Technologies Ltd, UK) and controlled with additions of either sulphuric acid (5% v/v) or ammonium hydroxide (15% v/v). A glycerol reservoir was linked to the base control (ammonia hydroxide) and fermenter by using a double peristaltic head pump (Applikon, Schiedam, Holland). During pH control, i.e. as cells produce acetate, glycerol was added to the fermenter at the same rate as the ammonium hydroxide and thus avoiding glycerol oscillation in the fermentation media. The glycerol reservoir was disconnected before the lactose induction. When the OD reached 50 the fermenter was induced with lactose (60 g.L^{-1}) and the temperature was adjusted to 27°C in order to reduce specific growth rate and promote correct folding of the Fab' antibody fragment. The 20 L fermentation was run for a total of 48 h before harvesting. The final cell biomass concentration and Fab' antibody fragment concentration were 100 g.L^{-1} (WCW) and 200 mg.L^{-1} respectively.

65
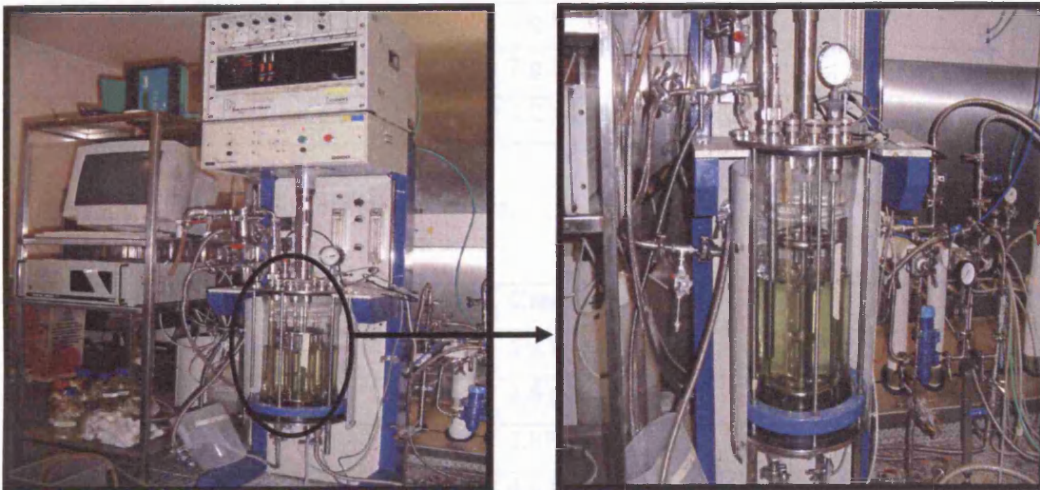
Figure 2.1   The Applikon 20 L fermenter used to generate W3110 *E. coli*.

Compound	Concentration
NaCl (VWR International, UK)	1 g.L^{-1}
Yeast extract (OXOID Ltd., UK))	2 g.L^{-1}
Phytone (Becton Dickinson Ltd., UK)	3.2 g.L^{-1}

Table 2.1   Preparation of complex media.

Compounds	Concentration
$(NH_4)_2SO_4$	5 g.L^{-1}
NaH_2PO_4	2.8 g.L^{-1}
KCl	3.87 g.L^{-1}
Citric acid	4 g.L^{-1}
Glycerol	30 g.L^{-1}
Trace elements*	10 mL.L^{-1}
$MgSO_4.7H_2O$	1 g.L^{-1}
Chloramphenicol	0.025 g.L^{-1}

Table 2.2   Preparation of defined media (*See Table 2.3).

Compounds	Concentration
Citric acid	100 g.L^{-1}
$CaCl_2.6H_2O$	5 g.L^{-1}
$ZnSO_4.7H_2O$	2.46 g.L^{-1}
$MnSO_4.4H_2O$	2 g.L^{-1}
$CuSO_4.5H_2O$	0.5 g.L^{-1}
$CoSO_4.7H_2O$	0.427 g.L^{-1}
$FeCl_3.6H_2O$	9.67 g.L^{-1}
H_3BO_3	0.03 g.L^{-1}
$NaMoO_4.2H_2O$	0.024 g.L^{-1}

Table 2.3   Preparation of trace elements.

2.4 Fermentation of DH5α *E. coli* with expression of plasmid pQR150 (20kB)

2.4.1 Sterilisation

All ancillaries and inoculum media were steam sterilised in an autoclave (The Sterilizing Equipment Company Ltd., Leicester, UK) at 121°C for 20 min. The 75 and 450 L fermenters were filled with 45 and 300 L of 2xTerrific broth (Table 2.4) respectively and sterilised at 121°C with an overhead pressure of 1.2 bar for 20 min.

2.4.2 Inoculum preparation

Kanamycin (50 µg.mL^{-1}) was added to eight sterilised 2 L baffled shake flasks containing 0.5 L 2xTerrific broth (Table 2.4) through a sterile 0.2 µm filter in a laminar flow hood. Each flask was inoculated with a vial (250 µL) from the working cell bank and left to incubate in a G25 shaker (New Brunswick Scientific Ltd, UK) at 250 rpm and 37°C for 12 h. The optical density (OD) was monitored at an absorbance of 600 nm using the DU-spectrophotometer (Beckman Instruments Ltd., High Wycombe, UK). On reaching an OD of 4.5, a total of 2.25 L was used to inoculate the 75 L fermenter.

2.4.3 75 L fermenter inoculation

A 75 L fermenter vessel (LH 1075 series stainless steel vessel, Inceltech, Slough, UK) was used to scale up production (Figure 2.2). All data was logged using the MTX PROPACK software (Acquisition Systems, Berkshire, UK). The working volume of the 75 L fermenter was 45 L of which 5% (v/v) was shake flask inoculum. The agitation rate and airflow rate were set at 500 rpm and 25 L.min^{-1} respectively. The pH was set at 7 +/- 0.5 and monitored using a Mettler Toledo pH probe (Mettler Toledo Ltd, UK). The pH was controlled with additions of either sulphuric acid (1M) or sodium hydroxide (1M). Dissolved oxygen tension (DOT) was measured using a Mettler Toledo DOT probe (Mettler Toledo Ltd, UK) and maintained at 30%. Foaming was controlled by the addition of sterile polypropylene glycol antifoam

(2000 grade) (Fisher Scientific, UK). The working temperature was fixed at 37°C. The fermenter was left to run for approximately 12 h until an OD of 30 was achieved. The media was then used to inoculate the 450 L fermenter.

2.4.4 Production at the 450 L scale

The production of DH5α *E. coli* was carried out in a 450 L fermenter vessel (Chemap AG, Volketswil, Switzerland) (Figure 2.2). All data was logged using the MTX PROPACK software (Acquisition Systems, Berkshire, UK). The working volume of the vessel was 300 L of which 5% (v/v) was inoculum from the 75 L fermenter vessel. The agitation rate and airflow rate were set at 200 rpm and 150 L.min^{-1} respectively. The pH was set at 7 +/- 0.5 and monitored using a Mettler Toledo pH probe (Mettler Toledo Ltd, UK). The pH was controlled with additions of either sulphuric acid (0.1M) or sodium hydroxide (4M). Dissolved oxygen tension (DOT) was measured using a Mettler Toledo DOT probe (Mettler Toledo Ltd, UK) and maintained at 30%. Foaming was controlled by the addition of sterile polypropylene glycol antifoam. The working temperature was fixed at 37°C. The fermenter was left to run for approximately 12 h until an OD of 30 was achieved. The material was crash-cooled to 12°C. Any material designated for future use was harvested using the CARR tubular bowl centrifuge (CARR separators Inc, MA). The final cell biomass concentration was 60 g.L^{-1} (WCW).

Compounds	Concentration
KH_2PO_4	4.62 g.L^{-1}
K_2HPO_4	25.08 g.L^{-1}
Tryptone	24 g.L^{-1}
Yeast Extract	48 g.L^{-1}
Glycerol	10 mL.L^{-1}
Kanemycin	50 µg.mL^{-1}

Table 2.4   Preparation of 2xTerrific broth.
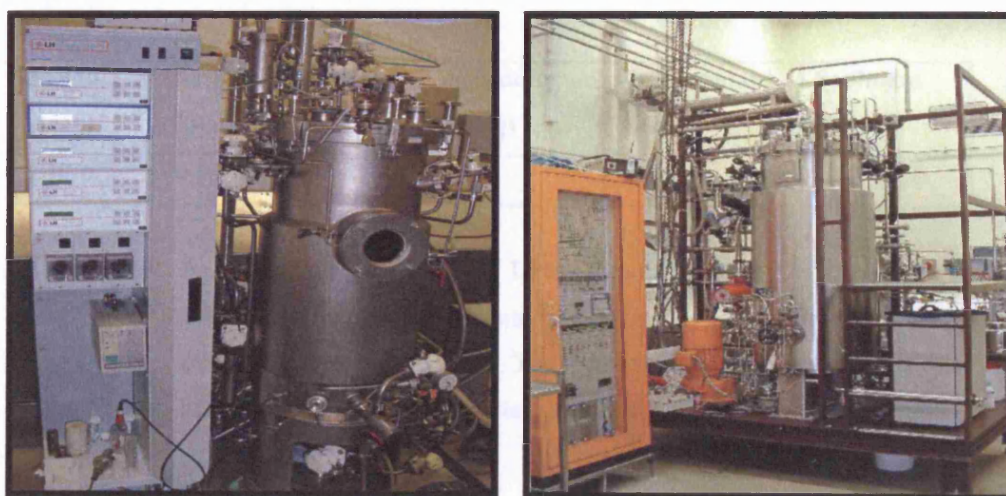
Figure 2.2   The Inceltech 75 L (left) and the Chemap 450 L (right) fermenter vessels used to generate DH5α *E.coli*.

2.5 Primary recovery and long-term storage of DH5α *E. coli* cells

DH5α *E. coli* cell recovery from the 450 L fermentation was performed using the CARR Powerfuge P6 tubular bowl centrifuge (CARR separators Inc, MA) because of its ability to achieve highly dewatered *E. coli* paste. The machine comprises of a 1 L bowl volume with a maximum rotational speed of 15000 rpm. The centrifuge was set to operate at 15000 rpm with a throughput of 60 L.h^{-1} using a Masterflex model 7518-12 pump (Barnant Co., Barrington, IL, USA) during cell harvesting. The centrifuge chamber was cooled via an outer glycol jacket. The OD (600 nm) of the supernatant was recorded using the DU-spectrophotometer (Beckman Instruments Ltd., High Wycombe, UK). On accumulating a full bowl, solids discharge was performed. The cell paste was stored at −80°C for future use.

E. coli strain	Clarification (%)	Feed (Kg)	Residue (Kg)	Supernatant (Kg)	Sediment (Kg)
DH5α	96	250	8	230	12

Table 2.5   A typical mass balance for DH5α *E. coli* recovery via the CARR Powerfuge tubular bowl centrifuge at a flowrate of 60 L.hr^{-1} and centrifugal rpm of 15000. The density of liquid supernatant was assumed to be the same as water i.e. 1kg/m^3.
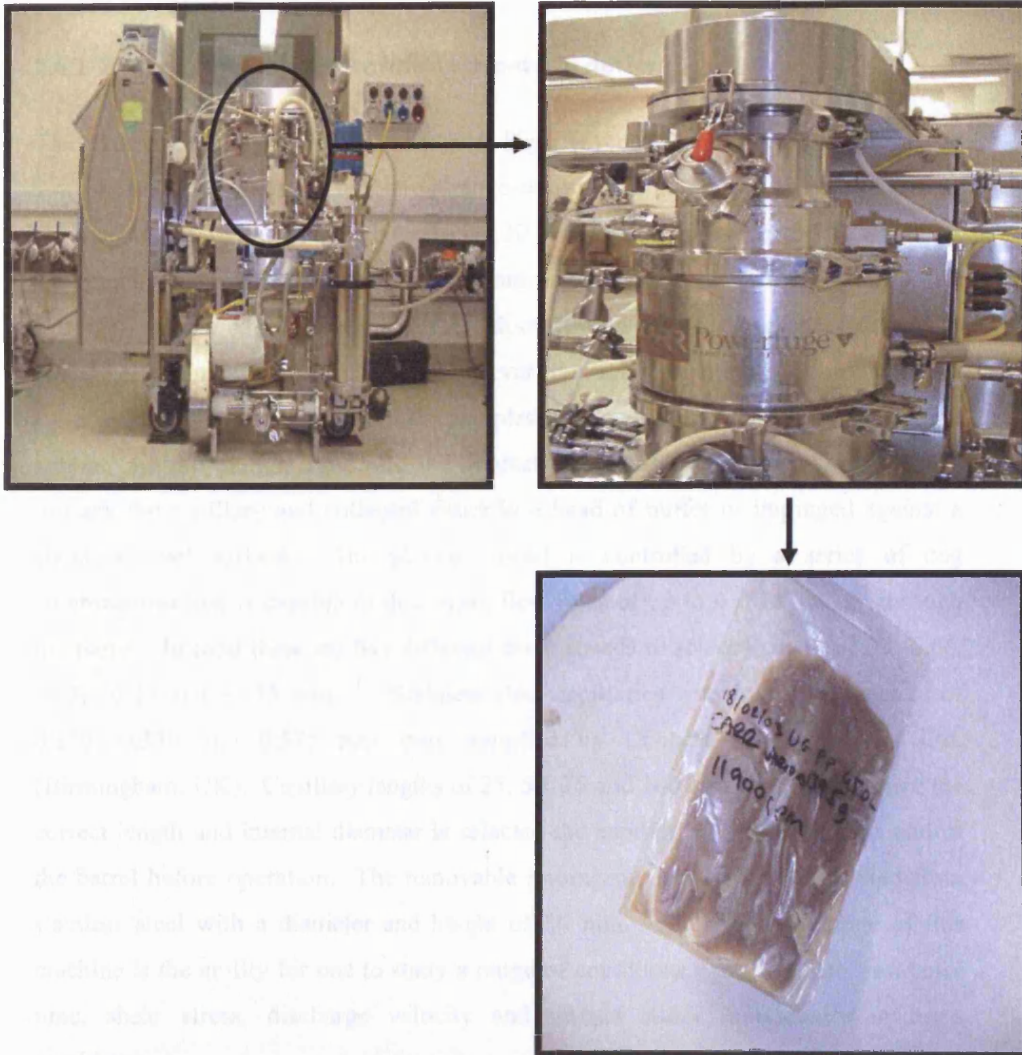
Figure 2.3   DH5α *E. coli* cell harvest using the CARR tubular bowl centrifuge. The feed was processed through the centrifuge at a flowrate of 60 L.h^{-1}. Upon saturation of the bowl, the solid phase was discharged with the aid of an internal scraper. The cell paste was packaged and left in long-term storage at –80°C.

2.6 Bioprocess equipment: general overview

2.6.1 Instron capillary device (ultra scale-down device)

The Instron capillary device (Instron Ltd, High Wycombe, UK) as shown in Figure 2.4 was modified in-house to study a range of stress conditions. The overall size of the machine including the outer frame is 120 cm high, 45 cm wide and 15 cm deep. The plunger and barrel are constructed from an aluminium alloy, i.e. Durell (Smith Ltd, UK), with a barrel diameter and length of 20 mm and 60 mm respectively. The barrel holds a maximum of 25 mL. However, throughout this study 10 mL volumes were used (refer to section 4.1.1). Samples are loaded into the barrel by pipette action. As the plunger descends and contacts the sample it is immediately forced through the capillary and collected either in a head of buffer or impinged against a stainless steel surface. The plunger speed is controlled by a series of cog combinations and is capable of delivering flow rates of up to 4×10^{-6} $m^3.s^{-1}$ through the barrel. In total there are five different drive speeds to select from i.e. 3.33, 6.66, 8.33, 10.33 and 13.33 $mm.s^{-1}$. Stainless steel capillaries with internal diameters of 0.250, 0.330 and 0.575 mm were supplied by Coopers Needle Works Ltd. (Birmingham, UK). Capillary lengths of 25, 50, 75 and 100 mm were used. Once the correct length and internal diameter is selected the capillary is screwed to the end of the barrel before operation. The removable impingement target is constructed from stainless steel with a diameter and height of 30 mm. The main advantage of this machine is the ability for one to study a range of conditions e.g. shear rate, residence time, shear stress, discharge velocity and impact either individually or as a combination.

2.6.2 Pilot-scale disc-stack centrifuges

2.6.2.1 CSA-1 disc-stack centrifuge

The CSA-1 hydro-hermetic disc-stack centrifuge as seen in Figure 2.5 (Westfalia Separator AG, Oelde, Germany) was used for the majority of the pilot-plant trials in this thesis. Design features of the device include a hydro-hermetic feed zone for reducing stress-related cell breakage, a cooling hood to prevent or reduce overheating

of the centrifuge bowl during operation and cleaning-in-place (CIP) capability. The machine specifications include a bowl liquid capacity of 0.6 L, a solid capacity of 250 mL and an operating bowl speed of 6100 to 9800 rpm (clockwise rotation). The machine is equipped with six discharge nozzles with the option of either partial (0.5 s opening time) or full discharge (1.0 s opening time). Further details can be found in Table 2.6. During separation of cell suspensions the dense solid phase is separated from the liquid phase in the active disc zone before accumulating around the periphery of the bowl. The operating water for controlling the discharge mechanism is supplied and maintained at a pressure of 2 bar via a Grundfos CR 2-50 pump (Grundfos pumps Ltd., Leighton Buzzard Beds, UK). The liquid phase is expelled through the top of the centrifuge via a centripetal pump with a backpressure of 0.5 to 1.5 bar to suppress air/liquid interfaces. Relevant CSA-1 dimensions and geometric features can be found in Figures 2.5 and 2.6 and Table 2.6.

2.6.2.2 SC-6 disc-stack centrifuge

The SC-6 hydro-hermetic disc-stack centrifuge as seen in Figure 2.7 (Westfalia Separator AG, Oelde, Germany) was used for comparative work with the CSA-1 centrifuge. A complete list of dimensions can be found in Table 2.7. New design features such as the novel hydraulic system provide more precise solid partial discharge times i.e. approximately 0.1 s and hence very dry solids. Similar to the CSA-1 hydro-hermetic design, the SC-6 centrifuge is characterised by having a hydro-hermetic feed zone. The bowl is temperature controlled via a cooling hood and base and has a maximum liquid capacity of 1.8 L with a solids holding space of 750 mL. The centrifuge bowl speeds range from 8000 to 12500 rpm. The machine is equip with eight discharge nozzles and during solids recovery either a partial or full discharge can be performed. For a partial discharge the pre-fill time can be set between 1 and 5 s, with 5 s giving the longest partial discharge. For all SC-6 centrifuge trials the pre-fill time was set at 3 s. The operating water for controlling the discharge mechanism is supplied and maintained at a pressure of 4.5 bar via a Grundfos CR 2-50 pump (Grundfos pumps Ltd., Leighton Buzzard Beds, UK). Solids discharged from the nozzles impinge against a collection bowl positioned 90 mm from the rotating centrifuge. Relevant SC-6 dimensions and geometric features can be found in Figure 2.7 and Table 2.7.
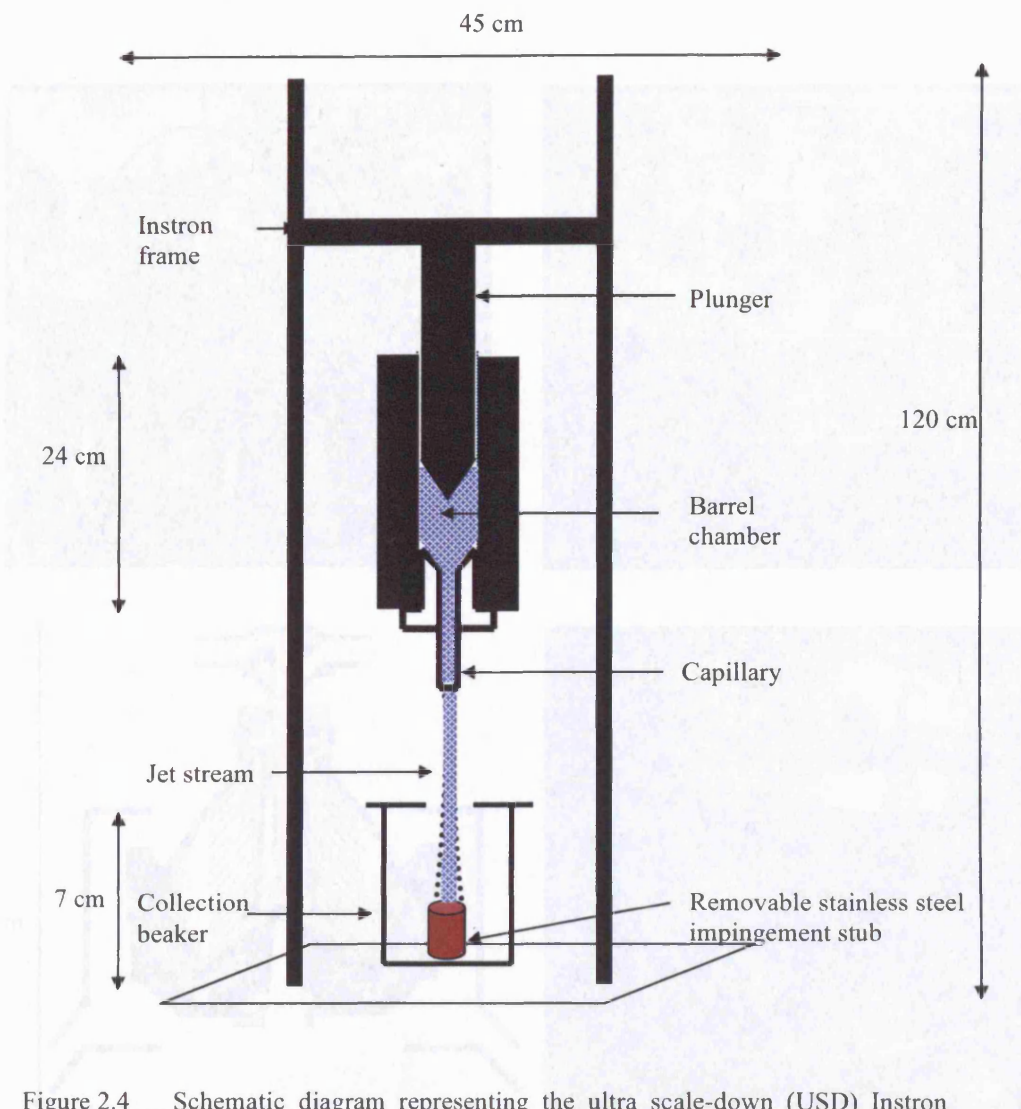
Figure 2.4   Schematic diagram representing the ultra scale-down (USD) Instron capillary device.
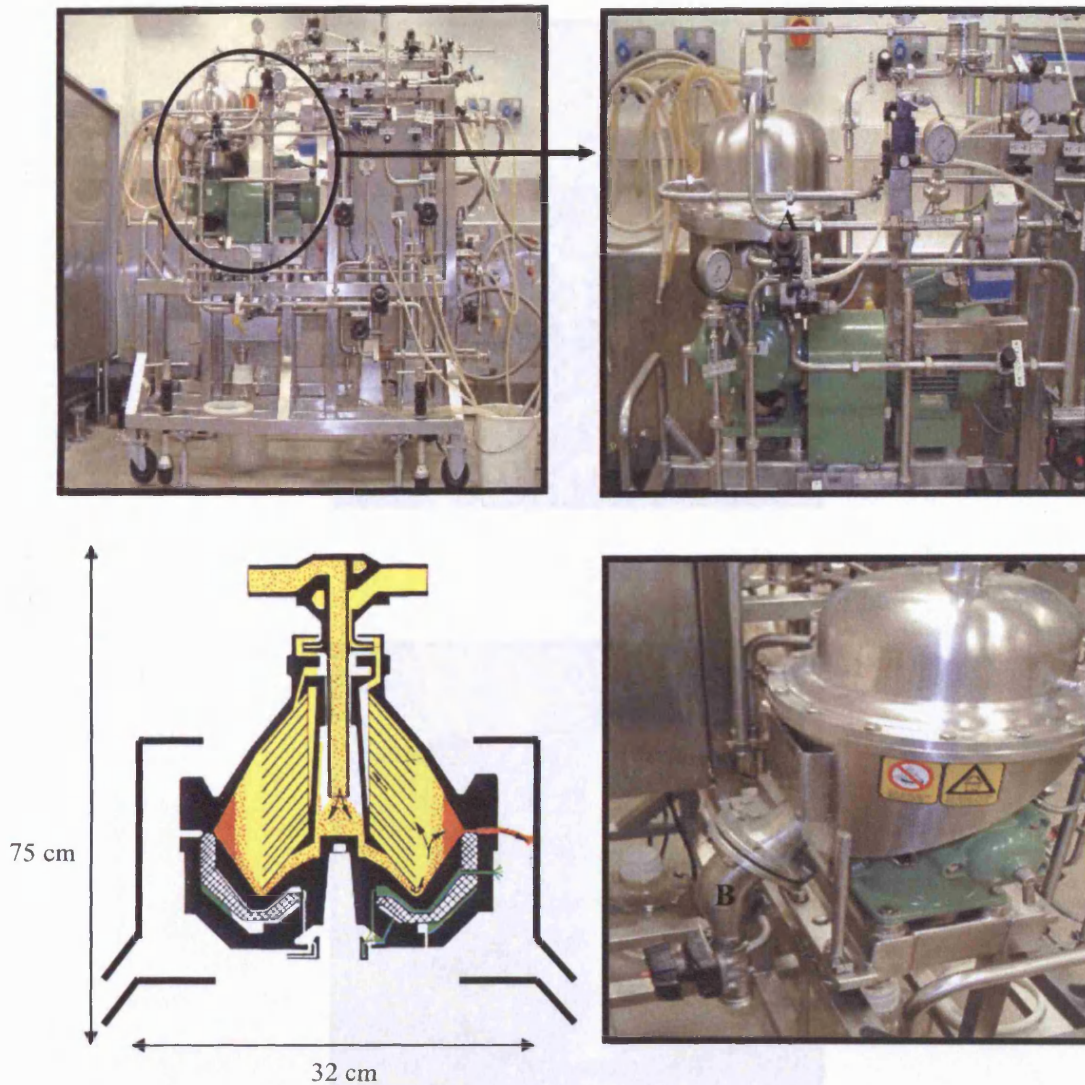
Figure 2.5   The Westfalia CSA-1 disc-stack centrifuge used for pilot-scale trials. Feed material entering the centrifuge is clarified with the clear phase removed via the supernatant pipe (A) and the solid paste collected via the discharge port positioned at the rear of the machine (B).

Figure 2.6   The Westfalia CSA-1 centrifuge bowl and the stack of separation discs. The geometry of the slots positioned along the centre of the bowl is rectangular.
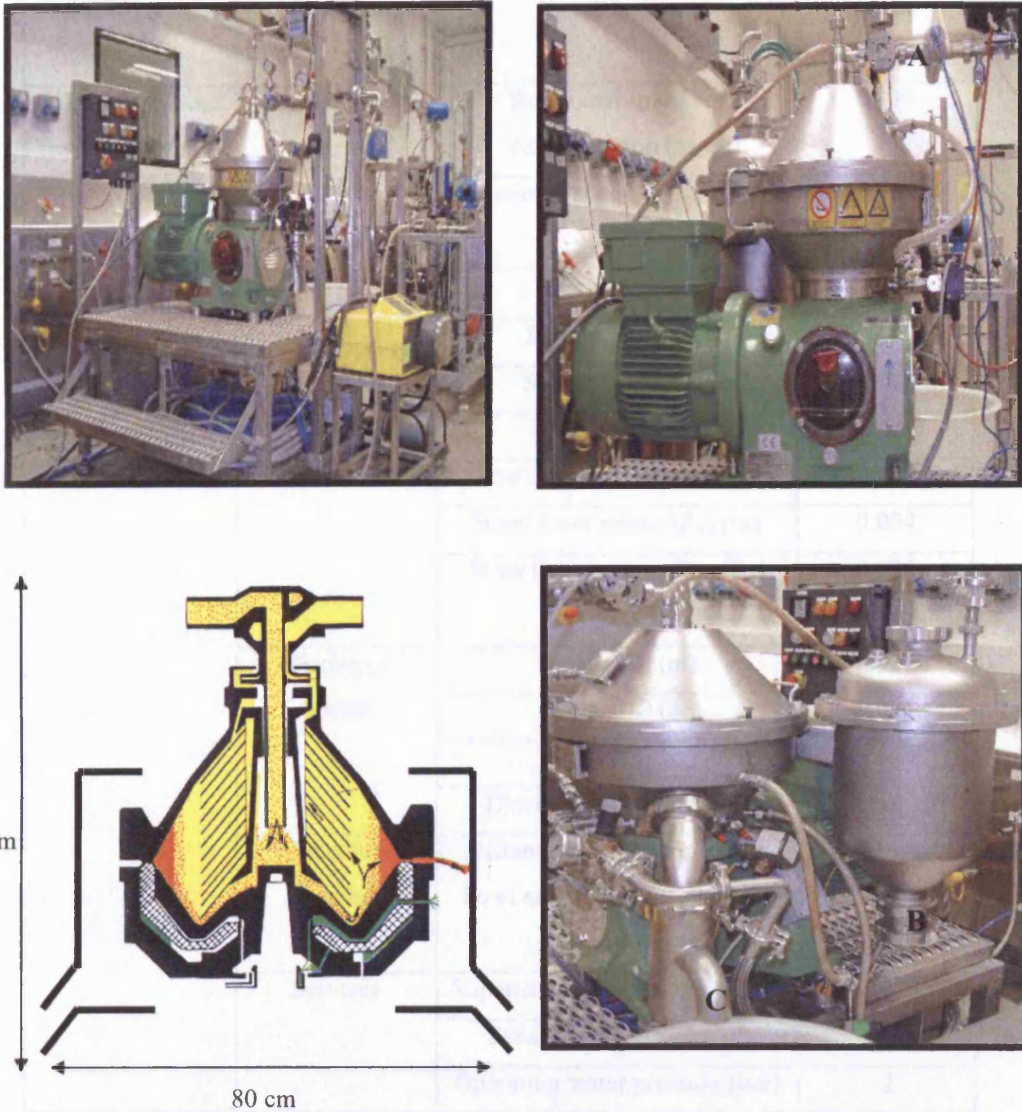
Figure 2.7   The Westfalia SC-6 hydro-hermetic centrifuge used for pilot-scale trials. Feed material entering the centrifuge is clarified with the clear phase removed via the supernatant pipe (A) and the solid paste collected via the discharge port positioned at the rear of the machine (B). Operating water is drained from the centrifuge through a port positioned at the rear of the bowl (C).

78

Centrifuge type	Feature	Specifications	Units
CSA-1 disc-stack (hydro-hermetic)	Centrifuge bowl	Rotational speed for centrifugation (rpm)	9800
		Rotational speed for discharge (rpm)	6100-9800
		Sigma (Σ) (m^2)	1710 †
		Bowl volume (L)	0.6
		Solid capacity (L)	0.25
		Flow rate ($L.h^{-1}$)	50-250
		Bowl outer radius (R_0) (m)	0.0995
		Bowl inner radius (R_1) (m)	0.084
		Inner liquid ring radius (R_2) (m)	0.025
	Discharge nozzle	Height (H) (m)	0.004
		Length (L) (m)	0.011
		Width (W) (m)	0.043
		Discharge speeds ($m.s^{-1}$)	51-82
	Collection chamber	Distance between centrifuge bowl and collection chamber (m)	0.090
	Services	Supernatant backpressure (bar)	0.5 – 1.5
		Feed inlet pressure (bar)	0.5
		Operating water pressure (bar)	2

Table 2.6   Relevant geometric dimensions and operating conditions for the CSA-1 centrifuge. † Sigma value for full centrifuge rotational speed.

Centrifuge type	Feature	Specifications	Units
SC-6 disc-stack (hydro-hermetic)	Centrifuge bowl	Rotational speed for centrifugation (rpm)	12500
		Rotational speed for discharge (rpm)	8000-12500
		Sigma (Σ) (m^2)	3647 †
		Bowl volume (L)	1.8
		Solid capacity (L)	0.70
		Flow rate (L.h^{-1})	50-3000
		Bowl outer radius (R_0) (m)	0.125
		Bowl inner radius (R_1) (m)	0.105
		Inner liquid ring radius (R_2) (m)	0.03
	Discharge nozzle	Height (H) (m)	0.0075
		Length (L) (m)	0.02
		Width (W) (m)	0.04
		Discharge speeds (m.s^{-1})	85-126
	Collection chamber	Distance between centrifuge bowl and collection chamber (m)	0.090
	Services	Supernatant backpressure (bar)	0.5 – 1.5
		Feed inlet pressure (bar)	0.5
		Operating water pressure (bar)	4.5
		Cooling supply pressure (bar)	5
		Air supply pressure (bar)	3

Table 2.7   Relevant geometric dimensions and operating conditions for the SC-6 centrifuge. † Sigma value for full centrifuge rotational speed.

2.7 Experimental design

2.7.1 Ultra scale-down (USD) studies of the effect of flow and impact conditions during *E. coli* cell processing

2.7.1.1 Preparation of cell suspensions

Frozen (-80°C) DH5α *E. coli* cell paste was left to thaw at room temperature for 2 h before re-suspending to a concentration of 300 mg.mL^{-1} (unless otherwise stated) in isotonic phosphate buffered saline (PBS) (0.01M PBS, 0.138M NaCl, 0.0027M KCl, pH 7) with a final suspension viscosity of 0.005 N.s.m^{-2}.

2.7.1.2 Effect of shear rate and residence time

To study capillary effects on cell integrity both the mass average shear rate and residence time were controlled by changing both the length and size of capillary used, and the plunger speed. The range of shear rates and residence times studied were up to 6.3 x 10^5 s^{-1} and 0.024 s respectively. The typical product of shear rate (s^{-1}) and residence time (s) (G_cT_i) during discharge in a large scale CSA-1 and SC-6 centrifuge is 30 and 40 respectively (Equation 13, Chapter 3). Samples were collected in a volumetric cylinder with a head of buffer of 100 mm depth positioned at 300 mm distance from the capillary tip. This method of sample collection has been shown to cause no cell breakage (Chapter 4, Figure 4.11). For multiple passes through the capillary, samples collected in the buffer were gently centrifuged for 3 min at 3500 rpm in a Beckman GS-6 series centrifuge (Beckman Instruments Inc., CA, USA); the buffer was separated from the cell sample and added back to the volumetric cylinder before re-circulating the cell sample through the capillary. Table 2.8 and 2.9 summarise the experimental arrangements for the mass average shear rate and the mean residence time investigations respectively.

2.7.1.3 Effect of viscosity/shear stress

The effect of shear stress was evaluated using capillary lengths of 50 mm and 100 mm, a capillary diameter of 0.33 mm, and residence times of 0.001, 0.002 and 0.006 s (Table 2.10). Cell suspensions were prepared with viscosity between 0.001 and 0.0065 $N.s.m^{-2}$; the behaviour of all samples were approximately Newtonian (Figure 2.10). The cell suspensions were then subjected to shear stresses of the order 10^3 to 10^4 $N.m^{-2}$ often experienced in centrifuges and homogenisers (Yim et al., 2000). Samples were collected in a volumetric cylinder with a head of buffer of 100 mm depth positioned at 300 mm distance from the capillary tip in order to eliminate secondary impaction effects. For multiple passes through the capillary, samples collected in the buffer were centrifuged for 3 min at 3500 rpm in a Beckman GS-6 series centrifuge (Beckman Instruments Inc., CA, USA); the buffer was separated from the cell sample and added back to the volumetric cylinder before re-circulating the cell sample through the capillary. Further experimental details can be found in Table 2.10.

2.7.1.4 Effect of impact

Impact studies were designed as illustrated in Table 2.11. The capillary G_cT_i was kept below 646 in order to minimise any capillary contributions to cell breakage (Chapter 4, Figure 4.5). A typical large-scale centrifuge such as the Westfalia CSA-1 disc-stack model will discharge over a velocity range 50 to 80 $m.s^{-1}$ with impact against a stainless steel collection bowl at a distance of 90 mm from the centrifuge bowl. To mimic these conditions samples were projected from the capillary over a velocity range up to 85 $m.s^{-1}$ at a stainless steel stub aligned at 90 mm from the capillary.

The effect of impact distance on cell breakage was conducted with a capillary length and diameter size of 50 mm and 0.33 mm respectively. The jet velocity was maintained at 49 $m.s^{-1}$ (G_cT_i <646) whilst changing the impact distance (10 mm to 300 mm) of the stainless steel stub.

A	Drive speed (mm.s^{-1})	Capillary diameter size (mm)	Capillary length (mm)	No of passes	Overall residence time (s)	Shear rate (x 10^5 s^{-1})
	13.33	0.33	100	12	0.024	6.3
	8.33	0.33	100	8	0.024	3.9
	6.66	0.33	100	6	0.024	3.2
	3.33	0.33	100	3	0.024	1.6
	13.33	0.575	75	6	0.024	1.2

B	Drive speed (mm.s^{-1})	Capillary diameter size (mm)	Capillary length (mm)	No of passes	Overall residence time (s)	Shear rate (x 10^5 s^{-1})
	13.33	0.33	100	6	0.012	6.3
	8.33	0.33	100	4	0.012	3.9
	6.66	0.33	100	3	0.012	3.2
	3.33	0.33	75	2	0.012	1.6

C	Drive speed (mm.s^{-1})	Capillary diameter size (mm)	Capillary length (mm)	No of passes	Overall residence time (s)	Shear rate (x 10^5 s^{-1})
	13.33	0.33	100	3	0.006	6.3
	8.33	0.33	100	2	0.006	3.9
	6.66	0.33	50	3	0.006	3.2
	3.33	0.33	75	1	0.006	1.6

D	Drive speed (mm.s⁻¹)	Capillary diameter size (mm)	Capillary length (mm)	No of passes	Overall residence time (s)	Shear rate (x 10⁵ s⁻¹)
	13.33	0.33	50	1	0.001	6.3
	8.33	0.33	50	1	0.0016	3.9
	6.66	0.33	50	1	0.002	3.2
	3.33	0.33	50	1	0.004	1.6

Table 2.8   Summary of conditions used to study the effect of mass average shear rate on DH5α *E. coli* cell breakage. Table A: Varying mass average shear rate with residence time fixed at 0.024 s. Table B: Varying mass average shear rate with residence time fixed at 0.012 s. Table C: Varying mass average shear rate with residence time fixed at 0.006 s. Table D: Varying mass average shear rate with residence time less than or equal to 0.004 s.

Drive speed (mm.s⁻¹)	Capillary diameter size (mm)	Capillary length (mm)	No of passes	Overall residence time (s)
6.66	0.33	50	1	0.002
6.66	0.33	100	1	0.004
6.66	0.33	50	3	0.006
6.66	0.33	50	5	0.01
6.66	0.33	100	5	0.02
6.66	0.33	100	7	0.028
6.66	0.33	100	13	0.052

Table 2.9   Summary of conditions used to study the effect of residence time on DH5α *E. coli* cell breakage. The mass average shear rate was fixed at 3.16×10^5 s⁻¹.

Drive speed $(mm.s^{-1})$	Capillary diameter size (mm)	Capillary length (mm)	No of passes	Overall residence time (s)
13.33	0.33	50	1	0.001
13.33	0.33	50	2	0.002
13.33	0.33	100	3	0.006

Table 2.10   Summary of conditions used to study the effect of mass average shear stress on DH5α *E. coli* cell breakage. Each condition was examined with suspensions of viscosity ranging from 0.001 to 0.006 $N.s.m^{-2}$.

Drive speed $(mm.s^{-1})$	Capillary diameter size (mm)	Capillary length (mm)	No of passes	G_cT_i	Velocity $(m.s^{-1})$
13.33	0.25	25	1	477	85
8.33	0.25	25	1	395	53
13.33	0.33	50	1	646	49
8.33	0.33	50	1	646	31
6.66	0.33	50	1	646	24
13.33	0.575	75	1	556	16
3.33	0.33	50	1	646	12

Table 2.11   Summary of conditions used to study the effect of discharge velocity on DH5α *E. coli* cell breakage. In all cases, G_cT_i was kept to a minimum i.e. below 646 to avoid cell breakage due to capillary related shear. The impact stub was fixed at 90 mm from the capillary tip.

2.7.2 Ultra scale-down (USD) prediction of *E. coli* cell recovery from high speed discharge centrifuges

2.7.2.1 Preparation of cell suspensions

In the following centrifugation study frozen material was used because of the convenience to do substantial experiments at small and large scale and to be assured of material consistency. Frozen ($-80°C$) DH5α *E. coli* cell paste was pre-treated with various freezing strategies to weaken the *E. coli* cells thus providing an insight into the recovery of cells with different cellular strength. Frozen ($-80°C$) DH5α *E. coli* cell paste was left to thaw at room temperature for 2 h. The cell paste was re-suspended to a concentration of 300 mg.mL^{-1} ($\mu = 0.005$ N.s.m^{-2}) in PBS buffer (0.01M, pH 7). One aliquot of the cell suspension was re-frozen at $-80°C$ and then thawed at room temperature for 2 h, a second aliquot was re-frozen at $-20°C$ and then thawed at room temperature for 2 h and a third aliquot immediately used for experimental trials. 200 mL of each freeze-thawed suspension was allocated for USD trials. The remainder of each suspension was diluted to a concentration of 50 g.L^{-1} in PBS buffer for pilot-scale trials.

Fresh W3110 *E. coli* cells (100 g.L^{-1}) and fresh DH5α *E. coli* cells (60 g.L^{-1}) were fed directly from the fermenter into the pilot-scale centrifuges. For USD trials a 1 L aliquot from each fresh *E. coli* feed suspension was spun down for 600 s at 10000 g in a Beckman J2-MI centrifuge with a JA10 rotor (Beckman, High Wycombe, UK) giving a paste resembling the centrifuge pre-discharge material with a viscosity of approximately 0.005 N.s.m^{-2}. Figure 2.8 illustrates the protein release for each batch of *E. coli* as a function of feed preparation before USD and pilot-scale studies.

2.7.2.2 Pilot-scale

The CSA-1 and SC-6 disc-stack centrifuges used during this study were installed with a hydro-hermetic feed zone in order to minimise cell breakage during entry of feed

into the separator (Boychyn et al., 2001). The centrifuges were temperature controlled at < 10°C during all experiments via cooled water circulating through the centrifuge hood. Cell suspensions were fed into both centrifuges under a pressure of 0.5 bar achieved with a flow rate of 56 L.h^{-1} and 100 L.h^{-1} for the CSA-1 and SC-6 respectively using a peristaltic pump (model 605DI, Watson Marlow, Falmouth, Cornwall, UK), which has previously been shown to cause no breakage to fragile particles (Clarkson, 1994). For the clarification of a cell suspension the centrifuges were programmed to operate at maximum rotational speed, i.e. 9800 rpm and 12500 rpm for the CSA-1 and SC-6 respectively.

On accumulating an estimated 250 mL of sediment in the holding space the peristaltic pump was switched off, the bowl speed was adjusted and allowed to stabilise before performing a partial discharge. The range of bowl speeds examined were from 6100 to 9800 rpm, and 8000 to 12500 rpm for the CSA-1 and SC-6 respectively. Partial discharges were performed with both centrifuges. Solid material collected post-discharge was re-suspended in clarified supernatant to the same initial feed concentration and immediately analysed. The centrifuges were rinsed with RO water between each experimental trial. As a control, cells were retrieved from the centrifuge prior to discharge and analysed. The procedure involved shutting the centrifuge down on accumulating a solids volume of 250 mL, dismantling the bowl, re-suspending the accumulated sediment in the supernatant and analysing for cell breakage.

2.7.2.3 Ultra scale-down

Cell suspensions of 10 mL (concentration 300 mg.mL^{-1}; μ = 0.005 N.s.m^{-1}) were processed through the USD capillary device (G_cT_i < 646) over a velocity range up to 85 m.s^{-1} (Table 2.11) at a stainless steel stub aligned at 90 mm perpendicular to the capillary tip. All experiments were carried out at room temperature with processed and unprocessed samples stored at 4°C unless otherwise stated. Figure 2.9 is a schematic illustration of the experimental design showing how the USD capillary device was tested in parallel with the pilot-scale centrifuges.

2.8 Off-line analytical techniques

2.8.1 Viscosity measurements

Sample viscosities were measured using a Rheomat 115 viscometer (Contraves Industrial Product, Middlesex, UK) with a concentric cylinder measuring system (Mettler Toledo Ltd, UK). Samples of 25 mL were exposed to shear rates ranging from 24.3 to 877.0 s^{-1}. The system temperature was maintained at 4°C by circulating cold water from a water bath through the cooling jacket. All torque readings were measured in triplicate. The torque readings were plotted on a log shear stress against log shear rate graph as shown in Figure 2.10 and the sample viscosities calculated as shown in Figure 2.11. To characterise the fluid behaviour the Ostwald-de Waele or power law is used ($\tau = K\gamma^{n}$, where τ is the shear stress, K is the consistency index, γ is the shear rate). The fluid behaviour index n is dimensionless. When $n=1$ the fluid exhibits Newtonian behaviour; when $n<1$ the fluid exhibits pseudoplastic behaviour; when $n>1$ the fluid is dilatant.

2.8.2 Intracellular protein release

The release of intracellular protein content was used as a quantitative measure of cell breakage and was measured using the Biorad Bradford assay (Bradford 1976). The method works by the reagent dye (i.e. Coomassie dye) binding specifically to amino acids such as tyrosine, cysterine and tryptophan. This activity can be monitored from the shift in optical density (OD) from 465 to 595 nm. Furthermore, the assay is colorimetric; as protein concentration increases the colour in the mixture intensifies.

Sample volumes of 2 mL were centrifuged for 15 min at 13000 rpm in a Biofuge model 13 centrifuge (Heraeus Sepatech, GmbH, Germany) to remove any particulate matter. 950 μL of Coomassie dye (Perbio Science Ltd, Cheshire, UK) was then added to 50 μL of supernatant in a 10 mm cuvette. The cuvette was then inverted five times to achieve good mixing and left to stand in the dark for 5 min at room temperature. The reaction was recorded at an OD of 595 nm using the Ultrospec 2000

spectrophotometer (Pharmacia Biotech, Cambridge, UK). The spectrophotometer was initially referenced with a cuvette of mixture 950 μL Coomassie dye to 50 μL reverse osmosis water. All samples were measured in triplicate.

All samples (unless otherwise stated) were analysed for protein immediately after experimentation. It is important to identify if slight variations in analysis timing contribute to the level of detected protein release. Figure 2.12 demonstrates that the release of protein is not governed by holding time between 0 to 48 h.

2.8.3 Periplasmic antibody fragment release

Loss of antibody fragments from the periplasmic space of W3110 *E. coli* cells upon centrifugal discharge was measured using an enzyme-linked immuno absorbent assay (ELISA). The ELISA assay works by initially forming antibody-antigen-enzyme linked antibody complexes, which interact with a colourless substrate to give a colour change that can be measured with a spectrophotometer. Figure 2.13 illustrates the sequence of events in a typical ELISA assay.

NUNC 96 well maxisorp immuno plates (Life Technologies Ltd, Paisley, UK) were coated with 100 μL of HP6045 mouse monoclonal antibody (2 μg.mL^{-1} in phosphate buffered saline (PBS)) (Celltech, Slough, UK) per well. The plates were covered with cling-film and stored at 4°C. After 24 h each plate was washed four times in PSB/T (0.05% Tween-20) buffer using the Columbus plate washer (Tecan UK Ltd, Reading, UK). The plates were then inverted and left to dry on tissue paper. Sample and standard volumes of 100 μL were added to the first row of wells and serially diluted down the plates with sample conjugate buffer. The standards were loaded at a concentration of 1 μg.mL^{-1} in sample conjugate buffer. The plates were covered with cling-film and incubated for 1.5 h at room temperature on the 3D rocking platform STR9 (Stuart Scientific, UK). The washing (four times in PBS) and drying of the 96 well plates were repeated. 100 μL of GD12 peroxidase (The Binding Site Ltd., Birmingham, UK) was added to each of the wells at a dilution of 1:2000 in sample conjugate buffer. The plates were incubated for 1.5 h at room temperature on the 3D

rocking platform STR9 (Stuart Scientific, UK). After a further wash and drying step 100 μL of substrate solution was added to each well and the OD at 630 nm was recorded using the Titertek Multiskan PLUS MK II microplate reader (Flow Laboratories, High Wycombe, UK) after 6 min. The PBS, sample conjugate buffer and substrate solution were prepared as shown in Table 2.12.

2.8.4 Complete cell breakage

Complete release of intracellular components (C_h) was characterised by measurements as a result of the use of the APV Manton Gaulin Lab 40 high pressure homogeniser (APV, Crawley, Sussex, UK). Samples with a volume and viscosity of 40 mL and 0.005 N.s.m^{-2} respectively were homogenised at 1200 bar for a total of 2 passes. The level of release under these conditions was assumed to be 100% i.e. no further release observed with multiple passes as shown in Figure 2.14. Figures 2.15 and 2.16 illustrate the gross change in cell appearance before and after homogenisation. For the majority of this thesis the release of intracellular protein was used as the marker for determining cell breakage unless otherwise stated.

The degree of cell breakage (C) is defined by:

$$\% \text{ Cell Breakage} = \left(\frac{C_s - C_f}{C_h - C_f} \right) x100 \qquad [2.4]$$

where C_s and C_f correspond to the concentrations of intracellular components released from the processed samples and feed respectively and C_h corresponds to the measured maximum concentration of intracellular components released as a result of homogenisation. C_f was approximately 0.24 and 2.7 mg.mL^{-1} and C_h was approximately 9.3 and 12 mg.mL^{-1} for small and large-scale experiments respectively (unless otherwise stated).

90
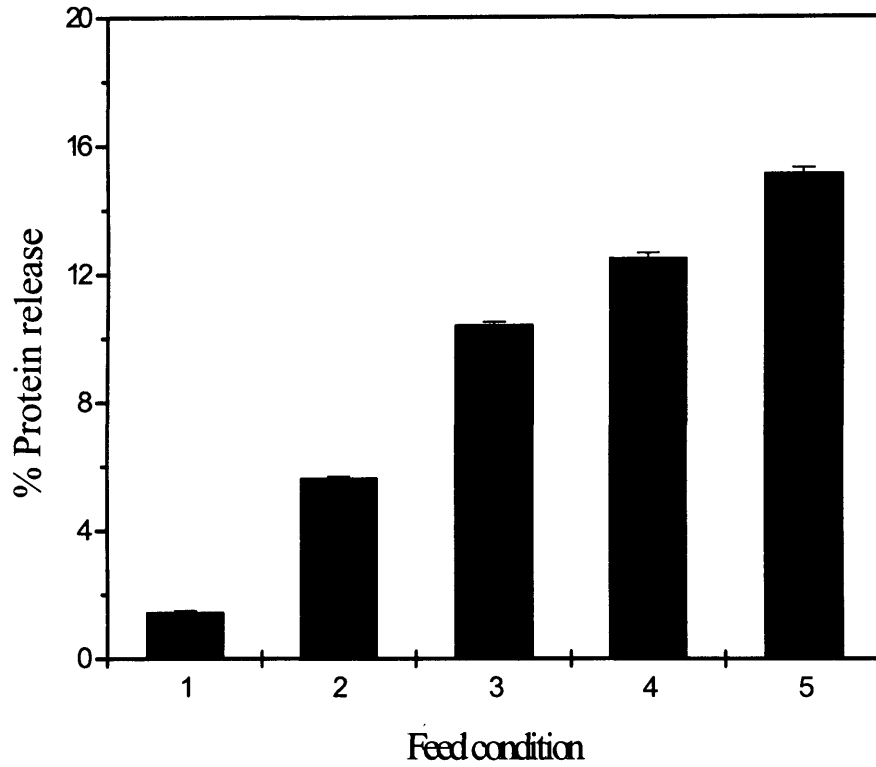
Figure 2.8   *E. coli* protein release as a function of feed preparation and before USD
and pilot-scale studies. Symbols: (1) Fresh W3110 *E. coli* cells (20 L);
(2) Fresh DH5α *E. coli* cells (450 L); (3) DH5α *E. coli* cells freeze-
thawed once from -80°C; (4) DH5α *E. coli* cells freeze-thawed twice
once from −80°C and then from -20°C; (5) DH5α *E. coli* cells freeze-
thawed twice from −80°C.
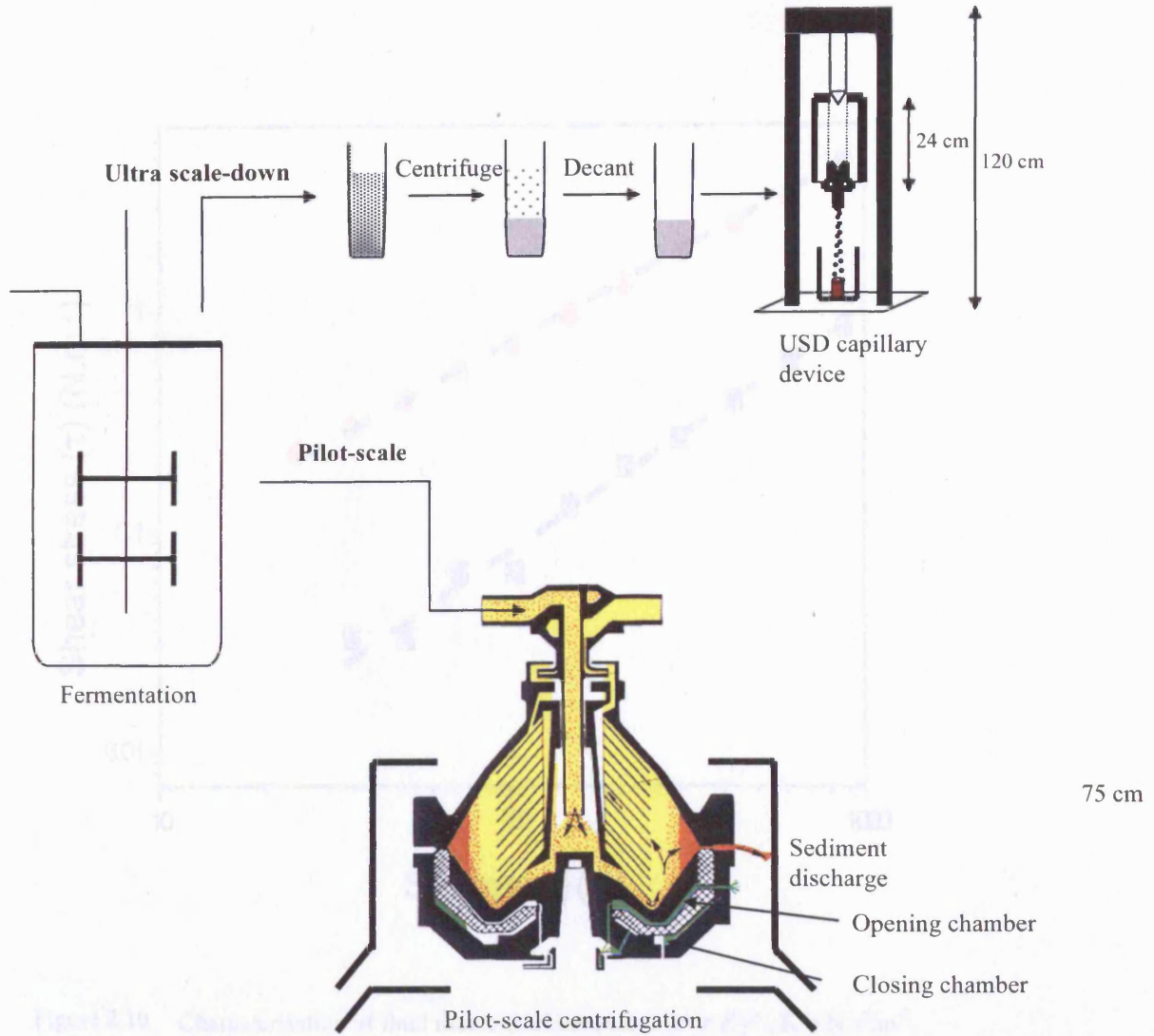
Figure 2.9   A schematic illustration of the USD procedure used to mimic pilot-scale centrifugal discharge. *E. coli* cell suspensions were fed through the pilot-scale centrifuge and recovered over a set of discharge velocities. A small volume from each feed suspension was spun down to give a paste resembling the centrifuge pre-discharge material. This paste was then processed through the USD capillary device.

92
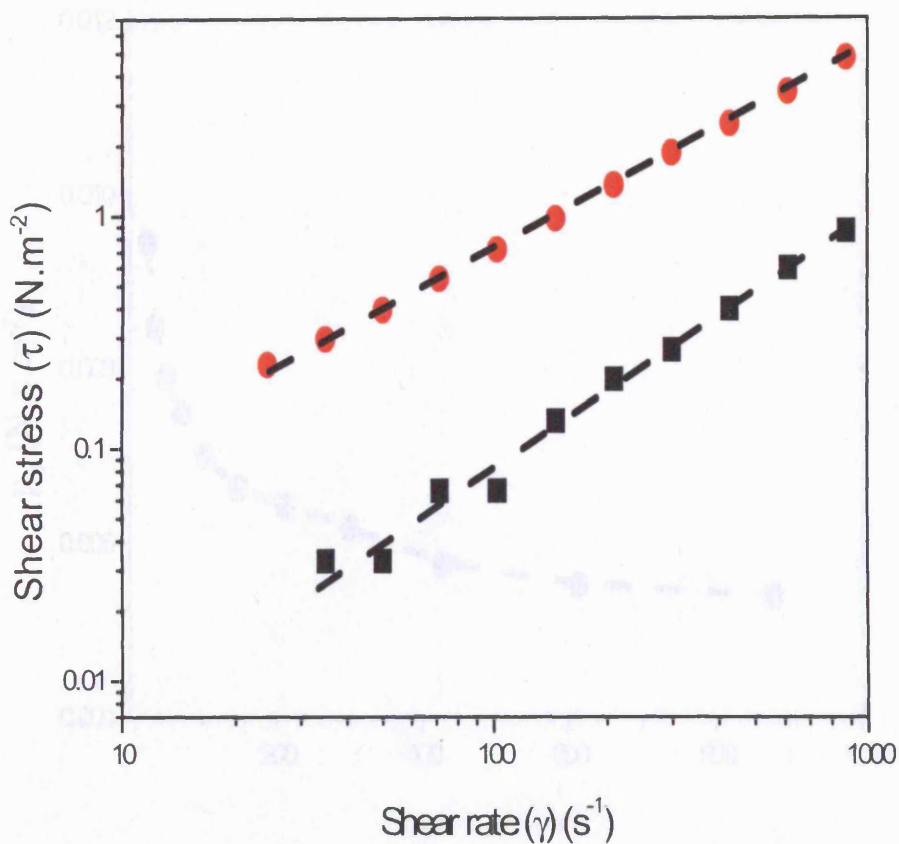
Figure 2.10   Characterisation of fluid rheological behaviour ($\tau = K\gamma^{n}$, K = N.s^{n}.m^{-2}, n = dimensionless). The apparent viscosity ($\mu_a = \tau/\gamma = K\gamma^{n-1}$) at high shear rate was used to characterise the material used in this thesis. Symbols: (●) Freeze thawed (from -80°C) DH5α *E. coli* cell suspension (300 mg.mL^{-1} WCW) showing slight evidence of pseudoplastic behaviour ($n = 0.9$) (R^2 of 0.99); (■) Reverse osmosis water with Newtonian behaviour ($n = 1.1$, K = 0.0009 N.s.m^{-2}) (R^2 of 0.99). All samples were measured in triplicate with the temperature maintained at 4°C.
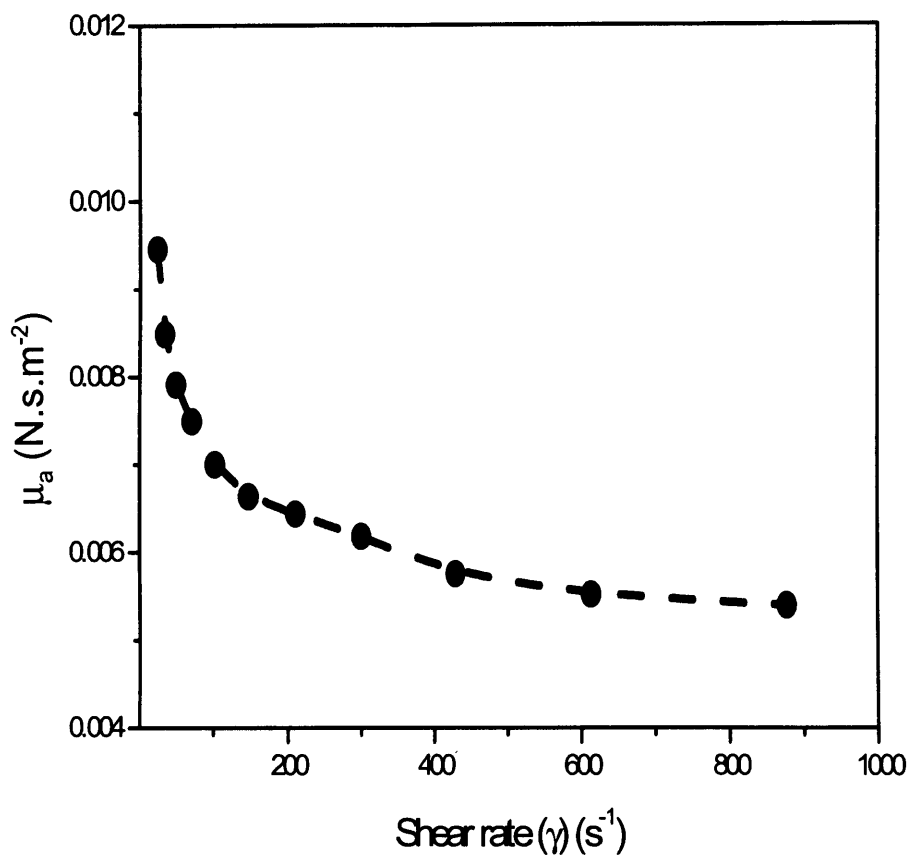
Figure 2.11   The relationship between apparent viscosity ($\mu_a = \tau/\gamma = K\gamma^{n-1}$) and shear rate for pseudoplastic *E. coli* suspensions used in this thesis. Symbol: (●) Freeze thawed (from -80°C) DH5α *E. coli* cell suspension (300 mg.mL^{-1} WCW, $\mu_a = 0.0053$ N.s.m^{-2}). All samples were measured in triplicate with the temperature maintained at 4°C.
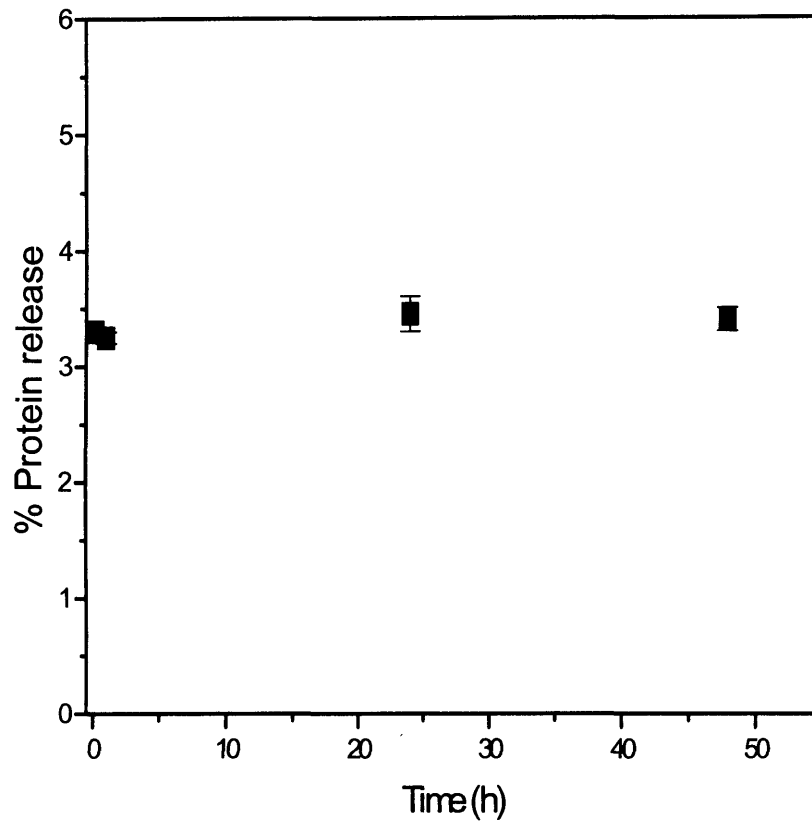
Figure 2.12   The effect of storing processed samples (G_cT_i of 646, impact velocity of 49 m.s^{-1}, impact distance (onto stainless steel stub) of 90 mm, viscosity of 0.005 N.s.m^{-2}) at 4°C on protein release as measured by the Coomassie method. No additional release is observed with delayed analysis.
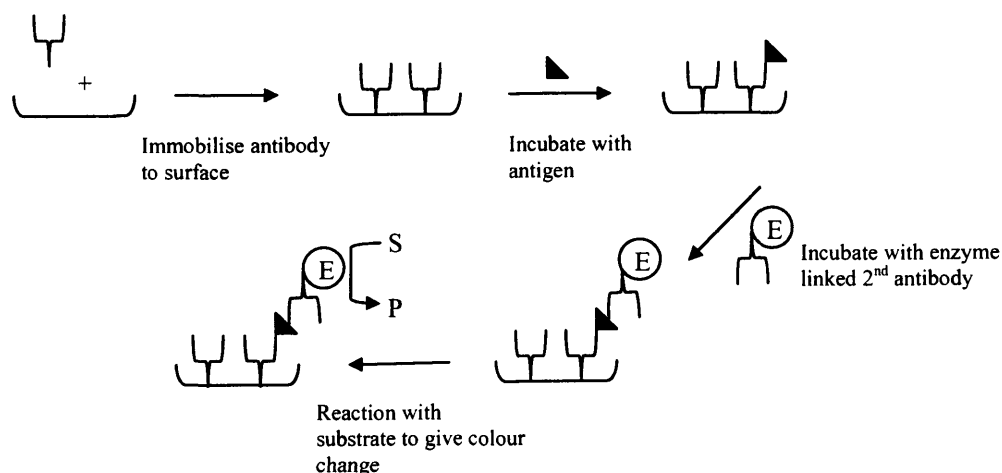
Figure 2.13   Schematic illustration of a sandwich ELISA.

	Reagents	Quantity
PBS (Buffer stored at 4°C)	Phosphate buffer	10 mM
	NaCl	145 mM
	Reverse osmosis water	1 L
Sample Conjugate Buffer (Buffer filtered and stored at 4°C)	Tris amino-methane	6.05 g
	NaCl	2.92 g
	Tween-20	0.1 mL
	Casein	1.0 g
	Reverse osmosis water	500 mL
Substrate solution (Substrate freshly prepared)	10 mg.mL^{-1} tetramethylbenzidine (TMB) in dimethylsulphoxide	100 μL
	0.1M (pH of 6) filtered sodium acetate/citric buffer	10 mL
	1 in 50 dilution of 30% H_2O_2 in water	100 μL

Table 2.12   Preparation of reagents for the ELISA assay.
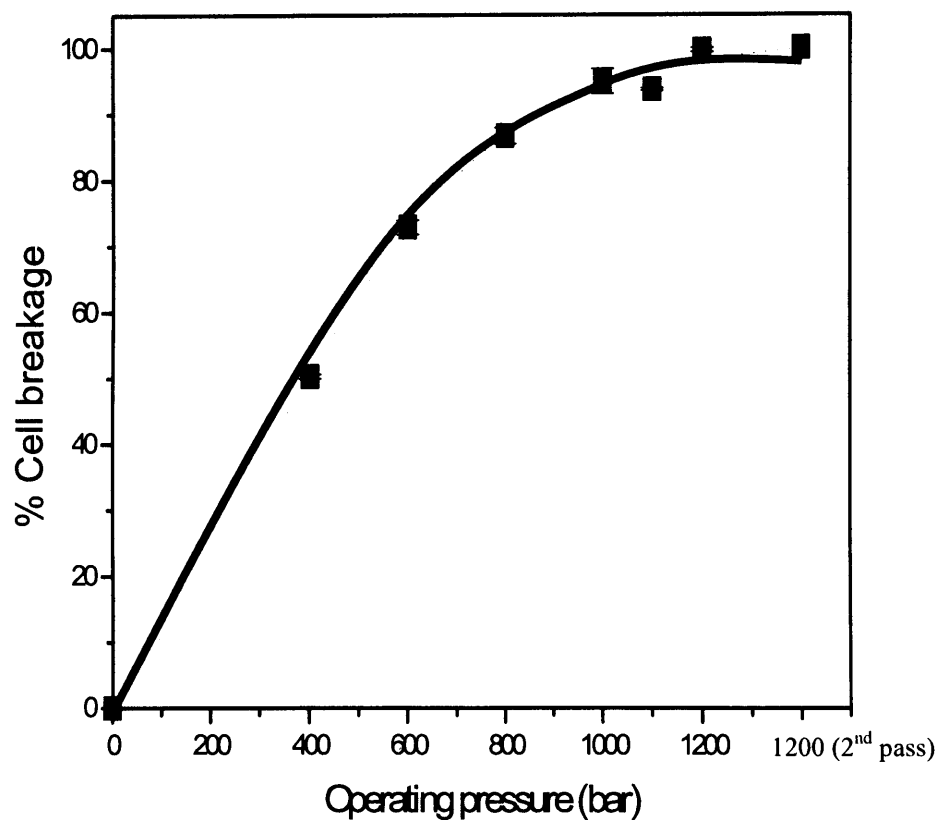
Figure 2.14   Cell breakage of W3110 *E.coli* as a function of the Lab 40 operating
pressure. Sample volumes of 40 mL were processed over a pressure
range of 0 to 1200 bar at a constant temperature of 4°C. All
experiments were performed in triplicate. Maximum cell breakage
was achieved at a pressure of 1200 bar (2 passes), where the cell
breakage was observed to plateau. Note: Identical results were
obtained for DH5α *E. coli*.

x10K   (A)   2μm   x10K   (B)
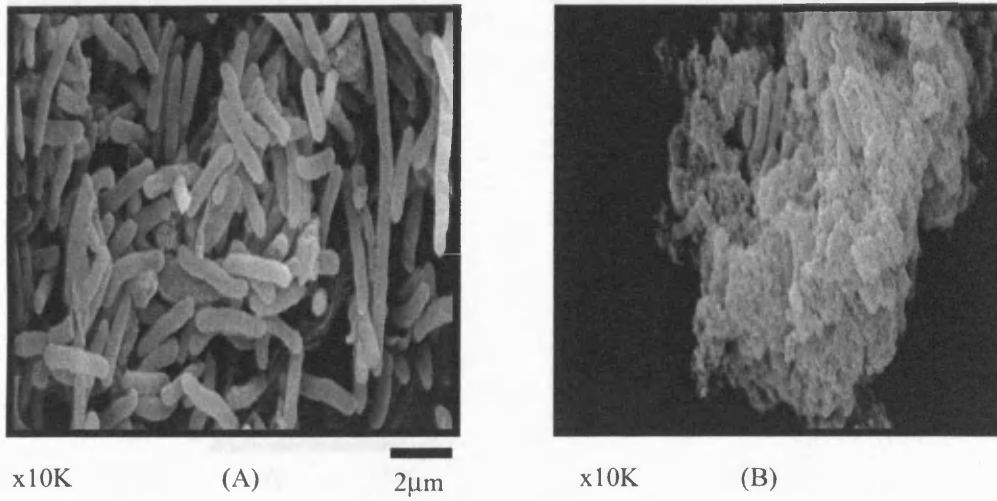
Figure 2.15   Scanning electron micrograph's of W3110 *E. coli* cells before (A) and after (B) exposure to a Lab 40 operating pressure of 1200 bar. (A) is characterised by rod shaped *E. coli* cells; (B) is characterised by a mass of debris clumped together.

x40K　　　　　(A)　　1μm　　　x40K　　　　(B)
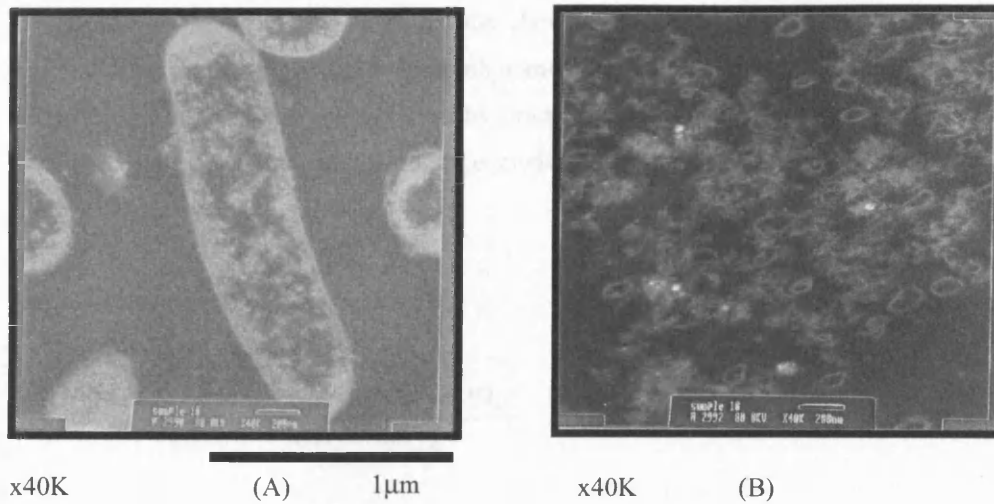
Figure 2.16　Transmission electron micrograph's of a W3110 *E. coli* cell before (A) and after (B) exposure to a Lab 40 operating pressure of 1200 bar. The *E. coli* cell in (A) is characterised as rod shaped with intracellular saturation. Homogenisation of the cell (B) leads to complete disruption with loss of intracellular material.

2.8.5 Centrifuge clarification efficiency

Optical density (OD) measurements of the clarified supernatant were performed at 600 nm using the Ultrospec 2000 spectrophotometer (Pharmacia Biotech, Cambridge, UK). A well-spun sample was obtained by centrifuging a representative feed sample for 30 min at 13000 rpm in the Biofuge model 13 centrifuge (Heraeus Sepatech, GmbH, Germany).

The clarification efficiency is defined by:

$$\%Clarification = \frac{(OD_f - OD_{ws}) - (OD_s - OD_{ws})}{(OD_f - OD_{ws})} \; x100 \qquad [2.5]$$

where OD_f, OD_s and OD_{ws} correspond to the optical density of the feed, supernatant and a well spun sample respectively.

2.8.6 Scanning electron microscopy (SEM)

Cells were concentrated by centrifugation (2 mL samples, 13000 rpm, 300 s). The cell proteins were fixed using a 2.5% (v/v) glutaraldehyde solution for 1.5 h. The fixing solution was removed by 3 rinses with PBS buffer (pH 7.4). The cell lipids were then fixed using 1% Osmium Oxide (Agar Scientific Ltd., Essex, UK) and left to stand for 1 h at 4°C. The fixing solution was removed by 3 rinses with PBS buffer (pH 7.4).

The fixed samples were serially dehydrated over a range of ethanol (VWR International, Lutterworth, UK) concentrations (25, 50, 75, 100 % v/v) for periods of 10 min before being transferred to a higher concentration. At 100% (v/v) ethanol concentration, the dehydrating agent was exchanged with fresh 100% ethanol over a 30 min period, at 10 min intervals.

Ethanol was replaced with 100% acetone via three consecutive washes at 5 min intervals before replacing with hexamethyldisilazane (HDMS) and soaking for 20 min. The cell pellet was spread over filter paper and left to air dry. Specimens were mounted onto stubs that were then spluttered with gold using the EMScope SC500 device (Emitech Ltd, Kent, UK) and observed using the Jeol JSM-5410LV scanning microscope (Joel Ltd, Toyko, Japan).

2.8.7 Transmission electron microscopy (TEM)

Cells were concentrated and fixed in the same manner as for the SEM. The fixed samples were serially dehydrated over a range of ethanol concentrations. At 100% (v/v) ethanol concentration, the dehydrating agent was exchanged with fresh 100% ethanol over a 30 min period, at 10 min intervals.

Ethanol was replaced with 100% propylene oxide (VWR International, Lutterworth, UK) via three consecutive washes at 10 min intervals before replacing with a resin/propylene oxide mixture of 1:3, 1:1 and 2:1 ratio for 40 min intervals. The resin comprised of dodecenyl succinic anhydrite (16 mL), Agar 100 (20 mL), methyl nadic anhydride (8 mL) and benzyldimethylamine (3 mL) (Agar Scientific Ltd., Essex, UK). The resin/propylene oxide mixture was then replaced with pure resin and left to stand at room temperature for 8 h. Polymerisation was carried out at 60°C for 12 h. Using a Ultramicrotone (Ultracut E, Leica Microsystems Ltd., Milton Keynes, UK) with a diamond knife, sections of 80 nm thickness were cut from the polymerised bulk material. The sections were placed onto a 200 mesh copper grid (Agar Scientific Ltd., Essex, UK) and stained with lead citrate solution for 10 min before viewing in a Jeol 1010 transmission electron microscope (Jeol Ltd. Toyko, Japan). Images were recorded on Kodak EM film (Agar Scientific Ltd., Essex, UK).

2.8.8 Flow cytometry

All flow cytometry measurements were performed using a Coulter Epics XL MCL (Coulter Corporation, Miami, USA). Flow cytometry has been used extensively used to study large cells such as mammalian cells (10-20 μm) (Davey et al., 1996) where small debris can be easily separated from the entities of interest. Unfortunately this technique becomes more difficult when moving to smaller particle sizes e.g. *E. coli* cells (1-2 μm) (Hewitt et al., 1998). The flow cytometry protocol was set-up according to Table 2.13.

Variables	Voltage	Gain
Forward scatter	105	5
Side scatter	74	50
FL1 filter (BOX)	581	1
FL3 filter (PI)	699	1
Baseline Offset	Activated	
Discriminator	5	

Table 2.13   Flow cytometry protocol settings. The discriminator eliminates background noise with higher values removing more noise.

The propidium iodide (PI) (Molecular Probes, UK) and bis-oxanol (BOX) (Molecular Probes, UK) dyes were selected for staining cells. PI was chosen because it provides information on the integrity of a cell membrane (Dangl et al., 1982). The stain binds to nucleic acids but cannot diffuse through an intact cytoplasmic membrane. The stain fluoresces at a wavelength of 630 nm (FL3 optical filter). BOX is lipophillic, anionic, and accumulates in the intracellular space provided the cell membrane is depolarised, hence it provides information on metabolic activity. The stain fluoresces at a wavelength of 525 nm (FL1 optical filter).

Cell suspensions were diluted with 0.2 μm filtered dulbecco's buffered saline (DBS, pH 7.2) to give approximately 5×10^3 cells.mL^{-1} (measured using the flow cytometer cell counter). To 1 mL of diluted sample, 5 μL of PI (200 μg.mL^{-1} in distilled water)

and 5 µL of BOX (10 mg.mL^{-1} in dimethyl sulphoxide) were added. Samples were vortexed for 10 s and left to stand for 30 s before analysing. The sample flowrate through the cytometer was set to "low" with the machine analysing between 150 to 200 cells.s^{-1}. The total time taken between each experiment and its analysis was < 10 min (unless otherwise stated).

3 THEORY

3.1 Ultra scale-down (USD) theory

3.1.1 Capillary flow

The challenge of working with high velocity capillary flow even of high viscosity suspensions is that the flow conditions are difficult to define with Reynolds numbers ($\rho v D_c/\mu$, with velocity, v, expressed as $Q/\pi R_c^2$) ranging from 1000-15000 i.e. from the laminar to transition regions. The length to diameter ratio for a capillary is typically 25 to 100 (Yim et al., 2000) which allows sufficient time for fully developed laminar or turbulent flow. However the suspensions are not homogeneous fluids but contain a high density of cells that are only two orders of magnitude smaller than the capillary diameter.

3.1.1.1 Laminar capillary flow

Most of the research in this field has been devoted to shear effects on animal cells (Papoutsakis et al., 1991; Petersen et al., 1988; Born et al., 1992; Zhang et al., 1993). Born et al. (1992) gives extensive insight into the behaviour of these cells to laminar shear stresses. Animal cells are generally considered susceptible to shear and other mechanical forces due to the lack of a protective cell wall. Under laminar conditions cells are assumed to deform giving rise to membrane tension, and with the tension exceeding the bursting membrane tension the cells become damaged (Born et al., 1992). This phenomenon has also been reported by Schmid-Schonbein et al. (1969) who worked with red blood cells. It was demonstrated that under stress flow, a red blood cell, like a liquid drop, could distort into a prolate ellipsoid. In this study we extend the literature to include effects of laminar shear on bacterial cells, namely *E. coli*.

The capillary flow may be characterised by the mass average shear rate (G_c) (Welty et al., 1984; Bell et al., 1982):

$$G_c = \frac{8}{15}\gamma_w \qquad [1]$$

where γ_w is the laminar shear rate at the capillary wall:

$$\gamma_w = \frac{4Q_c}{\pi R_c^3} \qquad [2]$$

and by the mean residence time (T_i):

$$T_i = \frac{\pi R_c^2 L_c}{Q_c} \qquad [3]$$

where R_c is the internal radius of capillary, L_c is the capillary length and Q_c is the capillary suspension flowrate.

The capillary mass average shear stress (τ) is defined by:

$$\tau = \mu G_c \qquad [4]$$

3.1.1.2 Transitional/turbulent capillary flow

It is widely accepted that biological cells, e.g. animal cells, are susceptible to turbulent environments (Zhang et al., 1993; Cherry et al., 1990; McQueen et al., 1989; McQueen et al., 1987; Abu-Reesh et al., 1989; Garcia-Briones et al., 1994), where cell damage is most often detected when the Kolmogorov microscale of turbulence falls below the cell size. However, Cherry et al. (1990) describes the turbulent disruption of single cell micro-organisms with average sizes less than the microscale of turbulence by assuming that disruption occurs by flow stresses inside the eddy.

Cells moving in and out of eddies experience a distribution of shear rates and shear stresses. Turbulent shear stresses have also been shown to cause greater cell damage than equal laminar stresses in a viscometer (Abu-Reesh et al., 1989). Although these reports demonstrate the detrimental effects of turbulent flow on cell survival, it is difficult to predict precisely how these forces will affect cell lines of different mechanical properties (Garcia-Briones et al., 1994).

The flow in a tube can be considered turbulent if the Reynolds number is above 4000 (Fox et al., 1994). The flow is usually characterised as being laminar close to the capillary wall and turbulent towards the centre (Fox et al., 1994; Zhang et al., 1993).

The mass average shear rate (G_c) in a turbulent environment is defined as (Zhang et al., 1993):

$$G_c = \sqrt{\frac{\varepsilon_T}{\mu_k m}}$$

[5]

where μ_k is the kinematic viscosity, m is the suspension mass, and ε_T is the total energy dissipation in the capillary tube defined as:

$$\varepsilon_T = \Delta P \pi R_c^2 U_c = \Delta P Q_c$$

[6]

where, ΔP is the pressure drop:

$$\Delta P = \bar{f} \rho \frac{L_c v_{max}^2}{2 D_c}$$

[7]

where v_{max} and $\bar{f}$ are the maximum velocity at the centre of the pipe and Fanning friction factor respectively given by:

$$v_{max} = \frac{U_c}{0.817}$$

[8]

$$\bar{f} = \frac{0.296}{[\mathrm{Re}(L_c / D_c)]^{0.2}}$$ [9]

where U_c is the capillary discharge velocity $(Q_c/\pi R_c^2)$.

3.1.2 Jet stream characterisation

A great deal of research has been conducted on understanding the profile of water jets (Haller et al., 2002; Shavlovsky, 1972; Summers, 1995; Yanaida et al., 1978; Yanaida 1974; Yanaida and Ohashi, 1978; Reichman et al., 1980; Olive et al., 1959; Vickers et al., 1980; Davies et al., 1980; Hrycak et al., 1969). However, in spite of this, there is still little understanding of the detailed structure and characteristics of water jets in air (Haller et al., 2002). Work by Yanaida and Ohashi (1978) considers the droplet region of a high velocity water jet. They divide the jet into three distinct zones, namely, the continuous flow region, the droplet flow region and the diffused flow region, as illustrated in Figure 3.1.

Near the nozzle there is relatively little change in jet structure with the majority of the fluid moving in a coherent central stream. Based on work conducted by Davies et al. (1980) it can be assumed that the velocity remains approximately constant within the continuous region of flow. Between the potential core length (X_c) and the break-up point (X_b) fine droplets begin to develop as a result of the shear effect from the adjacent stationary air. On reaching the break-up region (X_b), aerodynamic forces dominate over the flowing fluid stream and hence a decrease in velocity of the stream is observed. Shown below are equations used to determine potential core length (X_c) and break-up length (X_b) of a typical jet stream.

The potential core length of a jet over both laminar and turbulent conditions is given by (Shovlovsky, 1972):

$$\frac{X_c}{2R_0} = A - (6.8\times10^{-5}\times\mathrm{Re})$$ [10]

where X_c corresponds to the potential core length, R_0 is the orifice radius (equal to R_c in this paper) and A is a constant of between 85 and 112 depending on the type of nozzle used. Alternatively, for sufficiently high capillary Re (> 170,000) Yanaida (1974) has shown:

$$X_c = 0.97 \left(\frac{2R_0}{0.237} \right)^2$$
[11]

Hrycak et al. (1969) has shown that for Re between 1000 and 10,000 the size of the potential core varies considerably and that the potential core length (X_c) is dependant on nozzle diameter for Re between 2000 and 10,000. Since the Re for the following experiments was calculated to be a maximum of 3300 (unless otherwise stated), Equation 10 was used to calculate X_c. In addition, Yanaida et al. (1978) also expresses the relationship between the break-up length (X_b) and the potential core length of the jet (X_c), as shown in Equation 12. This jet distance (X_b) has, from cutting technology, been identified as the optimum point at which maximum energy dissipation occurs (Yanaida et al., 1978).

$$X_b = 3.55X_c$$
[12]

3.1.2.1 Consideration of droplet impact

A free jet leaving a nozzle will possess a potential core, which will diminish in size and velocity with increasing distance from the nozzle. The extent of jet decay is dependant primarily on surface tension and aerodynamic forces, with a growing layer of droplets appearing adjacent to the diminishing jet core to form a multi-component flow consisting of inner core fluid, the surrounding air flow, and droplet flow. A great deal of research in the field of jet technology has shown that with increasing distance from the nozzle, the factors that contribute to jet efficiency are the central core jet pressure but to a greater extent liquid droplet impact (Vickers et al., 1980; Olive et al., 1959; Reichman et al., 1980).

The fluid flow associated with high velocity impinging droplets is complicated and no full understanding has yet been derived (Haller et al., 2002). However, to explain why droplets may be the most effective form (i.e. highest energy storage) of a free jet the work by Lesser et al. (1983) should be considered. Their work seeks to understand the pressure distribution beneath a water droplet collapsing on a rigid surface at high velocity. The droplets were observed to compress and with the immediate arrival of preceding droplets continue to deform. This leads to changes in pressure usually referred to as the Water Hammer Pressure (WHP), created where a shock wave is introduced into the system (Figure 3.2A). This form of pressure is much larger than conventional jet impact pressures (Summers, 1995). This series of events may play a significant role in the initial loss of cell integrity as will be discussed later.

The compression of droplets leads to the formation of a jet from the contact edges between the droplet and impact surface (Figure 3.2B) and the rapid disappearance of these droplet structures (Figure 3.2C). To explore this phenomenon in more depth, reference is made to work conducted by Chalmers et al. (1991) and Cherry et al. (1992). Although these authors deal with bubbles as opposed to droplets, the mechanism involved with the loss of the spherical structures are suggested to be the same. On rupture of a bubble, the rim retracts at a rapid acceleration rate from stationary state to a velocity of ~3 $m.s^{-1}$ before bursting in ~2 ms (Cherry et al., 1992), and as such the intense hydrodynamic forces associated with this motion can be sufficient to cause cell rupture or worse still, cell death in and around the vicinity of the bursting bubble (Chalmers et al., 1991). Smaller bubbles have been found to be more harmful to cells (Handa et al., 1987; Wu et al., 1990), since the forces are more profound because of the large bubble surface area to volume ratio.
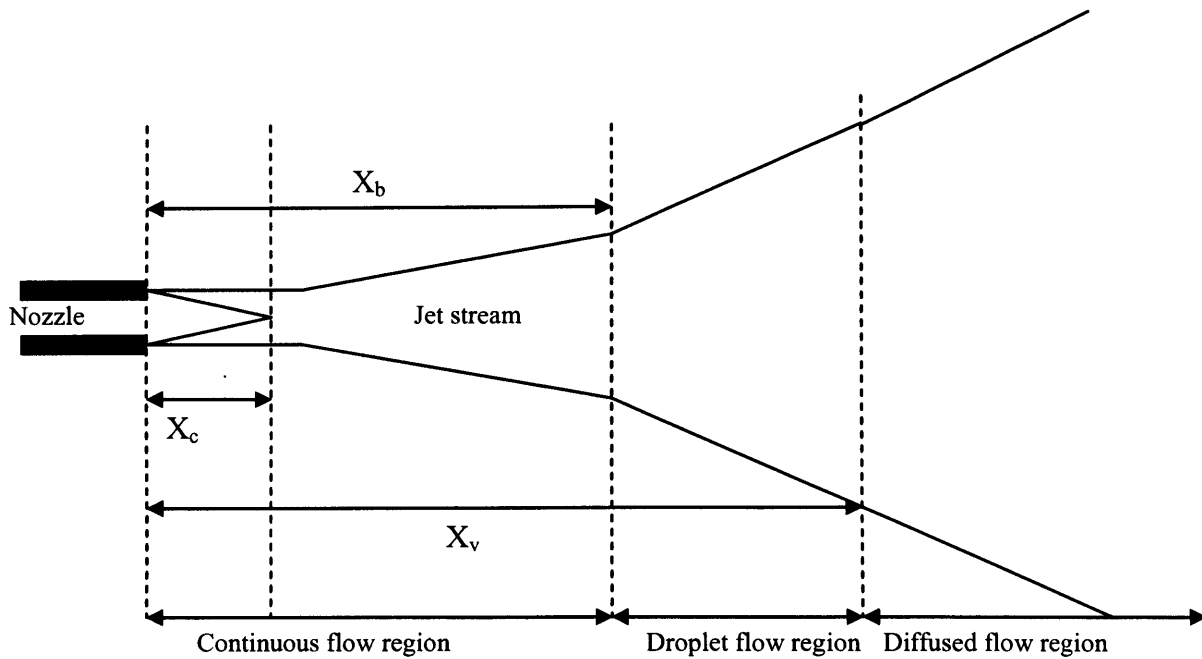
Figure 3.1   Schematic representation of a typical fluid stream exiting the capillary nozzle where X_c is the potential core, X_b is the break-up length and X_v is the droplet flow length.

Liquid drop

Cells

Contact edge

Shock wave

Compressed liquid

A

Nicking of bubble wall

Shock front

Jetting

B

Rim retraction

Cell breakage

C
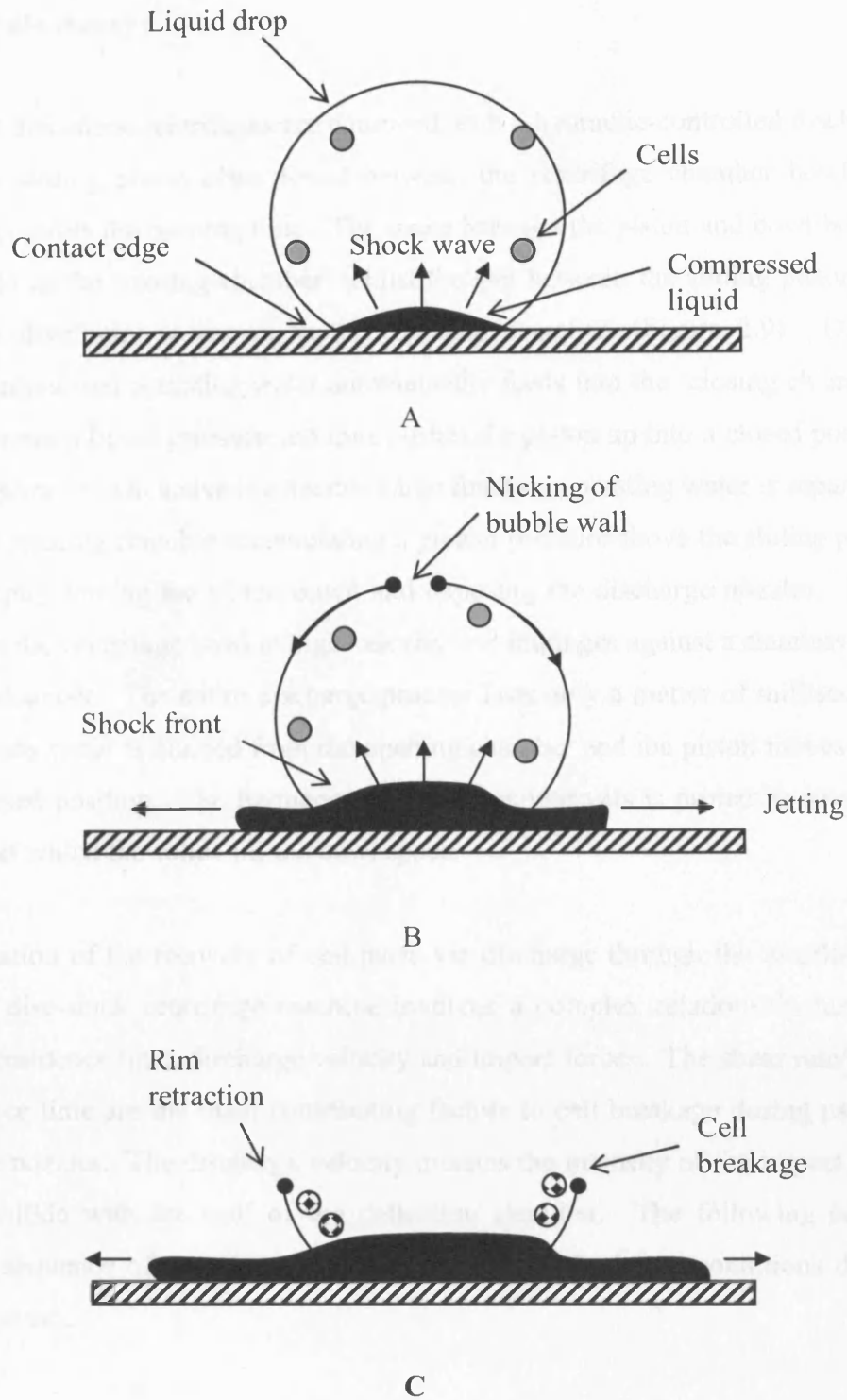
Figure 3.2   Schematic illustration of a droplet impacting on a rigid surface. (A) The shock front creates a high water hammer pressure environment. (B) The shock front overtakes the contact edge and forms a jet, whilst a nick develops on the droplet surface and begins to propagate. (C) The droplet rim retracts at high acceleration generating high energy dissipation and cell damage.

3.2 Pilot-scale theory

Intermittent disc-stack centrifuges are equipped with a hydraulic-controlled discharge feature. A sliding piston often found between the centrifuge chamber bowl and distributor controls the opening time. The space between the piston and bowl bottom is referred to as the 'closing chamber' whilst the gap between the sliding piston and base of the distributor is known as the 'opening chamber' (Figure 2.9). During operation pressurised operating water automatically feeds into the 'closing chamber', which generates a liquid pressure and thus pushes the piston up into a closed position sealing the nozzles. On activating the discharge function operating water is separately fed into the opening chamber accumulating a greater pressure above the sliding piston before abruptly forcing the piston down and exposing the discharge nozzles. Solid paste leaves the centrifuge bowl at high velocity and impinges against a stainless steel collection chamber. The entire discharge process lasts only a matter of milliseconds before process water is drained from the opening chamber and the piston moves back into the closed position. The frequency of discharge intervals is primarily governed by the rate at which the solids fill the bowl space.

Characterisation of the recovery of cell paste via discharge through the nozzles of a continuous disc-stack centrifuge machine involves a complex relationship between shear rate, residence time, discharge velocity and impact forces. The shear rate/stress and residence time are the main contributing factors to cell breakage during passage through the nozzles. The discharge velocity dictates the intensity of the impact force as solids collide with the wall of the collection chamber. The following section details the sequence of equations used to approximate discharge conditions during product recovery.

3.2.1 Nozzle shear rate

The G_cT_i (i.e. the product of mass average shear rate and mean residence time) for laminar flow through a centrifuge nozzle is given by:

$$G_cT_i = \frac{256QL}{15\pi D_h{}^3 U_p}$$ [13]

where Q is the centrifuge nozzle flow rate, L is the discharge nozzle length, U_p is the centrifuge discharge velocity and D_h is the hydraulic diameter of the rectangular nozzle given by:

$$D_h = \frac{2WH}{W + H}$$ [14]

where W and H are the width and height of the nozzle respectively.

The Reynolds number (Re) of suspension flowing through a rectangular nozzle is given by:

$$Re = \frac{\rho_N U_p D_h}{\mu}$$ [15]

where ρ_N is the suspension density and μ is the suspension viscosity.

3.2.2 Solids discharge velocity

The centrifuge discharge pressure (*P*) is given by (Ruthven 1997):

$$P = \frac{\rho_N}{2} \omega^2 (r_1^2 - r_2^2)$$

[16]

where r_1 is the bowl inner radius (i.e. outer radius of suspension within bowl), r_2 is the radius of the inner liquid ring (i.e. centripetal pump radius), and ω is the angular velocity of the bowl $(= 2\pi N)$.

The centrifuge discharge velocity (U_p) for a fully opened nozzle centrifuge is given by (Ruthven 1997):

$$U_p = \sqrt{\frac{2P}{\rho_N}}$$

[17]

4. RESULTS

The following section deals with two issues, namely ultra scale-down (USD) studies of the effect of flow conditions on *E. coli* cell processing and USD prediction of *E. coli* cell recovery from high speed discharge centrifuges. The first set of results seek to examine the nature of high-speed capillary flow discharged in the form of a free jet into a collection vessel, and the potential effect of this flow on cell integrity. The USD device selected for this study was the Instron capillary device requiring only mL quantities of test material. Numerous parameters were evaluated including the effect of capillary shear and residence time, sample viscosity, discharge velocity and impact configuration. Ultimately such a device could be used to predict cell recovery in continuous- or intermittent-discharge centrifuges of the disc stack variety commonly used in the bioprocessing sector. The nature of capillary flow and discharged jets, and their impact on collection surfaces, is reviewed here.

The second section focuses on discharge recovery of sensitive *E. coli* cells from an intermittent disc-stack centrifuge where the frequency and duration of solids discharge is controlled by the operator. This type of centrifuge is commonly used for medium feed solids concentration between 1 and 4% (Ruthven 1997). Intermittent discharge provides longer residence times and better dewatering of solids than continuous separators, often at the expense of disc space and reduced bowl throughput. Solid paste leaves the centrifuge bowl at high velocity and impinges against a stainless steel collection chamber. The entire discharge process lasts only a matter of milliseconds. The frequency of discharge intervals is primarily governed by the rate at which the solids fill the bowl space. Factors such as a high flow rate and a high cell density broth will give greater rates of solid accumulation. Higgins et al. (1978) and Gray et al. (1972) reported cell disruption during recovery of *E. coli* cells using intermittent discharge disc-stack centrifuges. Here cells growth on defined media yielded significantly greater protein release (~20%) compared with cells grown on complex media (~10%). However the region in the centrifuge causing such disruption was not identified and hence also the mechanism of cell damage could not be interpreted.

Our study aims to identify the factors involved with the disruption process and to mimic and understand the events which occur in large-scale centrifuges using ultra scale-down (USD) tools. This will be in much the same fashion as for characterising the feed zones of continuous high-speed centrifuges where rotating disc devices have formed the basis of the USD mimic (Boychyn et al., 2001, 2004).

4.1 Effect of process parameters on cell breakage

4.1.1 Effect of USD sample volume on experimental accuracy

When developing a USD device it is necessary to identify the minimum volume of process material capable of generating representative results. Figure 4.1 illustrates the effect of using different sample volumes on cell breakage during processing. Sample viscosities were fixed at 0.005 $N.s.m^{-2}$ with a capillary shear rate, residence time and velocity of 3.96 x 10^5 s^{-1}, 0.0016 s and 31 $m.s^{-1}$ respectively. The impact distance was set at 90 mm, of which the target was a stainless steel stub. The results show that the capillary device is capable of operating with a lower limit of 10 mL without compromising on the accuracy of the experiment. Sample volumes of less than 10 mL show a deviation in accuracy and in general were more difficult to work with. In support of this, from visual observations sample volumes less than 10 mL were insufficient at generating a representative jet stream from the capillary and hence would hinder impact studies that rely on forming a fully developed jet.

4.1.2 Effect of shear rate

Here we evaluate the effect of shear within the capillary on the degree of cell breakage. Figure 4.2 illustrates the extent of disruption as a function of shear rate during flow within the capillary. Cell suspensions were fed through the Instron over a range of drive speeds and capillary nozzle sizes in order to achieve different shear rates. Four sample residence times were studied, 0.024, 0.012, 0.006 and < 0.004 s, all of which were achieved by recycling the process material through capillaries of different lengths. Figure 4.3 illustrates no significant correlation between centrifuge spin time between capillary passes and cell breakage suggesting that the cell breakage observed is essentially due to capillary shear conditions. The impact distance

measured from the capillary tip was, for all experiments, fixed at 300 mm; the impact surface was buffer of depth 100 mm. The total available protein for release was 9.3 mg.mL^{-1} (C_h, Chapter 2, Equation 2.4) of which ~3% was already extracellular in the feed (C_f = 0.24 mg.mL^{-1}, Chapter 2, Equation 2.4). Small but significant levels of extra protein release are observed for the capillary shear studies representing the consequence of cell damage during capillary flow.

The results demonstrate that for a fixed capillary residence time an approximately linear relationship (R^2 > 0.84 to 0.98) might be assumed between shear rate and the degree of cell breakage. The results also demonstrate that increasing residence time leads to a greater degree of cell breakage. This observation will be addressed in more detail in the following section. One trend worth noting is the effect of shear rate on cell breakage when the residence time was fixed at < 0.004 s. Here it can be seen that regardless of the shear intensity, negligible protein release was detected. Even when exposing cells to shear rates (1.4 x 10^6 s^{-1}) several times higher than those experienced during large-scale centrifuge recovery of *E. coli*, no additional protein release is measured.

4.1.3 Effect of residence time

To clarify the effect of capillary residence time on the degree of cell breakage at a constant shear rate, cell suspensions were processed through a capillary at a shear rate of 3.16 x 10^5 s^{-1} over a range of exposure times achieved by varying the length of capillary and the number of passes and collected in a buffer of depth 100 mm at a standoff distance of 300 mm. The residence time within the generated shear field was varied between 0 and 0.052 s, where 0 s refers to the control. Figure 4.4 illustrates that at a fixed shear rate of 3.16 x 10^5 s^{-1} an increase in residence time results in greater levels of cell breakage. A short exposure time to the shear stress has no significant effect on cell integrity.

Figure 4.5 represents the logarithmic relationship between shear rate (G_c) and residence time (T_i) in the capillaries on cell breakage. Imposing a linear relationship (% cell breakage α ($G_c T_i$)^n, n = 1) yields a satisfactory fit (R^2 = 0.9) leading to further confidence in a linear relationship between breakage and shear rate (Figure 4.2) and

residence time (Figure 4.4). Cells subjected to an overall G_cT_i of < 1000 may be assumed to show negligible cell breakage (below measurement limit) and as such was used as a benchmark for excluding capillary responses from subsequent impaction studies. Figure 4.6 illustrates that no significant relationship is observed between cell breakage and number of passes through the capillaries, confirming that cell damage is largely due to the G_cT_i conditions along the capillary length.

4.1.4 Effect of viscosity/shear stress

A limited capillary shear study was carried out with feed suspensions of different concentration and hence viscosity. *E. coli* samples of viscosity ranging from 0.001 to 0.0065 N.s.m^{-2} were processed through a capillary of shear rate 6.3 x 10^5 s^{-1} and residence time of 0.001 to 0.006 s. Samples were collected in a head of buffer of height 100 mm at 300 mm distance from the capillary exit in order to eliminate impact effects. Figure 4.7 illustrates the effect of Reynolds number and sample viscosity on cell breakage. High cell breakage is evident under conditions of turbulent flow and high residence time. The degree of cell breakage drops as the viscosity increases or residence time decreases.

Figure 4.8 illustrates an increase in cell breakage with the extent of exposure to shear stress with an approximately linear relationship extending over a range of flow regimes from laminar to turbulent. The data was compiled by calculating the product of viscosity, shear rate and residence time and plotting against cell breakage (from Figure 4.7). Negligible difference is observed between the extent of cell breakage induced by laminar and turbulent shear stresses.

4.1.5 Effect of impact

To investigate the contribution of impact on the disruption of *E. coli*, a stainless steel surface was positioned at 90 mm from the capillary tip and perpendicular to the flow direction. Capillary discharge velocities studied ranged from 0 m.s^{-1} to 85 m.s^{-1}, where 0 m.s^{-1} refers to the control sample. Figure 4.9 illustrates the effect of capillary discharge velocity on the degree of cell breakage and demonstrates an approximately linear relationship (R^2 = 0.95). The highest accumulated capillary G_cT_i value over the

range of velocities studied is 646, which accounts for less than 0.3% cell breakage (Figure 4.5).

TEM images as shown in Figure 4.10 are used to examine further the effect of impact on cells. Figure 4.10A shows that for low discharge velocity minimal cell disruption occur, i.e. characterised by a large proportion of fully intact cells. However, for high discharge velocity as shown in Figure 4.10B, a variety of different cell forms are observed; from fully intact, distorted and leaky to ghost cells.

The effect of impact distance on the degree of cell breakage was studied, with results illustrated in Figure 4.11. In all cases the discharge velocity was fixed at 49 m.s^{-1} whilst the impact surface was positioned at different distances from the capillary ranging from 10 to 300 mm. A gradual increase in breakage is observed as impact distance increases, with maximum breakage occurring at an impact distance of 100 mm. With long impact distances, e.g. 300 mm, there is an observed decrease in degree of cell breakage.

It is possible to estimate the lengths of both the X_c and X_b regions of the fluid stream emerging from the capillary tip (Equation 10 and 12) (Figure 3.1). For a capillary with a nozzle diameter of 0.33 mm and a discharge velocity of 49 m.s^{-1}, X_c and X_b are estimated to be 28 mm and 99 mm respectively. The match of X_b with the distance at which maximum breakage occurs implies that the jet break-up into droplets may be a key mechanism in causing cell disruption.

TEM images presented in Figure 4.12 illustrate the changes that occur when passing the cells through the capillary device and impacting onto the stainless steel stub at different impact distances. According to Figure 4.11, cells impacted at 20 mm distance incur a relatively small amount of cell breakage, which is also evident in Figure 4.12A, depicted by the presence of a high proportion of fully intact cells, and only a minority of partially empty cells. Further increases in impact distance from 60 mm (Figure 4.12B) to 100 mm (Figure 4.12C) result in further observed cell damage represented by receding cell membranes, loss of cytoplasmic density and the existence of ghost cells. Hence, the trends observed in the TEM images demonstrate a strong consistency with the data distribution seen in Figure 4.11, whereby the degree of cell

breakage becomes more significant with increased impact distance up to the break-up point (X_b).

4.2 USD mimic of pilot-scale centrifuge discharge

4.2.1 Calibration of USD mimic of CSA-1 pilot-scale discharge recovery

Aliquots of frozen (-80°C) DH5α *E. coli* cell suspensions prepared from the same fermentation run were used to ensure consistent material was available for the initial calibration studies. Cell suspensions were processed through the USD capillary device for a range of discharge velocities with the discharge jet impacting on a stainless steel surface positioned at a distance of 90 mm. Multiple aliquots of the same cell suspension were processed through a CSA-1 disc-stack centrifuge. Cells recovered from the bowl (i.e. cells not discharged) showed no breakage.

The cell breakage accumulated from impact at high velocity is assumed to be proportional to KU^n, where K is a constant, U is the discharge velocity and n is 1 (assuming a linear relationship between cell breakage and discharge velocity (Chan et al., 2006)). The data in Figure 4.13 is presented on a log log axis with a linear least best fit line drawn through both large and small scale data with n constrained to 1. An overlap of the two correlations is not expected considering the different geometries of the USD and the disc-stack discharge systems and differences in the impact distance and angle. Hence a calibration factor of $K_{(CSA-1)}$, i.e. $U_c = 1.54U_p$, where $K_{(CSA-1)}$ equals 1.54 is used to correlate the results of the USD device with the full-scale CSA-1 centrifuge.

4.2.2 USD mimic of CSA-1 pilot-scale discharge recovery

Figure 4.14 is a log log plot showing the cell breakage for various freeze-thawed *E. coli* batches exposed to impact with a USD capillary discharge velocity range up to 85 m.s^{-1}. A linear least best fit line, where n is 1, is extrapolated from each set of data and is used to predict pilot-scale recovery for the same material. Cells from the same

120

batch were processed through the centrifuge with the discharge condition adjusted using the calibration factor of $K_{(CSA-1)}$ to account for differences between both scales. The pilot-scale recovery data over a velocity operating range of 56 to 82 $m.s^{-1}$ compares well with USD predictions for differently prepared material.

The application of the method to predict the recovery of fresh DH5α (450 L) and fresh W3110 (20 L) *E. coli* cells immediately after a fermentation is also evaluated (Figure 4.15). An approximately linear correlation is again observed between cell breakage and increasing USD discharge velocity which when extrapolated gives reasonable agreement with results for cells recovered in the disc stack centrifuge. Here the lower extent of cell breakage when handling fresh rather than frozen cells is successfully predicted.

4.2.3 USD mimic of SC-6 pilot-scale discharge recovery

The effect of a different centrifuge scale/design on cell breakage was also studied as shown in Figure 4.16. The cell breakage for freeze-thawed (from -80°C) DH5α *E. coli* cells is obtained for a USD discharge velocity range up to 85 $m.s^{-1}$. A linear least best fit line is drawn through the USD data with n constrained to 1.

Considering the difference between the CSA-1 and SC-6 design, a new calibration factor is required for a successful USD mimic. Aliquots of the same cell suspension were discharged in the SC-6 over a velocity range of 85 to 132 $m.s^{-1}$ with the results recorded on the log log plot in Figure 4.16. The same principle of line of least best fit with n having a value of 1 is used. A calibration factor $K_{(SC-6)}$ of 2.95 is used to align SC-6 data to USD results. The accuracy of this formula is verified by predicting the recovery of a fresh W3110 *E. coli* batch as shown in Figure 4.17. Small-scale results are plotted on a log log graph with a line of least best fit where n is 1. The line is extrapolated to predict large-scale recovery of the same material. To verify the prediction cells were processed through both the CSA-1 and SC-6 centrifuges with the data subsequently adjusted with calibration factors $K_{(CSA-1)}$ or $K_{(SC-6)}$.

The parity plot in Figure 4.18 is used to compare all measured % cell breakage from large scale centrifuge runs with the predicted % cell breakage obtained from running the USD capillary device. The dashed line, with slope of 1, represents a 100% mimic accuracy. The majority of data lies close to the dashed line illustrating a good agreement between measured and predicted cell breakage. In addition the parity plot demonstrates the robustness of the mimic with reasonably accurate predictions of both fresh and freeze thawed material.

ELISA analysis was carried out on all W3110 *E. coli* cell samples in this thesis to detect release of antibody fragments. Negligible release was reported for all small-scale and CSA-1 conditions. However, recovery of W3110 cells in larger centrifuges begins to illustrate the negative effects that discharge has on loss of product as shown in Figure 4.19. In Figure 4.19 there is clear evidence of greater loss of product with higher discharge velocities as seen with the SC-6. The data also shows the effectiveness of reducing velocity before discharge on product recovery with the difference in % product loss observed between the highest and lowest SC-6 discharge condition to be approximately 5 %.

4.2.4 Effect of impact on cell physiology

The effect of impact at high discharge velocity on cell damage was further analysed using flow cytometry. Figure 4.20 examines physiological changes to W3110 *E. coli* cells processed through the USD capillary device to mimic discharge at the lowest CSA-1 centrifuge speed. Propidium iodide (PI) and bis-oxanol (BOX) stains were used for cell examination, providing information on the integrity and polarity of a cell respectively. Each plot in Figure 4.20 is divided into 4 quadrants to allow for general characterisation of cells. Quadrant F1 represents permeabilised cells staining positively with PI, quadrant F2 represents dead cells staining positively with both PI and BOX, quadrant F3 represents healthy cells with no staining and quadrant F4 represents depolarised cells staining positively with BOX. Figure 4.20A shows the physical state of W3110 *E. coli* cells immediately after a 20 L fermentation. The majority of cells (91.3%) are characterised as intact and metabolically active, i.e. PI and BOX negative, with only 0.6% of cells in quadrant F2 i.e. dead cells. The main change as a result of discharge is an increase in the number of cells stained BOX

positive from 4.9% to 22.3% and thus reducing the number of healthy cell entities to 76.2% (Figure 4.20B). There is no evidence of cell permeabilisation, i.e. no PI response immediately after impact. Storing the processed samples at room temperature (25°C) for 1 h (Figure 4.20C) and 2 h (Figure 4.20D) yields a further small drop in the number of healthy cells, i.e. healthy cell numbers decrease from 76.2% to 73.4% after 2 h holding time. The depolarised (i.e. damaged) cells, generated by impact, are more sensitive than healthy cells to storage showing significant signs of degradation over the 2 h holding period with the number of cells staining both PI and BOX positive observed to increase from 0.6% to 6.8% and 8.1% after 1 h and 2 h storage respectively.

Flow cytometry was also used to compare the nature of cell damage by discharge from the CSA-1 pilot-scale centrifuge and USD capillary device. Figure 4.21A denotes fresh DH5α *E. coli* cells after a 450 L fermentation with 87% of cells in the feed characterised as healthy and 2.4% reported to be dead. The changes in cell physiology as a result of discharge from the disc-stack centrifuge (Figure 4.21B) and the USD capillary device (Figure 4.21C) are similar with cells from the healthy population observed to spread across into quadrant E4 and show signs of depolarisation. The number of dead cells is observed to increase from 2.4% in the original feed to 7.4% and 11.1% for pilot-scale centrifuge discharge and USD capillary discharge respectively.
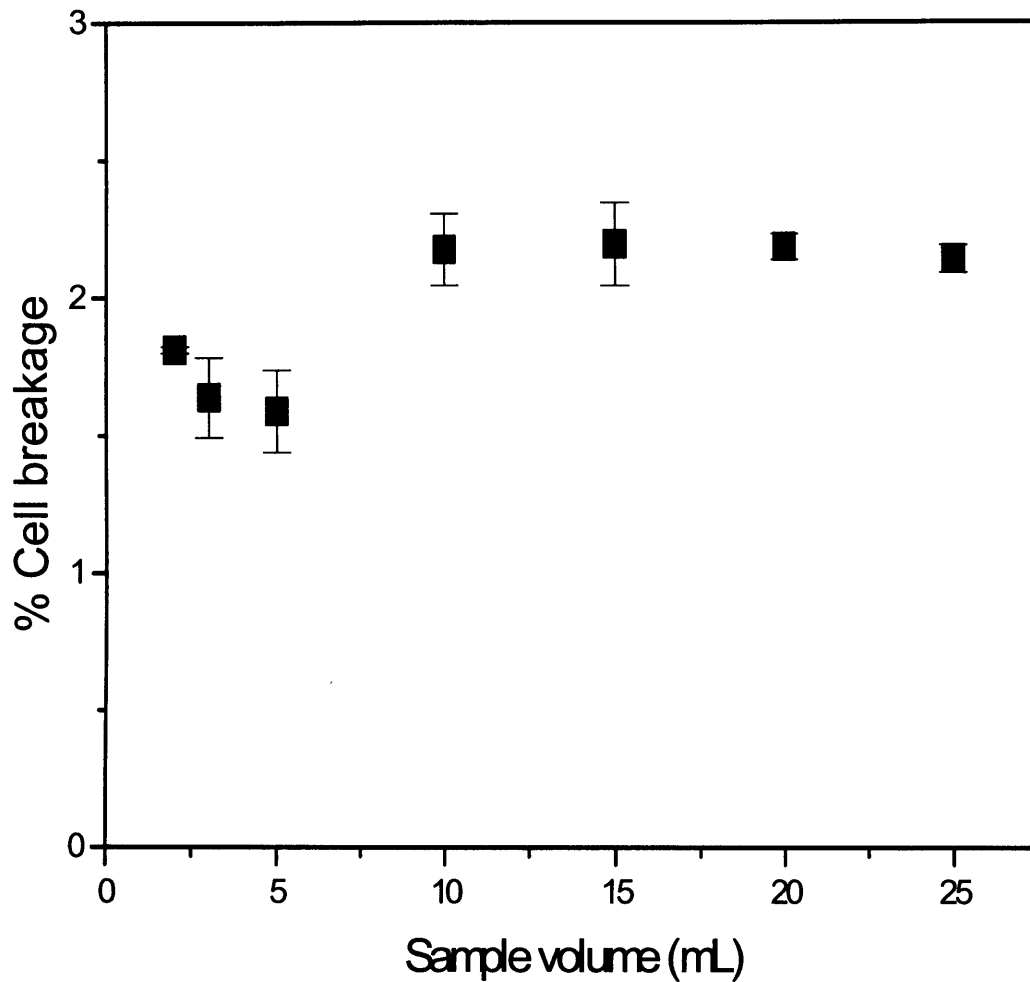
Figure 4.1   DH5α *E. coli* cell breakage as a function of capillary sample volume size. Sample viscosities were fixed at 0.005 $N.s.m^{-2}$ with a capillary shear rate, residence time and velocity of 3.96 x $10^5 s^{-1}$, 0.0016 s and 31 $m.s^{-1}$ respectively. Samples were impacted on a stainless steel target positioned at 90 mm from the capillary tip. All experiments were performed in triplicate.
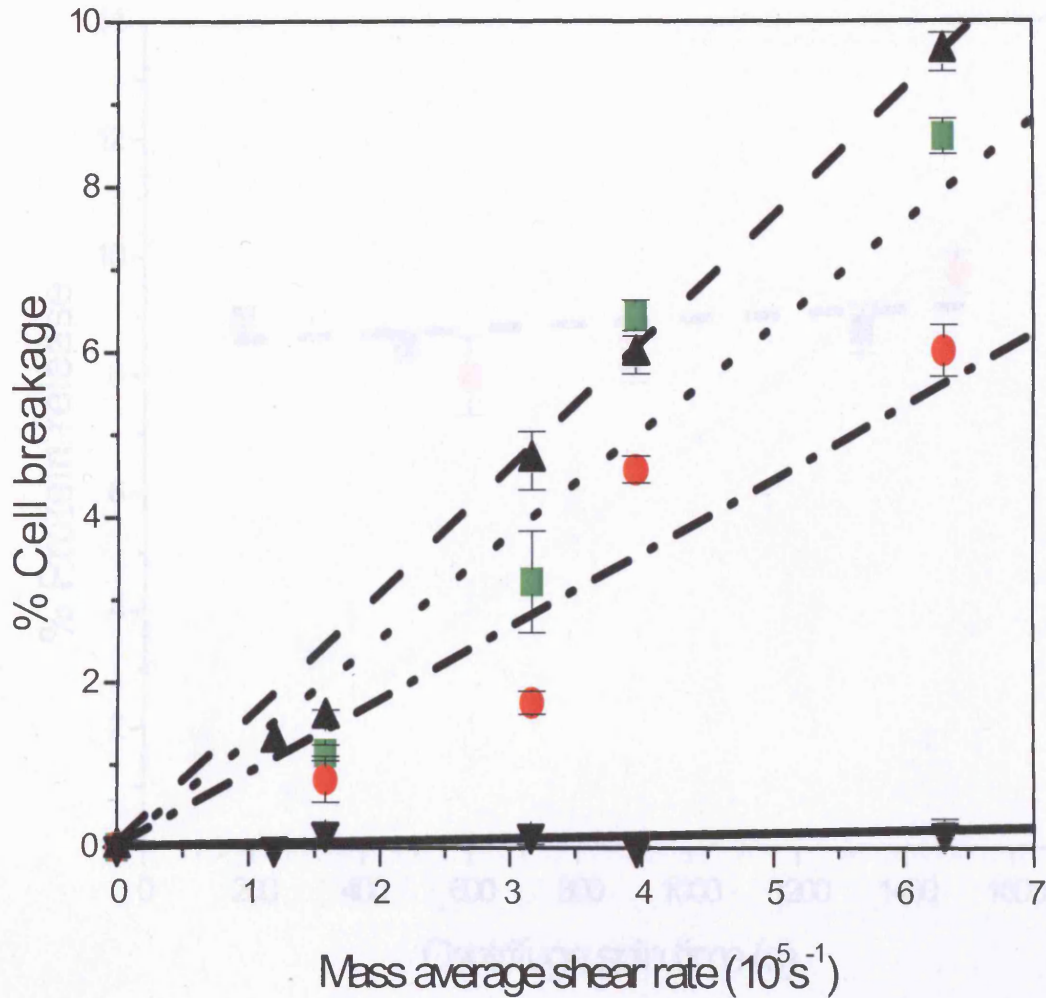
Figure 4.2   DH5α *E. coli* cell breakage as a function of mass average shear rate. Impact effects were avoided by collecting samples in a head of buffer at 300 mm distance from the capillary exit. Viscosity was fixed at 0.005 N.s.m^{-2} (Newtonian) with laminar flow conditions. The residence time and correlation co-efficient (R^2) are: (▲) 0.024 s, 0.98; (■) 0.012 s, 0.90; (●) 0.006 s, 0.84; (▼) 0.004 s, 0.98. Note: A mass average shear rate of 14 x 10^5 s^{-1} with a residence time of 0.00045 s generated 0 % cell breakage.

Figure 4.3   DH5α *E. coli* cell protein release per unit exposure to shear as a function of bench top centrifuge spin time. *E. coli* samples (μ =0.005 N.s.m^{-2}) were exposed to a capillary shear rate of 6 x 10^5 s^{-1} and a residence time of 0.003 s (i.e. three cycles of 0.001 s residence time) and collected in a head of buffer of depth 100 mm. Symbols: (●) Centrifuge rotational speed of 8000 rpm; (■) Centrifuge rotational speed of 12000 rpm. The lack of a significant trend (R^2 of 0.15) indicates that centrifuge spin time does not contribute to cell breakage.
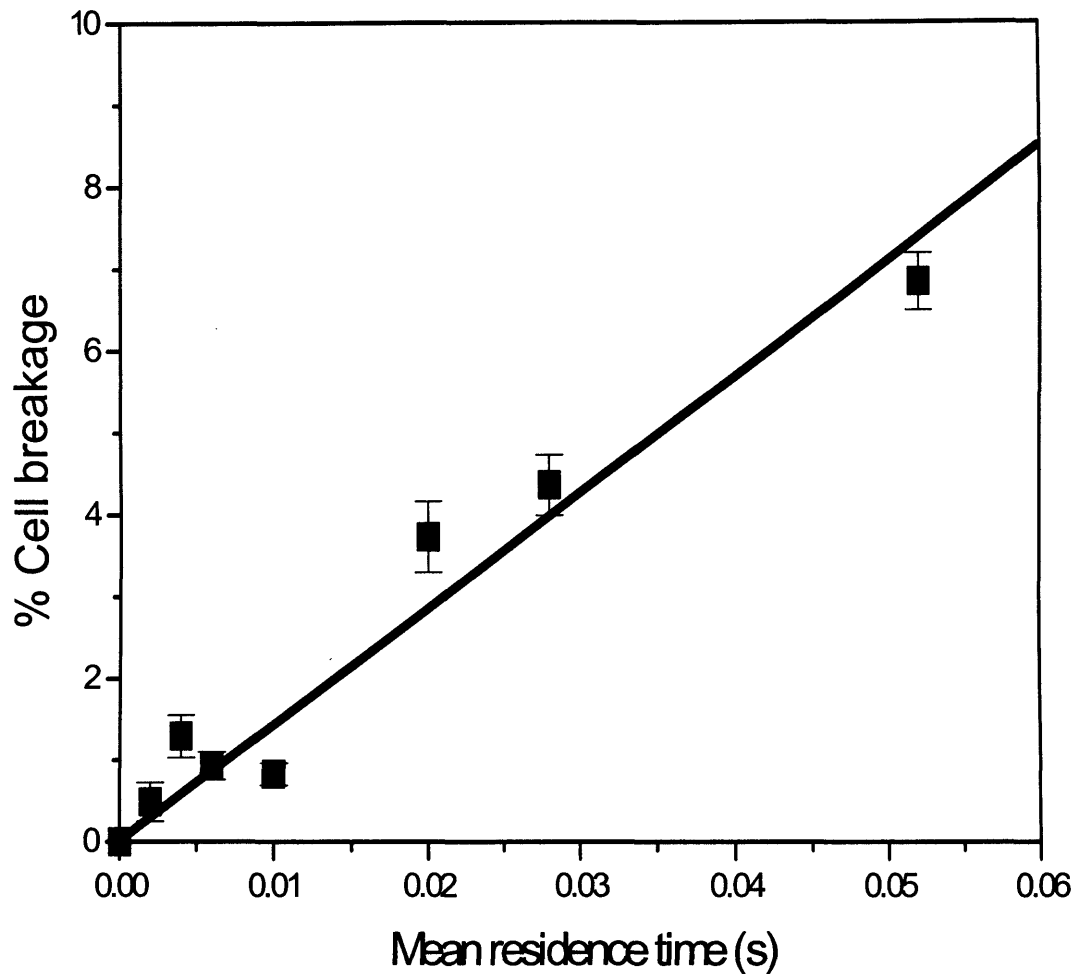
Figure 4.4   DH5α *E. coli* cell breakage as a function of residence time in the capillary. The mass average shear rate was fixed at 3.16 x 10^5 s^{-1}. Impact effects were avoided by collecting samples in a head of buffer at 300 mm impact distance from the capillary. Viscosity was fixed at 0.005 N.s.m^{-2} (Newtonian) with laminar flow conditions. Regression analysis (R^2) for the line of best fit was 0.94.
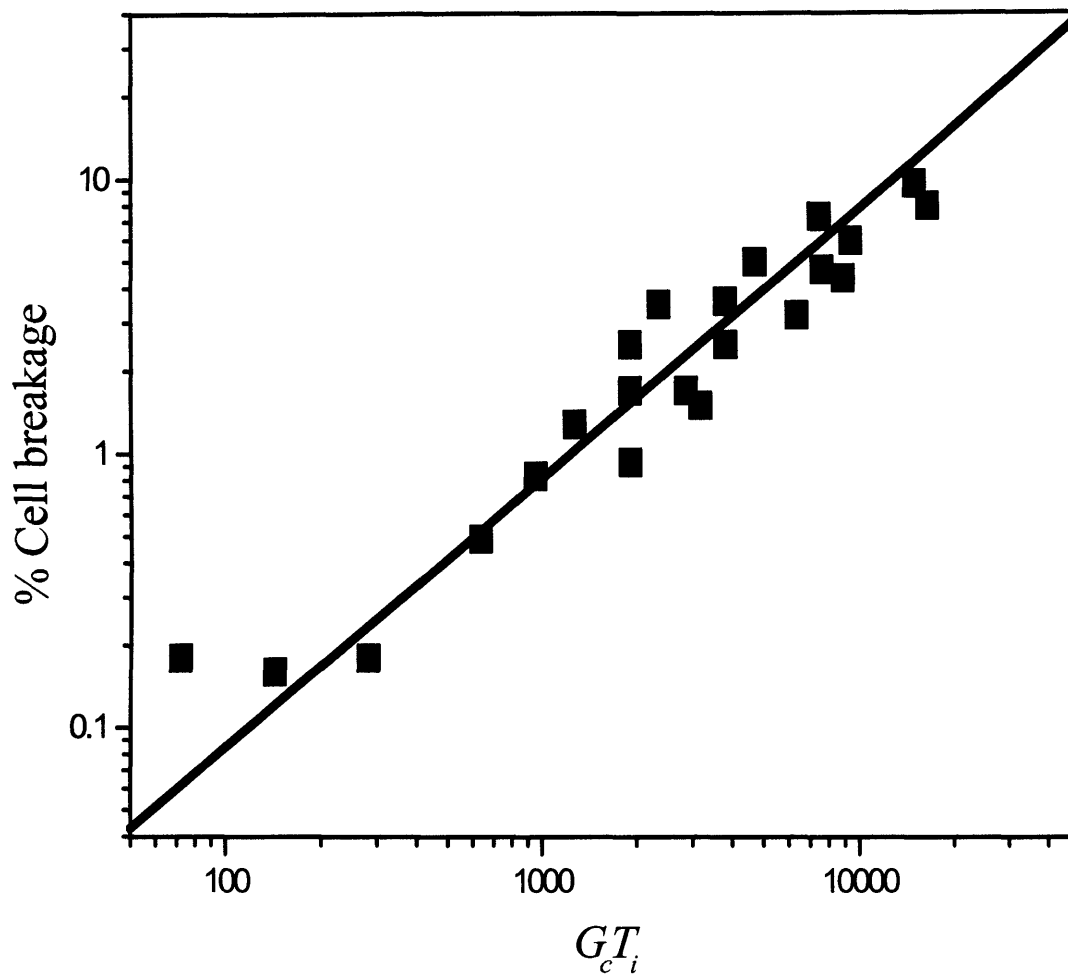
Figure 4.5   DH5α *E. coli* cell breakage as a function of the product of mass average shear rate and residence time (G_cT_i). Regression analysis (R^2) for the line of best fit was 0.9 (% cell breakage α $(G_cT_i)^n$, n = 1).
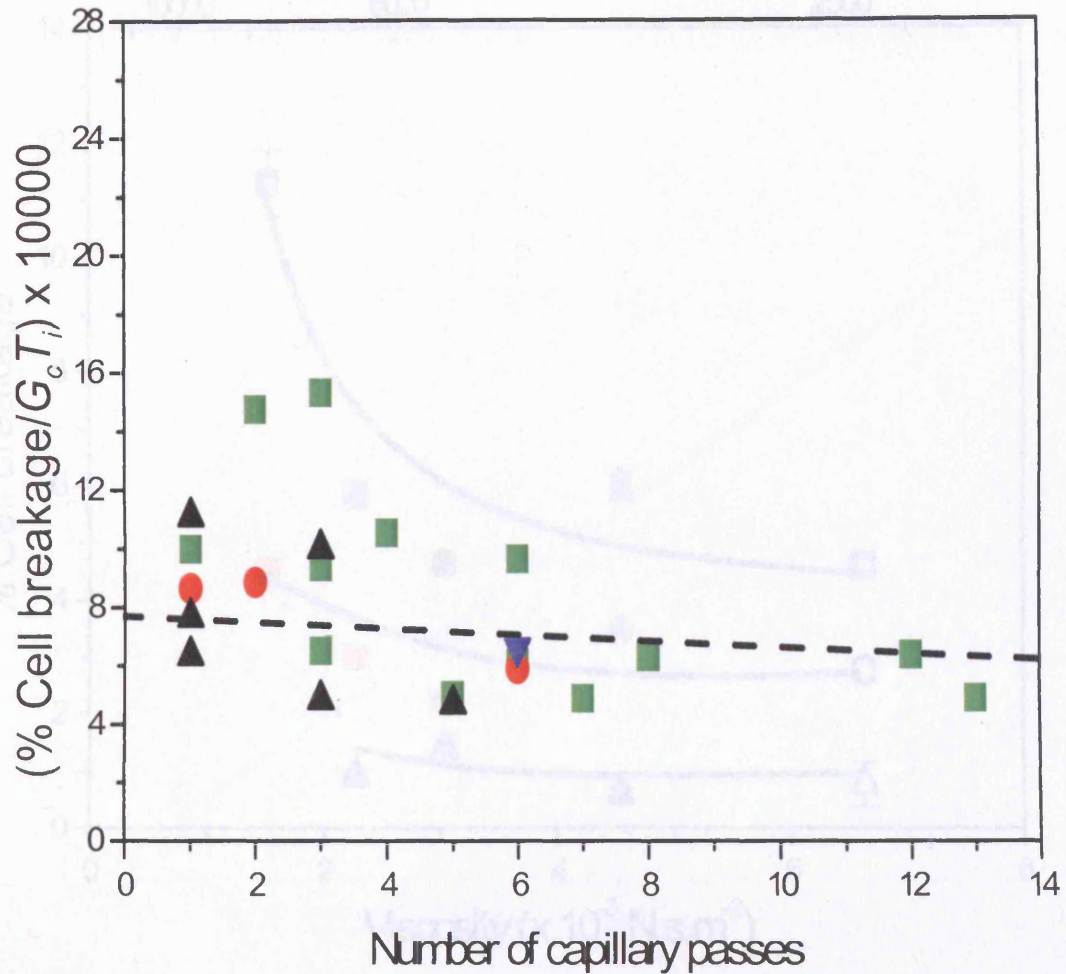
Figure 4.6   DH5α *E. coli* cell breakage per unit exposure to shear (G_cT_i) as a function of the number of capillary passes to explore if entrance or exit effects made a significant contribution to the breakage. A range of capillary lengths were tested, with processed samples collected in a head of buffer positioned at 300 mm distance from the capillary. The capillary length and internal diameter are: ($\blacksquare$) 100 mm, 0.33 mm; ($\bullet$) 75 mm, 0.33 mm; ($\blacktriangle$) 50 mm, 0.33 mm; ($\blacktriangledown$) 75 mm, 0.575 mm. The lack of a significant trend in the least squares best fit (---) (R^2 of 0.26) indicates breakage is due to shear in the capillary rather than due to entrance and exit effects.
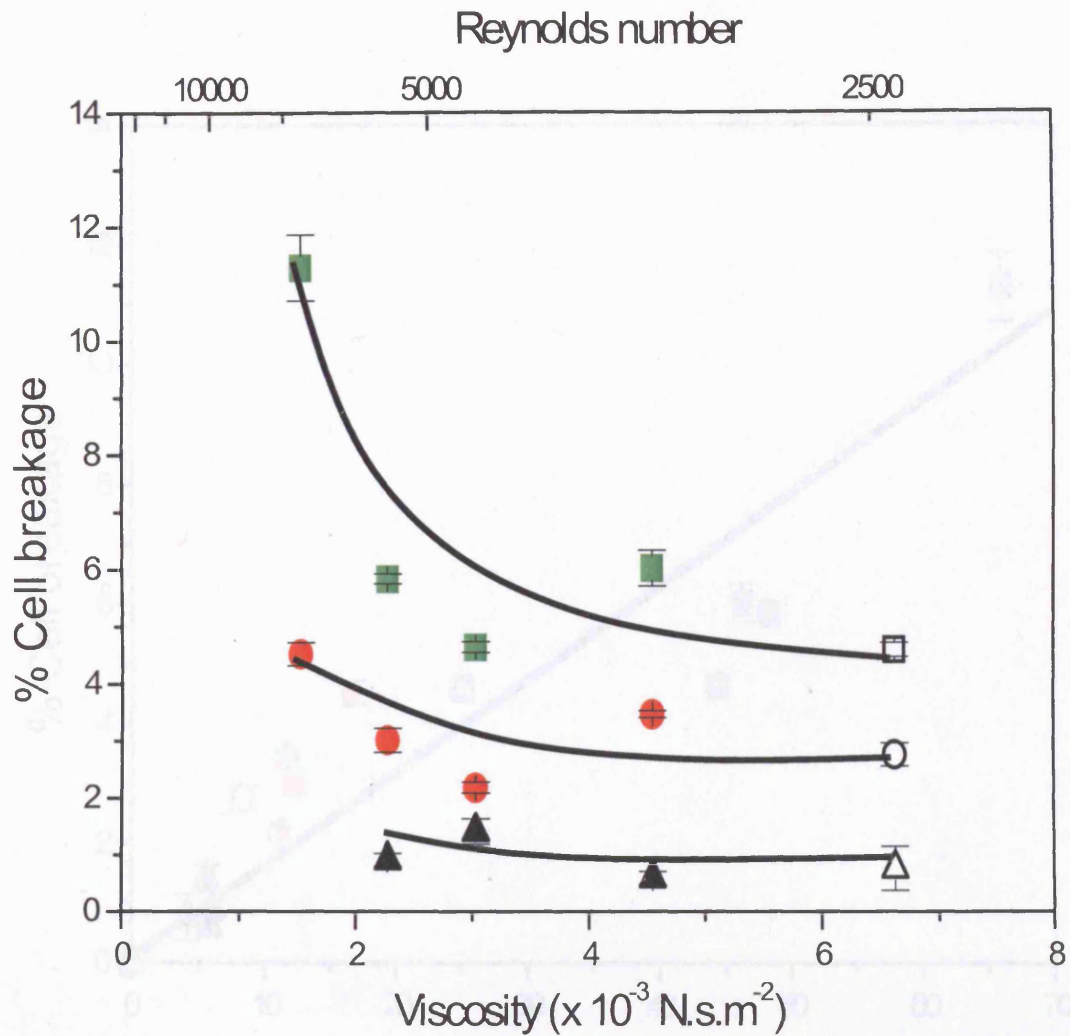
Figure 4.7   Effect of varying viscosity and hence Reynolds number (Re) on DH5α *E. coli* cell breakage at a fixed shear rate of 6.3 x 10^5 s^{-1}. Impact effects were avoided by collecting samples in a head of buffer at 300 mm distance from the capillary exit. Mean residence time: (■, □) 0.006 s; (●, ○) 0.002 s; (▲, △) 0.001 s under (□, ○, △) laminar and (■, ●, ▲) turbulent capillary flow regimes. Lines drawn are best fit by eye.
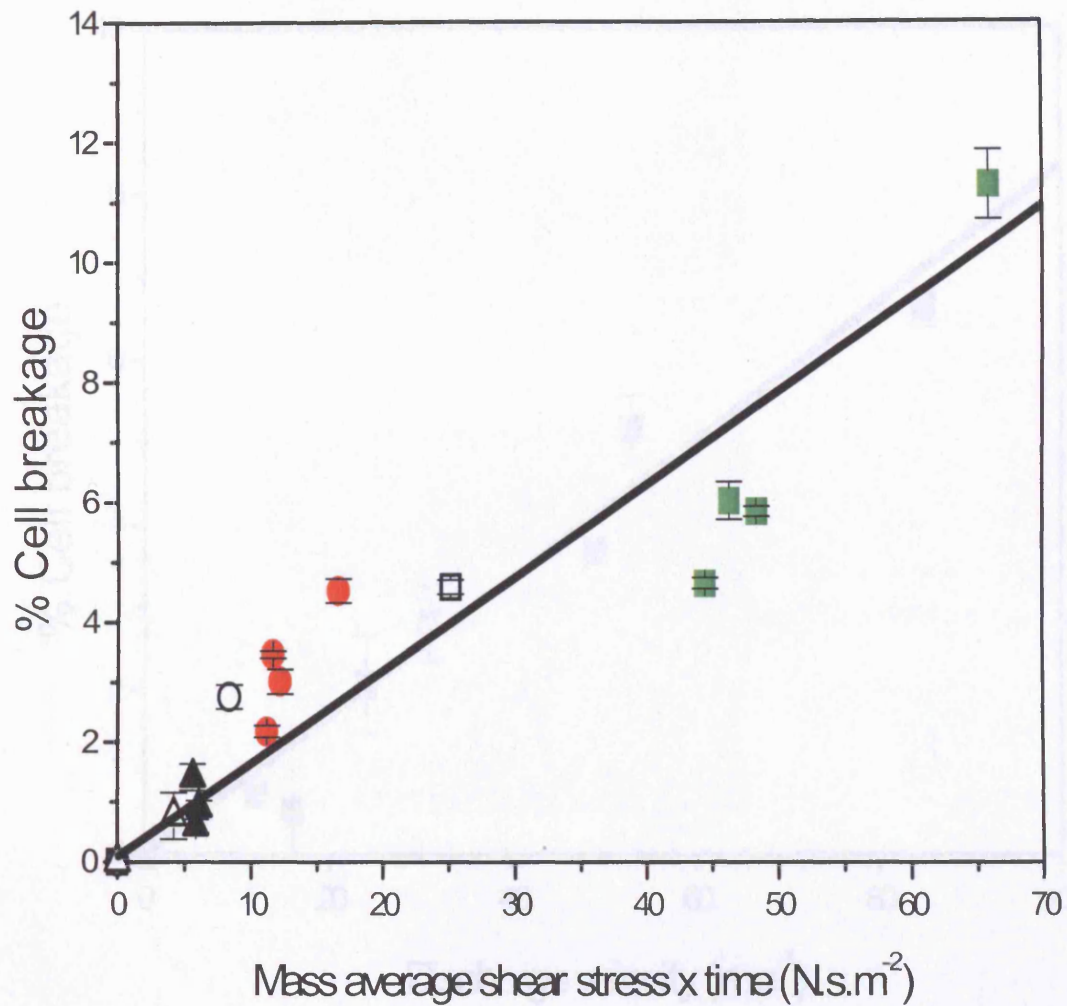
Figure 4.8   Effect of varying the product of mass average shear stress and exposure time on DH5α *E. coli* cell breakage under (□, ○, Δ) laminar and (■, ●, ▲) turbulent capillary flow regimes (R^2 of 0.82). Residence time: (■, □) 0.006 s; (●, ○) 0.002 s; (▲, Δ) 0.001 s.
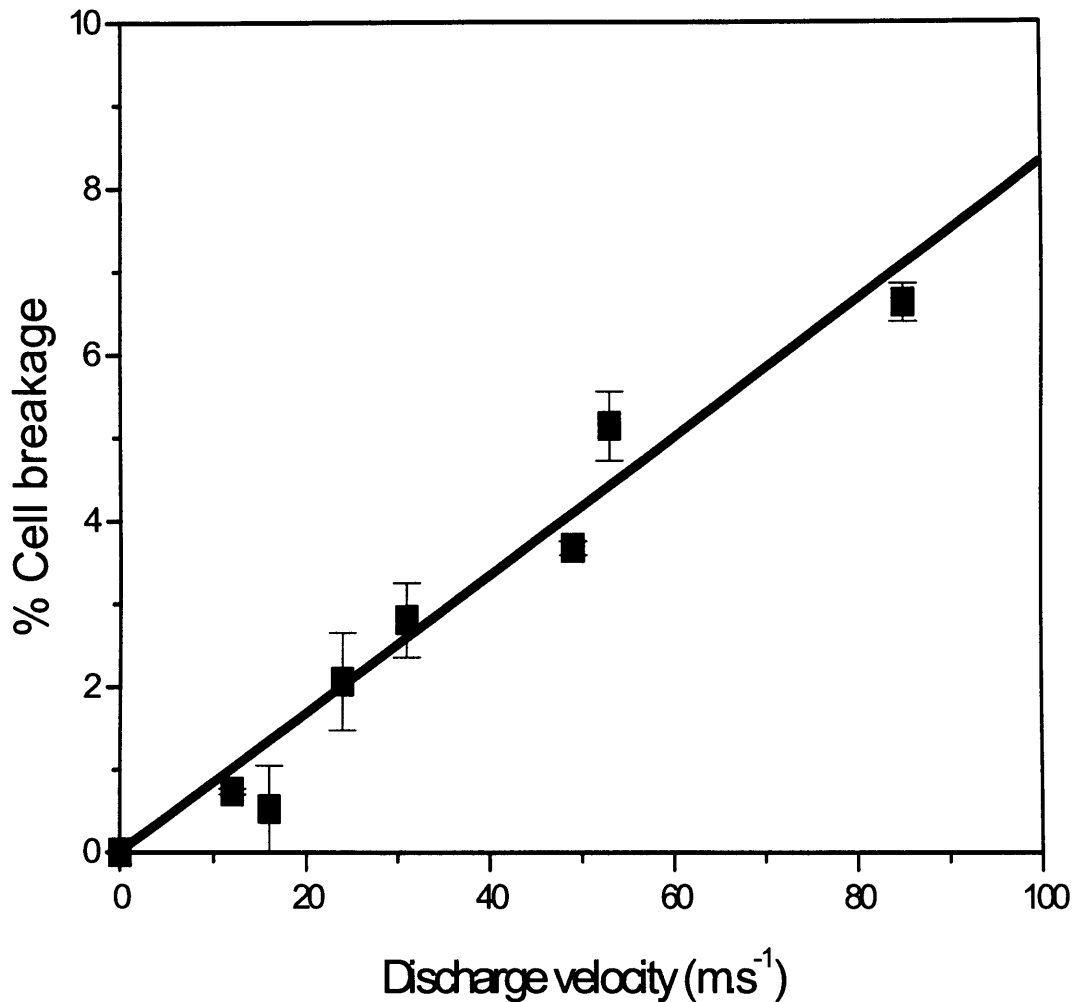
Figure 4.9   DH5α *E. coli* cell breakage as a function of discharge velocity. In all cases a stainless steel stub was fixed at an impact distance of 90 mm from the tip of the capillary. Viscosity was fixed at 0.005 N.s.m^{-2} (Newtonian) with laminar flow conditions. G_cT_i was maintained below 646 to eliminate capillary cell breakage. The results demonstrate a steady growth in cell breakage as the discharge velocity is increased. Regression analysis (R^2) for the line of best fit was 0.95.
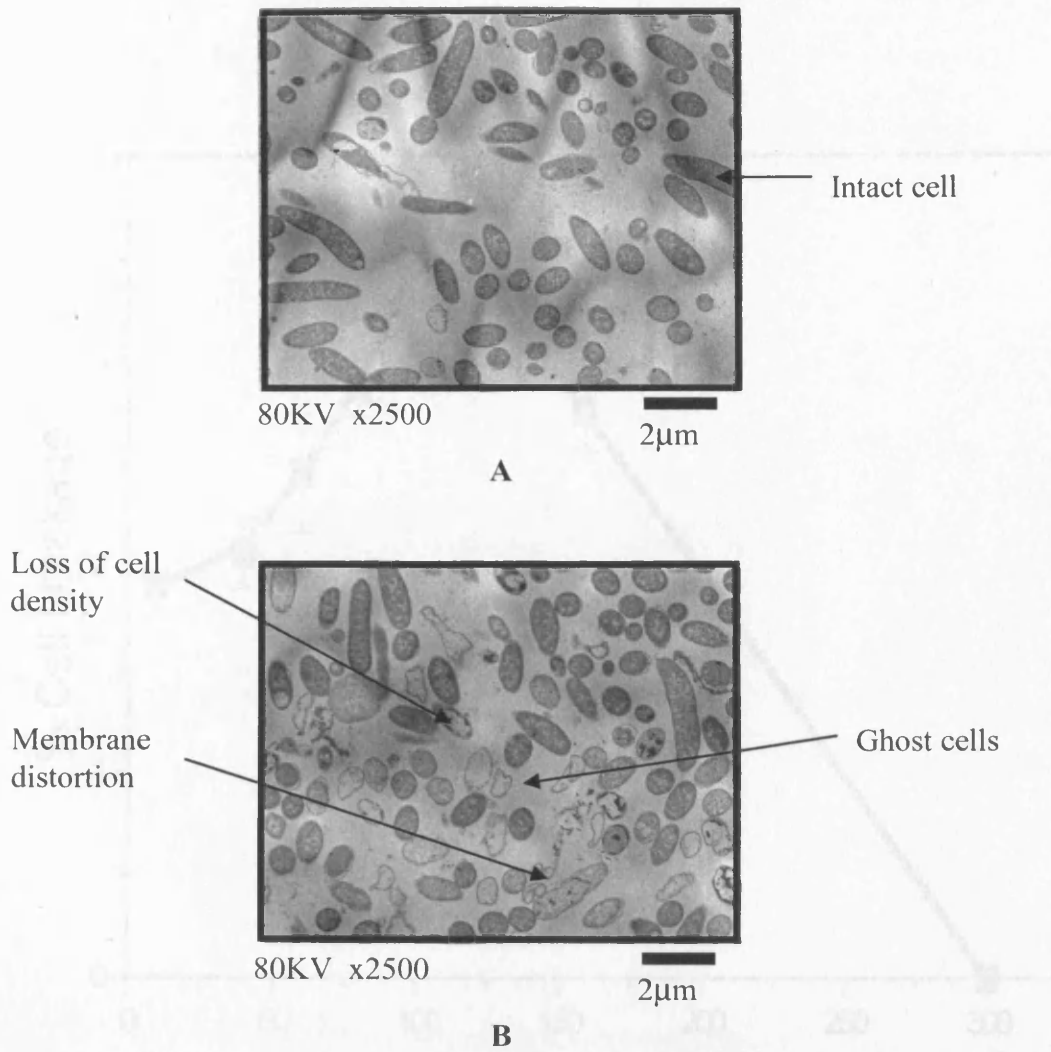
Figure 4.10   Representative (5 cm^2) cross-sectional TEM images of DH5α *E. coli* cells discharged at velocities of (A) 12 m.s^{-1} and (B) 85 m.s^{-1} onto a stainless steel stub fixed at an impact distance of 90 mm.   Samples A and B were exposed to a $G_cT_i < 646$.
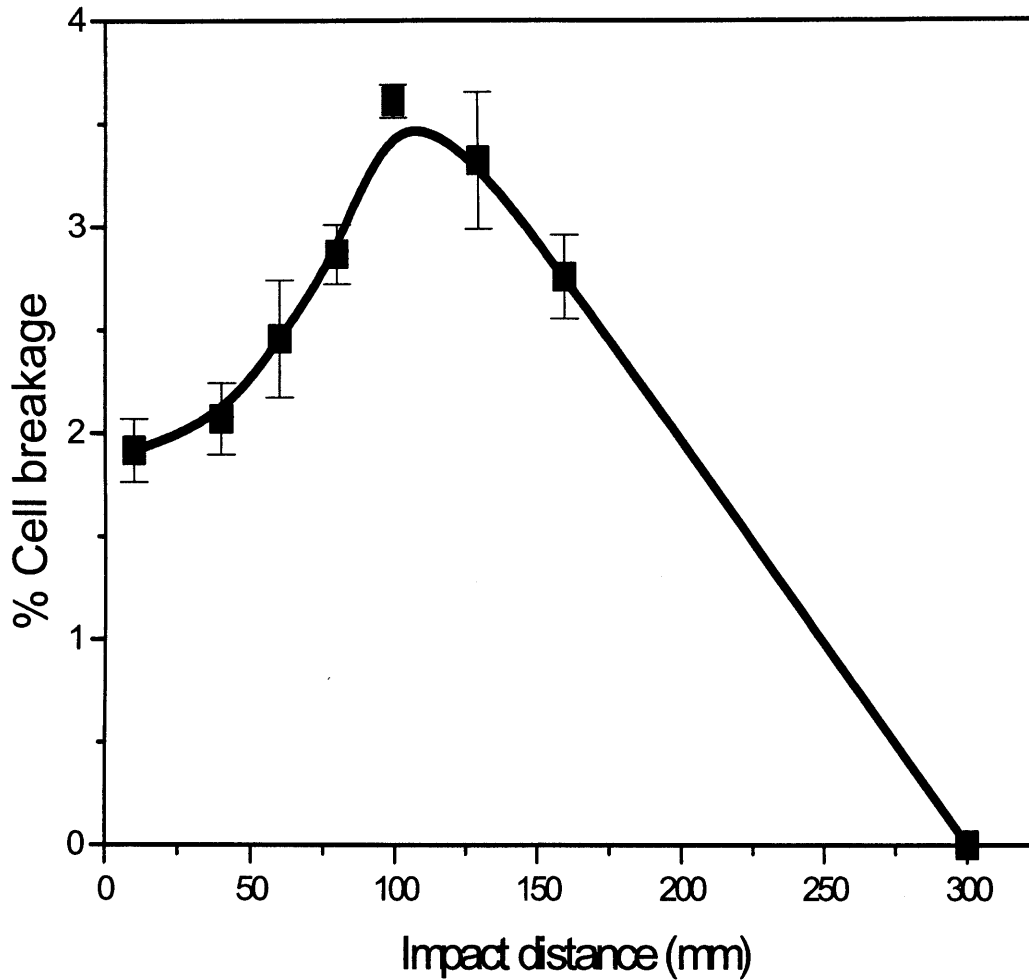
Figure 4.11   Effect of changing the stainless steel stub impact distance on DH5α

E. coli cell breakage. Impact velocity and G_cT_i were fixed at 49 m.s^{-1}

and below 646 respectively. Viscosity was fixed at 0.005 N.s.m^{-2}

(Newtonian) with laminar flow conditions. Note: The data point at

impact distance 300 mm was the result of collecting the jet in a head of

buffer. Line drawn is best fit by eye. Each point is the average of

triplicate runs; range is 95% confidence fit.

Intact cell

80KV x2500   A   2µm

Receding cell membrane

80KV x2500   B   2µm

Loss of cell density

Ghost cells

80KV x2500   C   2µm
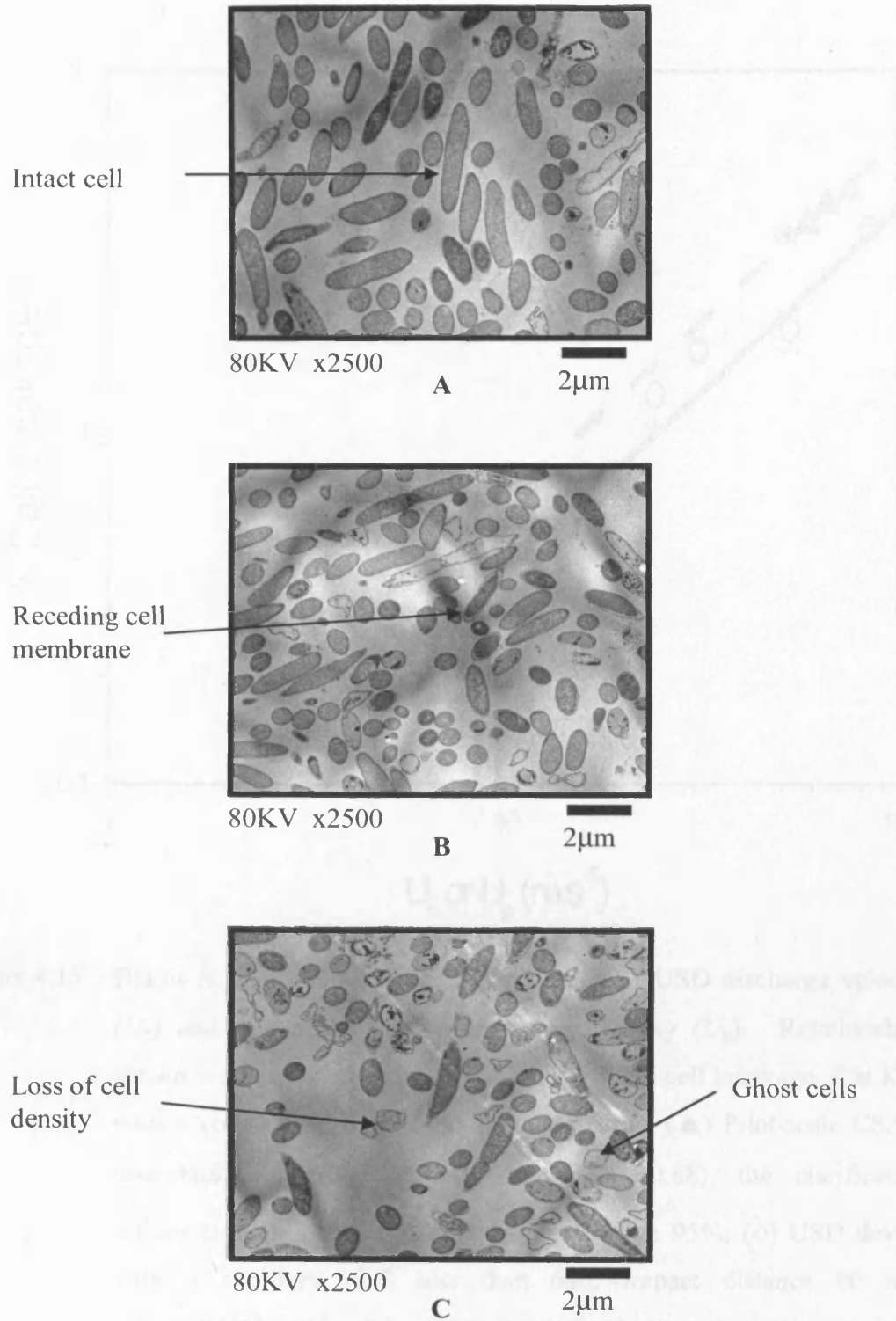
Figure 4.12   Representative (5 cm^2) cross-sectional TEM images of DH5α *E. coli* cells exposed to a G_cT_i of 646 and discharge velocity of 49 m.s^{-1}. Samples were impinged onto a stainless steel stub at an impact distance of (A) 20 mm; (B) 60 mm; (C) 100 mm.
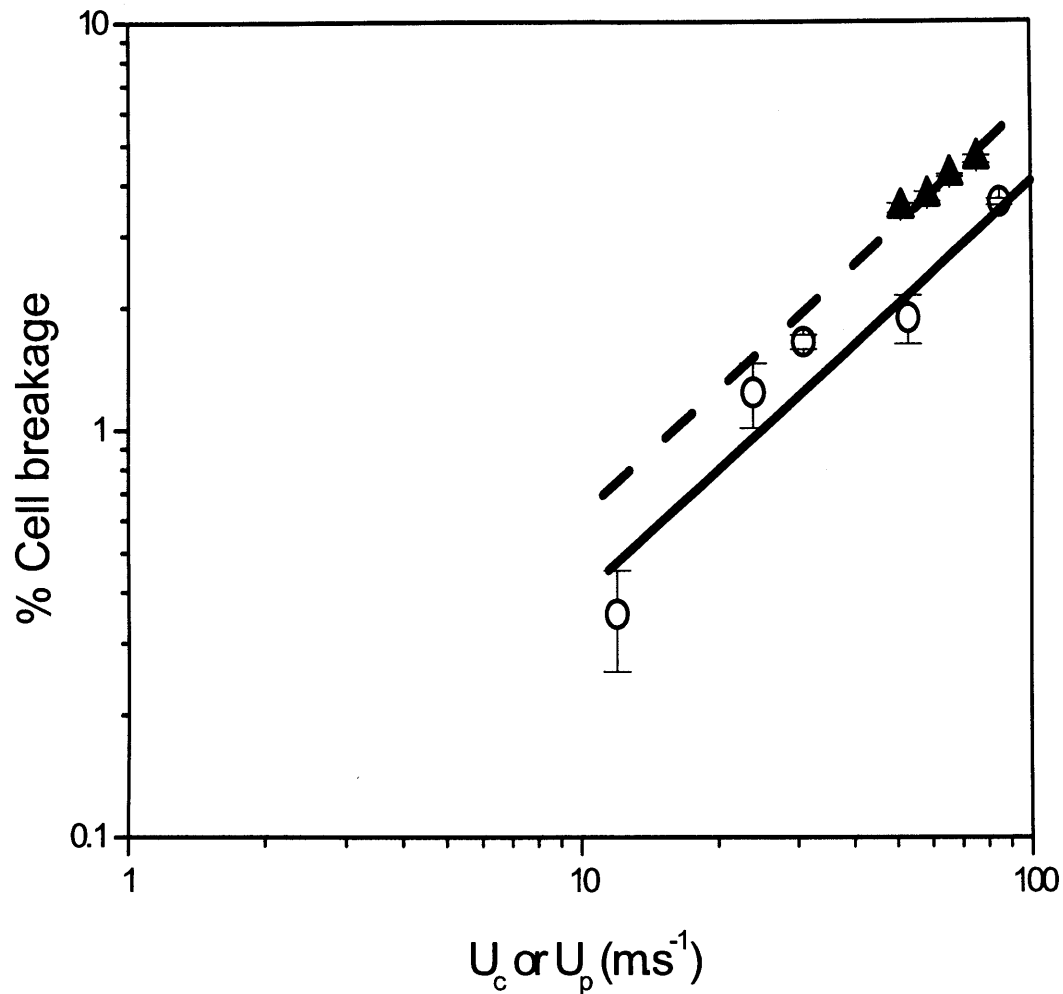
Figure 4.13   DH5α *E. coli* cell breakage as a function of USD discharge velocity
(U_c) and pilot-scale CSA-1 discharge velocity (U_p).   Relationships
shown are least squares best fits of the form % cell breakage, C α KU^n
with n constrained to a value of 1.   Symbols: (▲) Pilot-scale CSA-1
disc-stack centrifuge ($C = 0.063U_p$, $R^2 = 0.88$), the clarification
efficiency at pilot-scale was maintained above 95%; (o) USD device
with a capillary G_cT_i less than 646; impact distance 90 mm
($C = 0.041U_c$, $R^2 = 0.9$).   Pilot-scale and USD experiments were
performed in duplicate and triplicate respectively.   Frozen cells (freeze-
thawed from −80°C) used for calibration purposes.   Calibration factor
to align centrifuge and USD results, $K_{(CSA-1)}=0.063/0.041=1.54$.
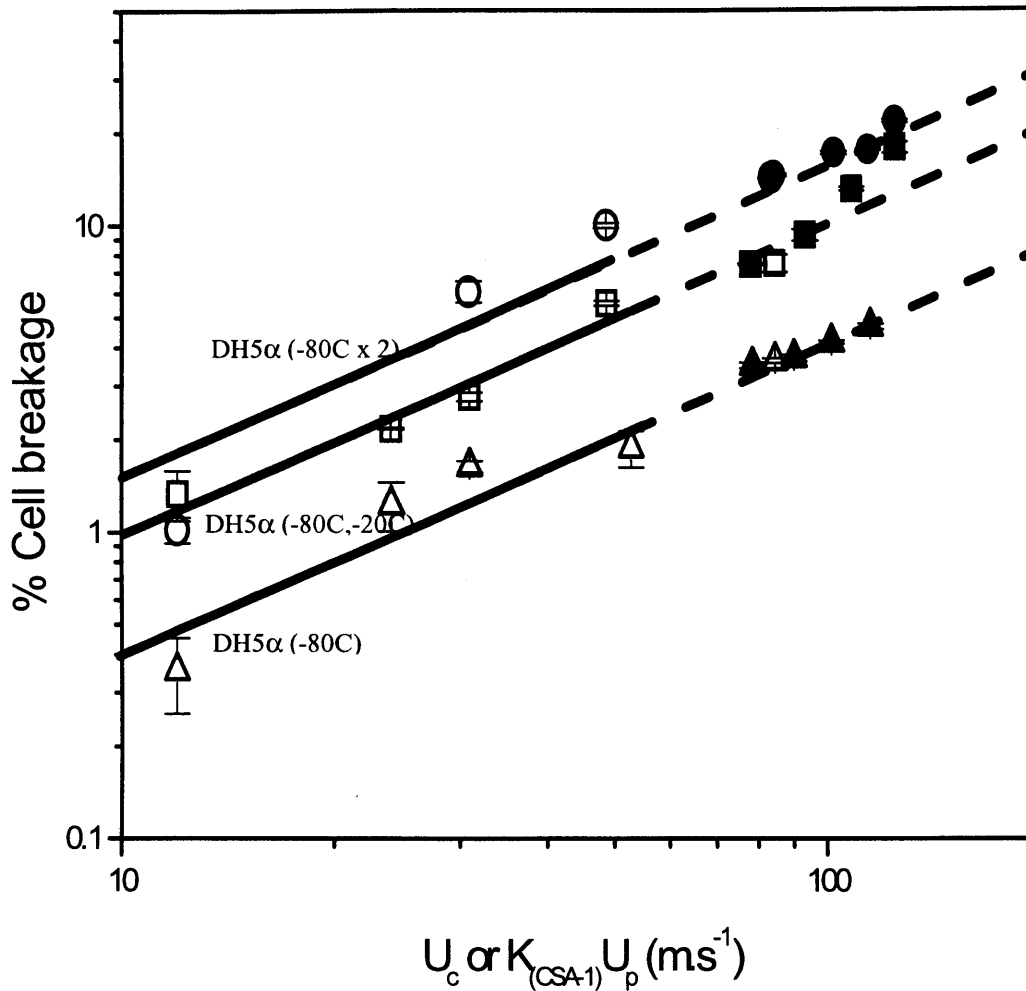
Figure 4.14

DH5α *E. coli* cell breakage as a function of (o, □, Δ) USD discharge velocity (U_c) and (●, ■, ▲) pilot-scale CSA-1 discharge velocity (U_p) with a calibration factor of $K_{(CSA-1)}$, where $K_{(CSA-1)}$ has a value of 1.54. Least squares best fit shown, $C \propto U^n$ with n set at 1: Cell preparation methods: (●, o) DH5α *E. coli* cells freeze-thawed twice from −80°C ($C = 0.154U_c$, $R^2 = 0.968$); (■, □) DH5α *E. coli* cells freeze-thawed twice once from −80°C and then from -20°C ($C = 0.098U_c$, $R^2 = 0.99$); (▲, Δ) DH5α *E. coli* cells freeze-thawed once from -80°C (see Figure 4.13, $C = 0.041U_c$). USD: capillary G_cT_i less than 646; impact distance set at 90 mm. Pilot-scale and USD experiments were performed in duplicate and triplicate respectively.
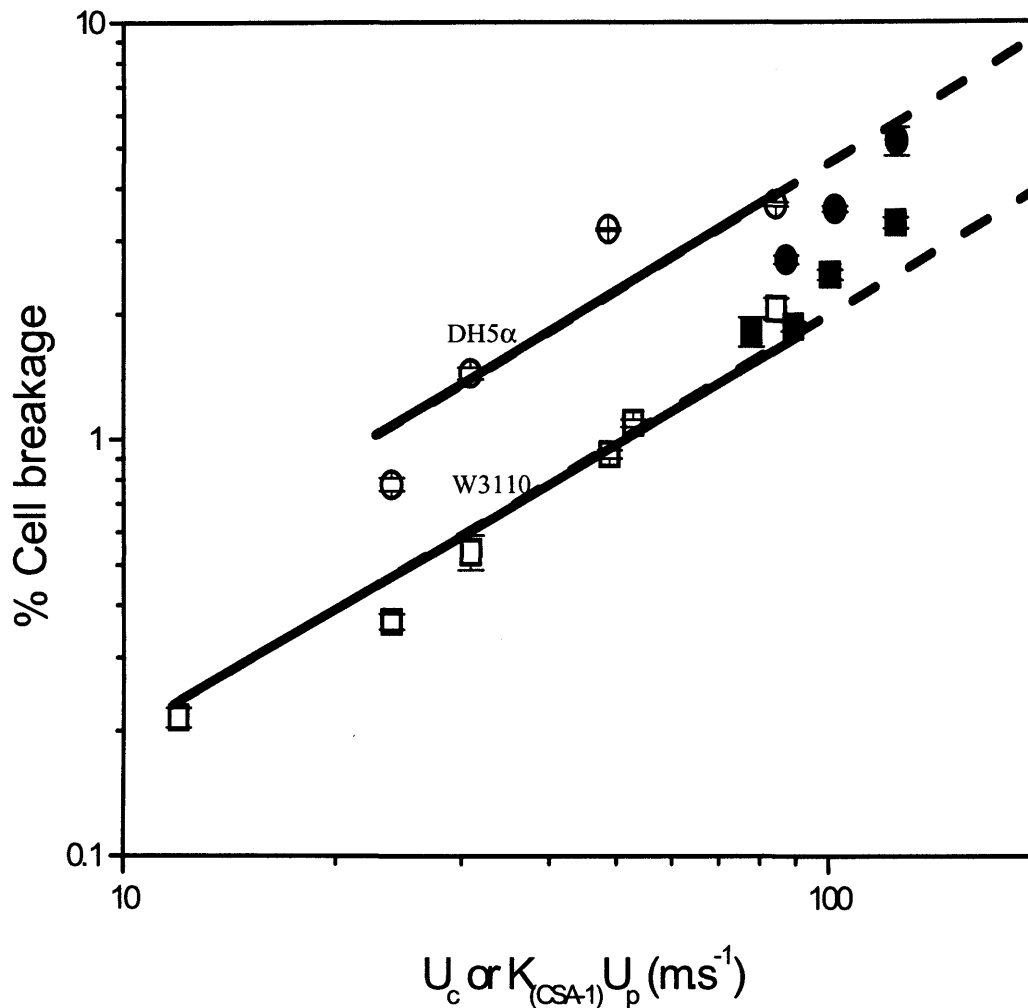
Figure 4.15   Fresh *E. coli* cell breakage as a function of (o, □) USD discharge velocity (U_c) and (●, ■) pilot-scale CSA-1 discharge velocity (U_p) with a calibration factor of $K_{(CSA-1)}$, where $K_{(CSA-1)}$ has a value of 1.54. Symbols: (●, o) fresh DH5α *E. coli* cells (450 L) ($C = 0.045U_c$, $R^2 = 0.92$); (■, □) fresh W3110 *E. coli* cells (20 L) ($C = 0.019U_c$, $R^2 = 0.97$). USD: capillary G_cT_i less than 646; impact distance set at 90 mm. Pilot-scale and USD experiments were performed in duplicate and triplicate respectively.
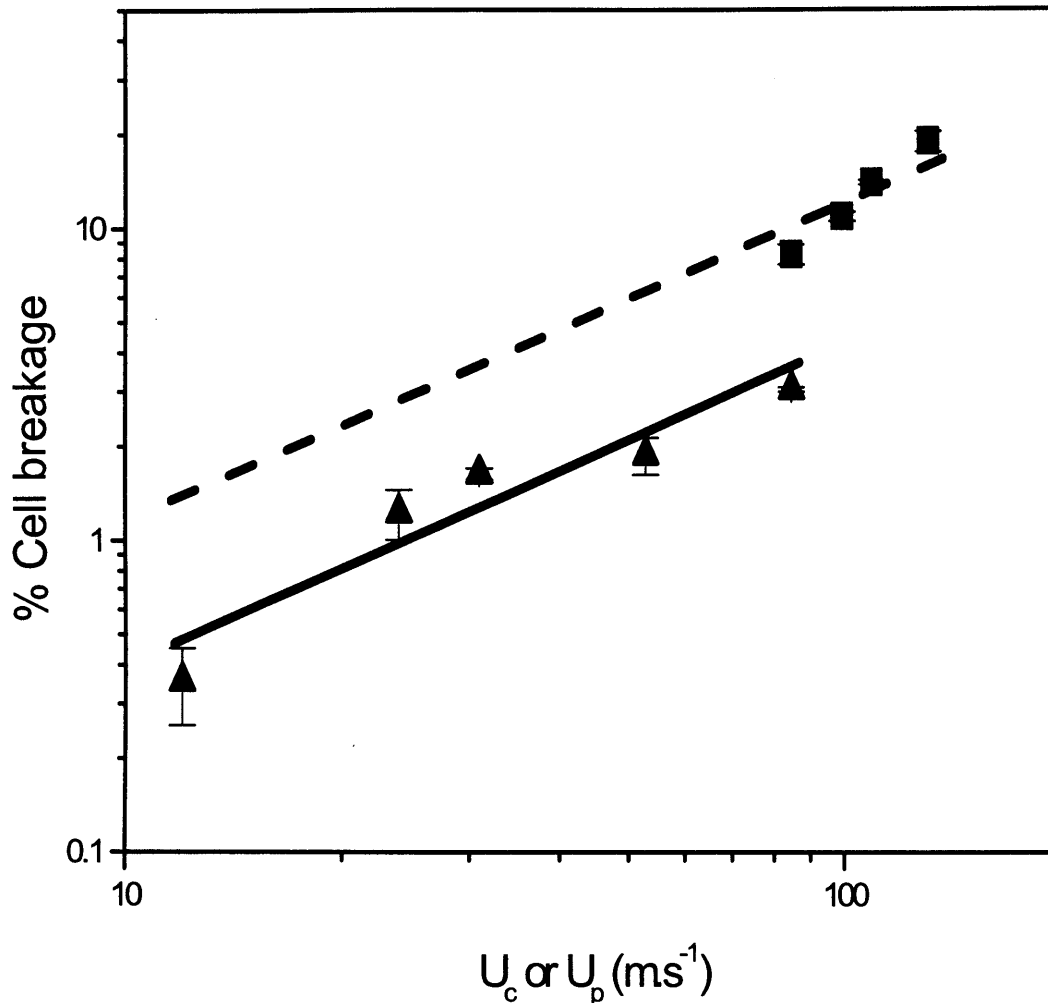
Figure 4.16   DH5α *E. coli* cell breakage as a function of USD discharge velocity (U_c) and pilot-scale SC-6 discharge velocity (U_p). Relationships shown are least squares best fits of the form % cell breakage, C α KU^n with n constrained to a value of 1. Symbols: (■) Pilot-scale SC-6 disc-stack centrifuge ($C = 0.118U_p$, $R^2 = 0.99$); the clarification efficiency at pilot-scale was maintained above 95%; (▲) USD device with a capillary G_cT_i less than 646; impact distance 90 mm ($C = 0.04U_c$, $R^2 = 0.91$). Pilot-scale and USD experiments were performed in duplicate and triplicate respectively. Frozen cells (freeze-thawed from –80°C) used for calibration purposes. Calibration factor to align centrifuge and USD results, $K_{(SC-6)} = 0.118/0.04 = 2.95$.
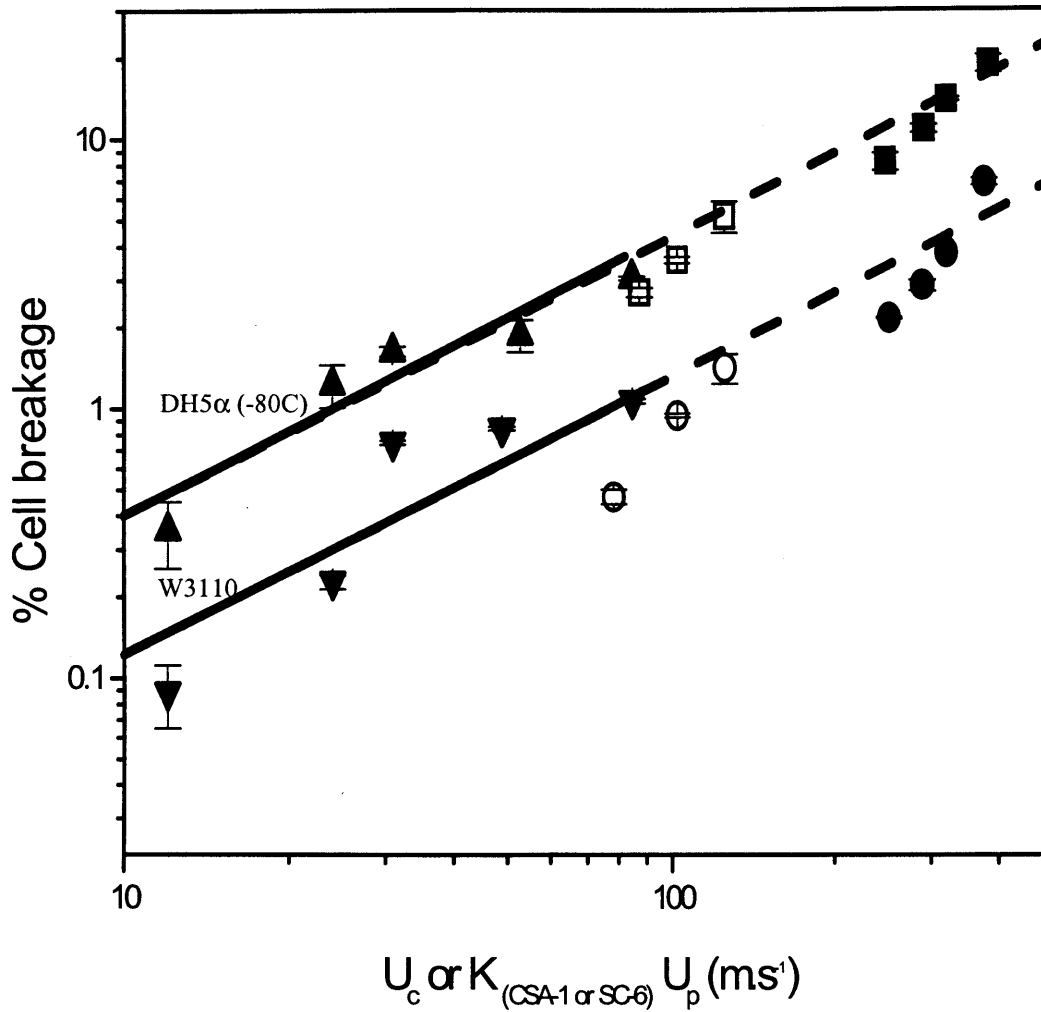
Figure 4.17 Cell breakage of (▲, □, ■) frozen DH5α *E. coli* and (▼, o, ●) fresh
W3110 *E. coli* cells (20 L) as a function of pilot-scale and USD
discharge velocity. Least squares best fit shown, C α U^n with n set at 1.
Symbols: (■, ●) Pilot-scale SC-6 discharge velocity with a calibration
factor of 2.95 ($K_{(SC-6)}$); (□, o) Pilot-scale CSA-1 discharge velocity with
a calibration factor of 1.54 ($K_{(CSA-1)}$); (▲, ▼) USD discharge velocity
($C = 0.04U_c$ for DH5α *E. coli*; $C = 0.013U_c$ for W3110 *E. coli*).
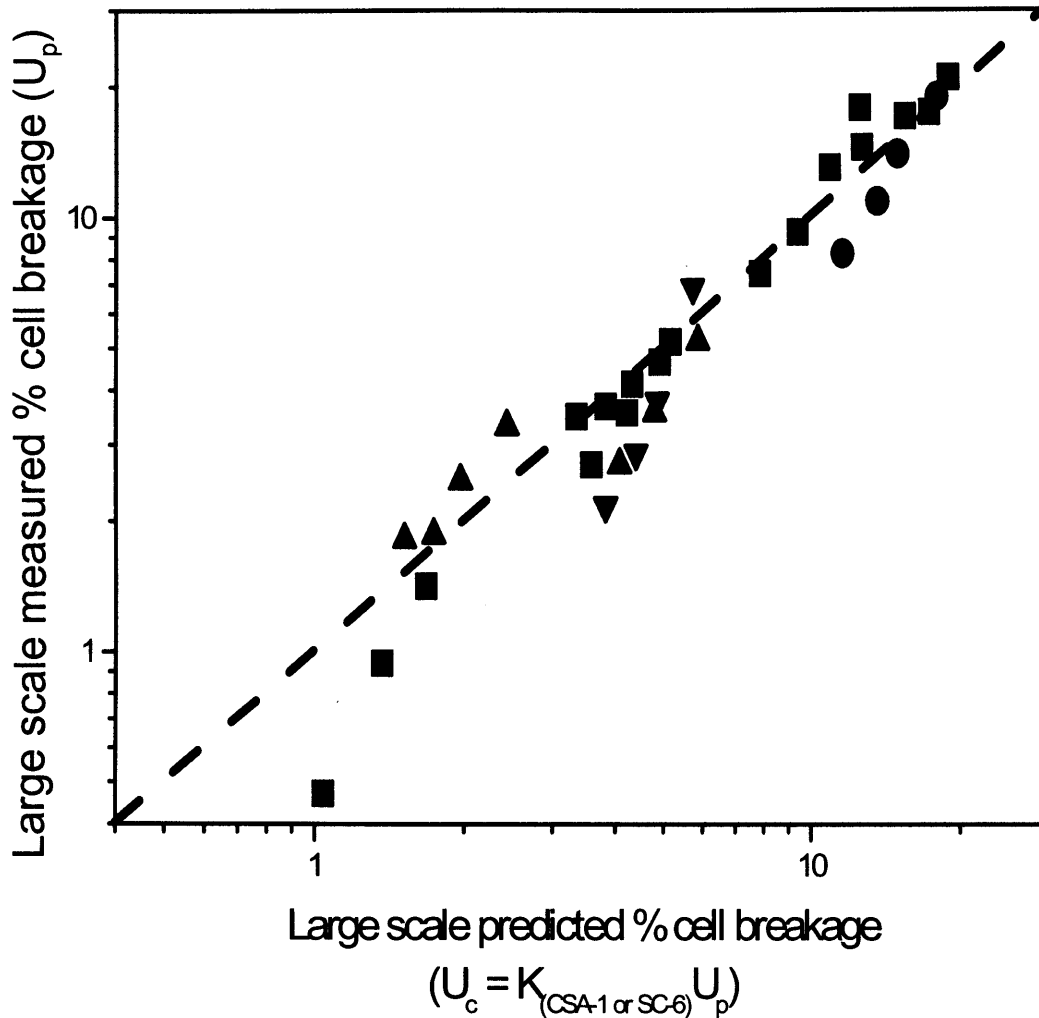
Figure 4.18 Parity plot comparing the measured % cell breakage acquired from large-scale trials to the predicted % cell breakage determined from USD trials. Symbols: (■) USD/CSA-1 comparison for freeze thawed material (DH5α *E. coli*); (▲) USD/CSA-1 comparison for fresh material (W3110 and DH5α *E. coli*); (●) USD/SC-6 comparison for freeze thawed material (DH5α *E. coli*); (▼) USD/SC-6 comparison for fresh material (W3110 *E. coli*).
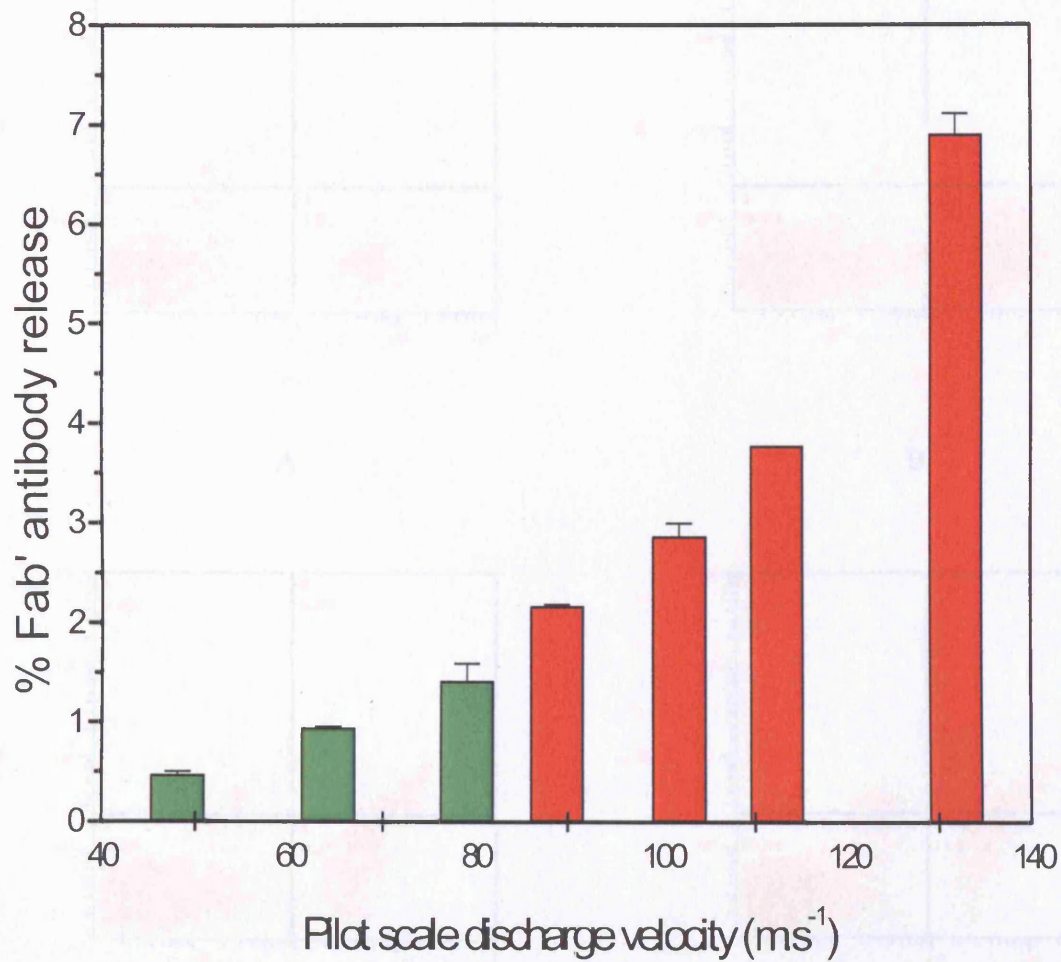
Figure 4.19   Loss of Fab' antibody fragment product from fresh W3110 *E. coli* cells
(20 L) as a function of pilot-scale discharge velocity. Symbols: (■)
Pilot-scale SC-6 discharge velocity; (■) Pilot-scale CSA-1 discharge
velocity. No Fab' product loss was detected from USD discharge.
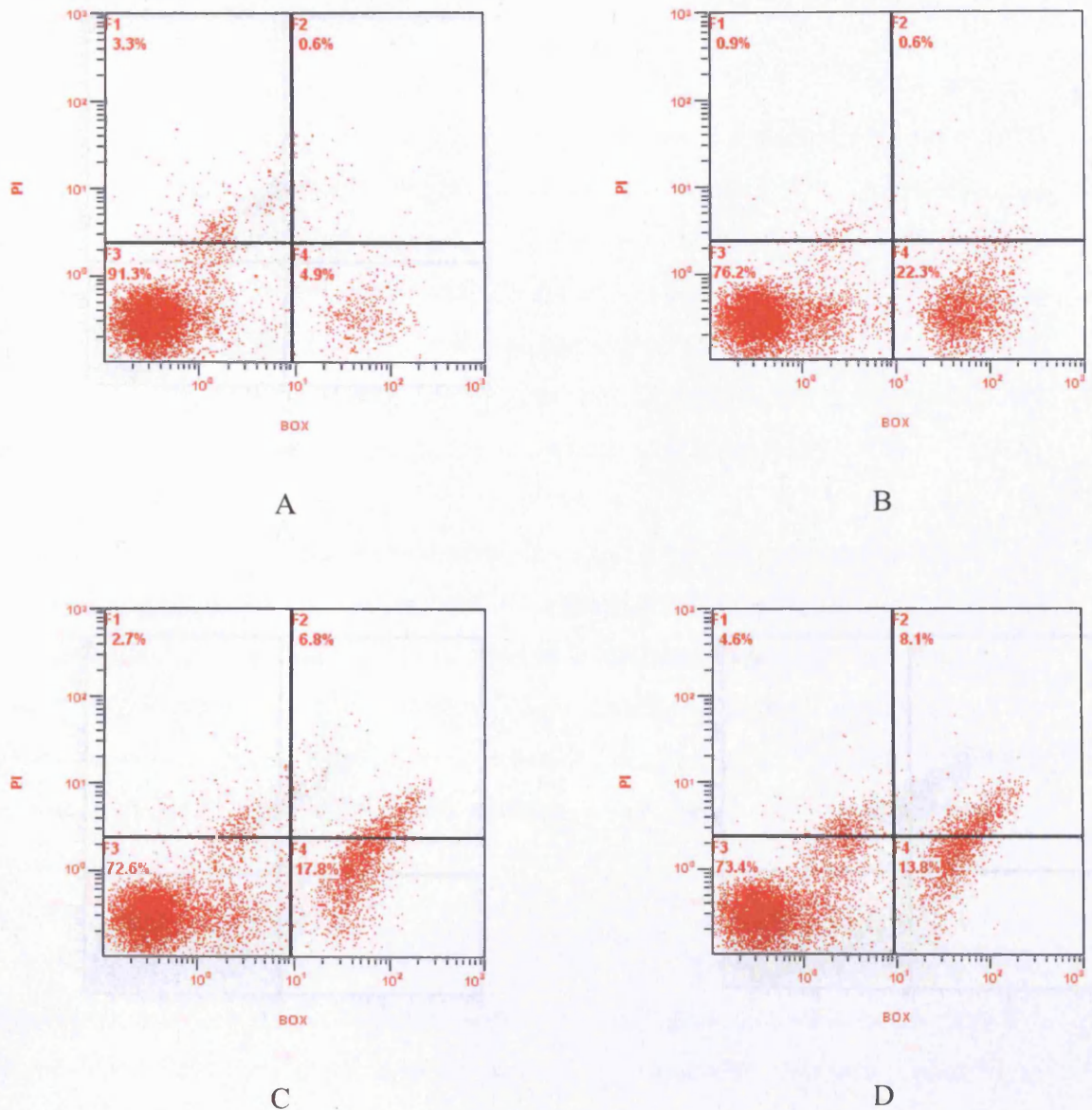
Figure 4.20   Effect of USD discharge velocity and holding time on fresh W3110 *E. coli* cell physiology. Symbols: (A) experimental control, no discharge; (B) USD discharge velocity of 85 m.s^{-1} with impact onto a stainless steel stub at 90 mm perpendicular to the capillary exit (holding time 0 h); (C) USD discharge velocity of 85 m.s^{-1} with holding time of 1 h at 25°C after impact; (D) USD discharge velocity of 85 m.s^{-1} with holding time of 2 h at 25°C after impact. Quadrants: (F1) PI positive staining, cells are permeabilised; (F2) PI and BOX positive staining, cells are dead with a depolarised permeabilised cytoplasmic membrane; (F3) PI and BOX negative staining, cells are healthy and polarised; (F4) BOX positive staining, cells are depolarised.
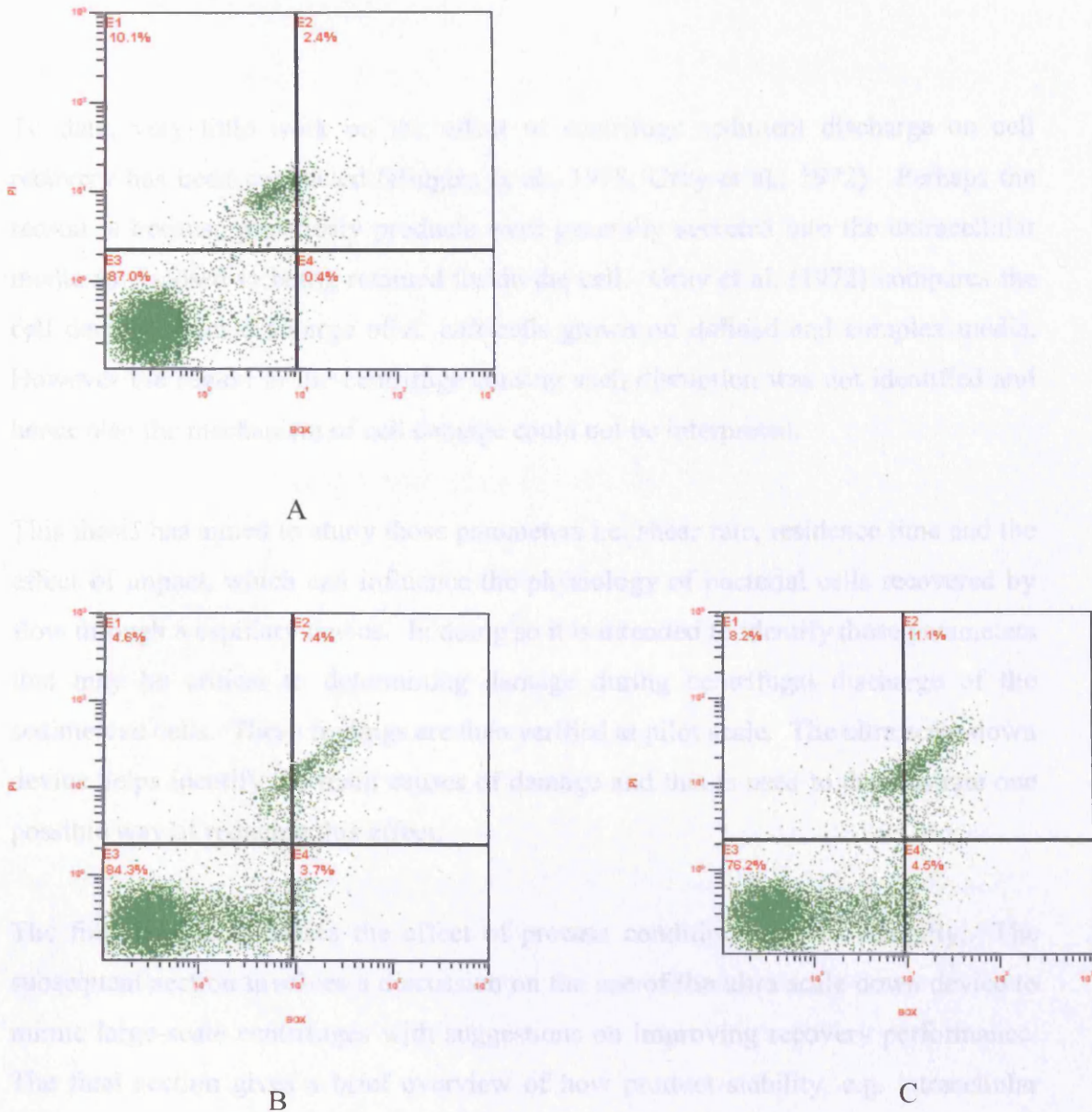
Figure 4.21   Comparison of fresh DH5α *E. coli* cell physiology after exposure to pilot-scale and the equivalent USD discharge velocity. Symbols: (A) experimental control, no discharge; (B) pilot-scale calibrated CSA-1 discharge velocity of 80 m.s^{-1} (i.e. original velocity of 52 m.s^{-1} x K$_{(CSA-1)}$ of 1.54) (holding time 0 h); (C) USD discharge velocity of 85 m.s^{-1} (holding time 0 h). Quadrants: (E1) PI positive staining, cells are permeabilised; (E2) PI and BOX positive staining, cells are dead with a depolarised permeabilised cytoplasmic membrane; (E3) PI and BOX negative staining, cells are healthy and polarised; (E4) BOX positive staining, cells are depolarised.

5 DISCUSSION

To date, very little work on the effect of centrifuge sediment discharge on cell recovery has been conducted (Higgins et al., 1978; Gray et al., 1972). Perhaps the reason is because previously products were generally secreted into the extracellular media as opposed to being retained inside the cell. Gray et al. (1972) compares the cell damage from discharge of *E. coli* cells grown on defined and complex media. However the region in the centrifuge causing such disruption was not identified and hence also the mechanism of cell damage could not be interpreted.

This thesis has aimed to study those parameters i.e. shear rate, residence time and the effect of impact, which can influence the physiology of bacterial cells recovered by flow through a capillary device. In doing so it is intended to identify those parameters that may be critical to determining damage during centrifugal discharge of the sedimented cells. These findings are then verified at pilot scale. The ultra scale-down device helps identify the main causes of damage and this is used to demonstrate one possible way of reducing this effect.

The first section discusses the affect of process conditions on cell integrity. The subsequent section involves a discussion on the use of the ultra scale-down device to mimic large-scale centrifuges with suggestions on improving recovery performance. The final section gives a brief overview of how product stability, e.g. intracellular plasmids, might be affected during typical high centrifuge operating conditions.

5.1 Examination of capillary process parameters on *E. coli* cell recovery

5.1.1 Effect of shear rate and residence time

High shear rates were shown to cause physiological changes to the *E. coli* and the extent of cell damage found to be dependant on the residence time within the shear field (Figure 4.2 and 4.4). These results correspond with previous observations (Shamlou et al., 1994; Levy et al., 1999) in which breakage of particles was found to be time dependant. Aloi et al. (1995) observed a similar time-dependant response with Sf-9 insect cells, demonstrating that exposure to shear after 4 h resulted in larger detectable calcium levels than after a 15 min exposure.

The effect of shear and residence time on cell integrity should give an indication of how processing conditions will affect cell recovery. Units such as homogenisers are commonly employed to operate at high pressures and hence high shear rate with residence time determined by the number of passes through the homogeniser valve (Keshavarz Moore et al., 1990; Maguire et al., 2003; Shamlou et al., 1995; Mosqueira et al., 1981). This equates to a high G_cT_i which is usually sufficient to disrupt even the most robust of cells (Mosqueira et al., 1981). With most centrifuge designs, feed suspensions are processed through a central inlet zone where initial contact is with a spindle nut rotating at bowl speed before dispersing into the centrifuge chamber where clarification occurs. Others have demonstrated through experiments and computational fluid dynamics modelling the existence of high mechanical forces within the feed zone (Boychyn et al., 2001; Neal et al., 2003). However particles accelerating towards the spindle nut impinge and deflect thus only a fraction of time is spent within the high shear field resulting in low G_cT_i values and hence little to no cell disruption. Cell recovery by the centrifuge will be discussed later.

5.1.2 Effect of shear stress

In the context of bioprocessing, unit operations often suffer from generating high shear stresses that can induce morphological changes to cells (Stathopoulos et al.,

146

1985; Levesque et al., 1989; Kretzmer et al., 1991), changes in metabolism (Edwards et al., 1989; Frangos et al., 1988) and loss of cell viability (Born et al., 1992; Zhang et al., 1993; Lange et al., 2001; Abu-Reesh et al., 1989). Our work (Figure 4.8) has shown that this form of stress only plays a key role in determining recovery performance if both the shear stress and residence time are sufficiently high. Under identical shear stress conditions a lower residence time was demonstrated to improve recovery of intact cells. For a disc stack centrifuge CFD analysis of the feed zone indicates maximum energy dissipation rates of $\sim$ 2 x 10^5 W.kg^{-1}, i.e. velocity gradients (G_c) of $\sim$4 x 10^5 s^{-1} (Boychyn et al., 2004). The volume of the high shear region is significantly less than 0.2 mL (Boychyn et al., 2004) giving maximum mean residence times less than 0.002 s for flow rates used in this study. Hence the G_cT_i value is less than 10^3 i.e. little to no breakage expected (Figure 4.5). Discharge nozzles are of the order of L:d ratio 2 where the product of G_cT_i may be estimated from Equation 13 (Chapter 3), giving G_cT_i values of the order of 50 again indicating little breakage this time in the discharge port (Figure 4.5). Abu-Reesh et al. (1989) suggested that the flow regime also plays a significant role in determining the survival rate of cells, where turbulent shear stress leads to a greater loss of cell viability than identical levels of laminar shear stress. In the limited studies reported here (Figure 4.8) on flow structure, laminar and turbulent flow give similar breakage rates for equivalent velocity gradients. However the laminar flow will have been only partially developed such that the nature of the disruptive forces on the cells will be similar to these in turbulent flow (extensional, impact, hydrodynamic). It is these conditions which will exist in very short sediment discharge zones of disc stack centrifuges.

5.1.3 Effect of impact

Besides *E. coli* cell damage by shear and residence time in the capillary, collection of material via impact on a stainless steel stub has also been demonstrated to cause cell damage. Hashish et al. (1980) previously reported a linear relationship between the impact velocity and cell breakage showing that breakage is initiated when the energy dissipation generated by impaction of the jet against a target exceeds the strength of the cellular material. From our laboratory-scale studies (Figure 4.9) we have shown that the discharge velocity leading to impact plays a vital role in cell breakage during

cell recovery from the capillary system. As the discharge velocity increases, the greater energy dissipation leads to more cell breakage and these observations are supported by Obara et al. (1995). For a fixed velocity, maximum extent of cell breakage was evident with changing impact distance (Figure 4.11). This might be caused by the changes in jet profile with increasing distance. At a distance close to the nozzle exit, jet pressure is the dominant factor causing cell breakage (Reichman et al., 1980). As fluid flows away from the capillary ($>X_c$), the shear effects generated by the stationary air disperses the layers of jet as very fine droplets with the quantity of these fine droplets increasing further down the continuous region. This feature maximizes at the break-up point (X_b) corresponding to a theoretical measurement of 99 mm for the current capillary system. The cause of cell damage may be due to a high frequency of droplets that generate forces in the form of shock waves and shear stresses during impact. At distances greater than the break-up point (X_b), the jet develops into a dominant diffusion flow, whereby aerodynamic drag leads to decay in jet velocity and formation of large droplets (Davies et al., 1980) and hence lower cell damage. Negligible cell damage due to impaction occurred when the impact distance was extended to 300 mm, where the jet had lost significant momentum.

5.2 Ultra scale-down mimic of a CSA-1 and SC-6 disc-stack centrifuge

A USD approach has been developed to help study experimentally process variables that affect cell viability during high velocity flow such as may occur during centrifuge discharge. The USD device, requiring only mL quantities of material, offers the prospect for early screening of process conditions and hence reduction in the time required for bioprocess development; for example, an understanding of how centrifuge processing affects material properties for subsequent purification stages.

Successful scale-down requires a detailed understanding of both large-scale and USD equipment behaviour. In earlier results (Figure 4.5) capillary shear contributions ($G_cT_i < 646$) accounted for negligible *E. coli* cell damage. For pilot-scale centrifuge discharge the nozzle G_cT_i was estimated to be less than 50 (Equation 13) and therefore assumed to have minimal effect on *E. coli* cell structure. This assumption could not

be physically verified because of the difficulties involved with separating shear contributions during discharge from impact in the large-scale machine. The principal behind our USD mimic of centrifuge discharge is similar to work conducted by Boychyn et al. (2000) where calibration factors accounted for non-ideal centrifuge flow. Our mimic was based on a calibration factor K_{CSA-1} and K_{SC-6} to account for differences in jet profile and impact configuration. The calibration factors were

derived from the expression $U_c^{\,n} = \dfrac{K_1}{K_2} U_p^{\,n}$, where K_1 is the pilot-scale constant, K_2 is

the small-scale constant, and n is the slope constrained to 1 (based on an approximately linear relationship observed between % cell breakage and discharge velocity as seen in Figure 4.9). The USD mimic gave good estimates of large-scale performance (Figure 4.18) for both W3110 and DH5α *E. coli* cells with varies pre-treatments. The weakening of cells lead to greater cell breakage which was successfully predicted at small-scale. For both centrifuges up to 50% difference in cell damage were recorded between the best and worst operating scenario, i.e. the lowest and highest centrifuge bowl rotational speed during discharge, and this was mirrored at the small-scale.

The use of flow cytometry analysis further supported the accuracy of our mimic by comparing and identifying the physiological changes that occur upon impact after discharge for both the USD and pilot-scale operations (Figure 4.21). Evidence of depolarisation immediately after impact was reported for both scales of operation. The % of dead cells also increased after discharge. One possible explanation for the overall trend observed is that the energy dissipation generated at impact travels through the cell structures in the form of shock waves (Chan et al., 2006) causing internal damage, e.g. damage to nucleic acids, proteins, enzymes and hence loss of cell functionality, i.e. loss of cell metabolism. As a result of metabolic inactivation the cells may no longer remain charged and therefore permit the entry of BOX stain. As the damaged cells degrade the membrane losses integrity and eventually permits entry of PI stain. Flow cytometry is however limited to only targeting living, permeabilised and depolarised cells. Other entities can also exist within a processed sample, namely ghost and semi-ghost cells of which the former can be considered completely dead (Chan et al., 2006; Lewis et al., 2004). Nebe-von-Caron et al. (2000)

suggest that as more intracellular material leaks from cells the number of lipophilic sites for BOX binding increases. This would be displayed as an enhanced BOX and normal PI response. In addition, cells with no cytoplasmic content (i.e. ghost cells) would only give an enhanced BOX response. Ghost cells staining BOX positive and PI negative would therefore give a false representation of the total number of dead cells present in the sample. Identifying the number of ghost cells in each quadrant is difficult and had not been carried out in this study.

Throughout this investigation the average large scale discharge velocities were calculated based on full bowl opening. However, the effect of opening time on velocity distribution has not been considered. Figure 5.1 gives a general overview of how the discharge time and corresponding nozzle opening differ between the CSA-1 and SC-6 centrifuges (Siegeler 1993). This relationship is dynamic and will vary with changes in centrifuge bowl speed. The opening times for the CSA-1 and SC-6 were approximated to be 0.5 and 0.1 s respectively (Siegeler 1993). Assuming that the solids ejection of 250 mL from both centrifuge bowls take 0.05 s and that unimpeded sediment flow is only initiated with a slot exposure height of 0.0038 m (i.e. full CSA-1 bowl opening), the CSA-1 discharges the sediment over an approximately constant velocity whereas the SC-6 is suspected to discharge over a range of velocities governed by the degree of nozzle opening. Preliminary calculations (not shown) estimate the average velocity during high speed SC-6 discharge to be as much as 25% higher than the original velocities calculated based on full bowl opening.

5.3 Effect of process conditions on viable intracellular plasmid product yield

This work has briefly examined the impact of feed condition and centrifuge operation on cell recovery. The interaction between operations is also significant in determining the overall process performance (Zhou et al., 1999; Groep et al., 2000). Examples of earlier work on process interactions include the effect of fermentation growth rate and growth phase on cell resistance to cell disruption and debris removal by centrifugation (Siddiqi et al., 1995; Hull and Middelberg 1993; Zhou et al., 1999). Zhou et al. (1999) demonstrate the complexity of these interactions and highlighted the

compromises that need to be made in order to achieve pre-specified goals. Here we briefly consider the impact of centrifuge processing of cells, expressing an intracellular product, e.g. DNA plasmids, on subsequent process performance. Recovery of intact cells and product from centrifugation is generally favoured because intact cells place very little additional burden on subsequent processing and maximum biological activity requires the product to retain its supercoiled form. However, damaged cells recovered from centrifuge discharge will begin to degrade quickly with the rate of cell death dependant on the extent of damage. During cell degradation, contamination of intracellular product with nucleases is possible leading to loss of viable product, e.g. DNA plasmids will degrade when in contact with nucleases and in addition nucleases will truncate other forms of DNA, such as chromosomal DNA, creating a mix of plasmid and chromosomal fragments of similar size that place a heavy burden on subsequent separation and purification steps (Hearle et al., 1994; Gray et al., 1973).

In this last section we briefly evaluate the effect of discharge conditions from the CSA-1 centrifuge and capillary device on product integrity i.e. supercoiled (SC) plasmid. SC-6 trials were not conducted due to insufficient supply of test material. The stability of the required SC isoform during processing is a key issue if it is to be used for therapeutic processes e.g. gene therapy and DNA vaccination (Marquet et al., 1995). To date, very few studies have addressed the issues relating to large-scale processing and purification of plasmid DNA (Levy et al., 1999; Theodossiou et al., 1997; Ciccolini et al., 1998). Levy et al. (1999) carried out extensive studies on plasmid sensitivity and demonstrated that plasmids were very prone to shear damage with an exponential decline in SC (29 kb) content with increasing shear rate. Total degradation of SC plasmid was observed at a shear rate of 9×10^5 s^{-1}. The ionic strength of DNA solution affects damage to plasmids; the extent of damage increasing with decreasing ionic strength. This is probably due to greater compaction of the molecule e.g. below the microscale of turbulence. The aim of the following section is to expand our current understanding of plasmid sensitivity to include the effects of centrifuge processing i.e. solids discharge and hold-up time between operations.

The effect of varying USD discharge velocity (with impact on a stainless steel stub) on DNA integrity was investigated using fresh and freeze thawed (from -80°C) DH5α *E. coli* cells expressing intracellular (20 kb) plasmids. All DNA analysis was kindly conducted by Simyee Kong and Ben Bourne of Biochemical Engineering, UCL. Processed samples were treated with an alkaline lysis step (Birnboim and Doly, 1979; Theodossiou et al., 1997) causing the breakdown of the cell wall and release of intracellular contents. The released DNA content was purified using a QIAprep Spin Miniprep kit (Qiagen Ltd, West Sussex, UK). The concentration of purified DNA was measured at an OD of 260 nm using the Biomate 3 spectrophotometer (Thermo Spectronic, Madison, WI, USA) before loading onto an agarose gel. Further methodology details can be found in Appendix 2. Figure 5.2 is a typical gel electrophoresis for processed plasmid pQR150 (20 kb) (from freeze thawed DH5α *E. coli*) showing an increase in the damaged DNA (represented by the smear extending from the linear isoform) with increasing USD discharge velocity. The formation of linear isoforms may be due to degradation of either the SC or OC isoforms or both during high velocity discharge. It is suggested that the recovery of intact SC isoform is also dependant on the biomechanical cell properties before and after processing. Figure 5.3 shows the stability of damaged plasmid (acquired from a USD discharge velocity of 85 m.s^{-1}) as a function of holding time after operation. Processed samples were held at room temperature of 25°C for periods of 0 to 6 h. The results illustrate the sensitivity of processed material with a decrease in SC plasmid DNA content and an increase in damaged DNA with longer holding times. However, negligible change in the SC plasmid DNA content was reported for holding unprocessed samples at 25°C between 0 and 6 h. One possible explanation for this observation is that the unprocessed cells are sufficiently stable and intact compared to processed cells where intracellular contamination of product may have occurred, e.g. contamination with nucleases, leading to the breakdown of SC to undesirable open circular and linear isoforms. These results support earlier flow cytometry data (Figure 4.20) where intact and living cells proved more stable than damaged cells over time i.e. by the end of the holding test damaged cells showed signs of cell death whereas intact cells remained reasonably stable.

Figure 5.4 compares the CSA-1 and USD recovery of SC plasmid product from a fresh 450 L DH5α *E. coli* fermentation with no significant plasmid degradation observed for both scales of operation. With reference to Figure 4.21, for the same *E. coli* batch, the majority of fresh DH5α *E. coli* cells were observed to survive large-scale and USD discharge and therefore it is reasonable to assume that in this case the cell intracellular environment was suffice to maintain the plasmid. The samples analysed in Figure 5.4 were all done immediately after experimentation with no further monitoring of the batch stability. Observations from Figure 4.20 suggest that damaged cells can become unstable and loss viability if held between operations which might also apply to Figure 5.4. The research conducted by Levy et al. (1999) and the characterised plasmid behaviour to discharge and holding time reported here increases awareness and appreciation of the difficulties in recovering and purifying plasmids at large-scale.
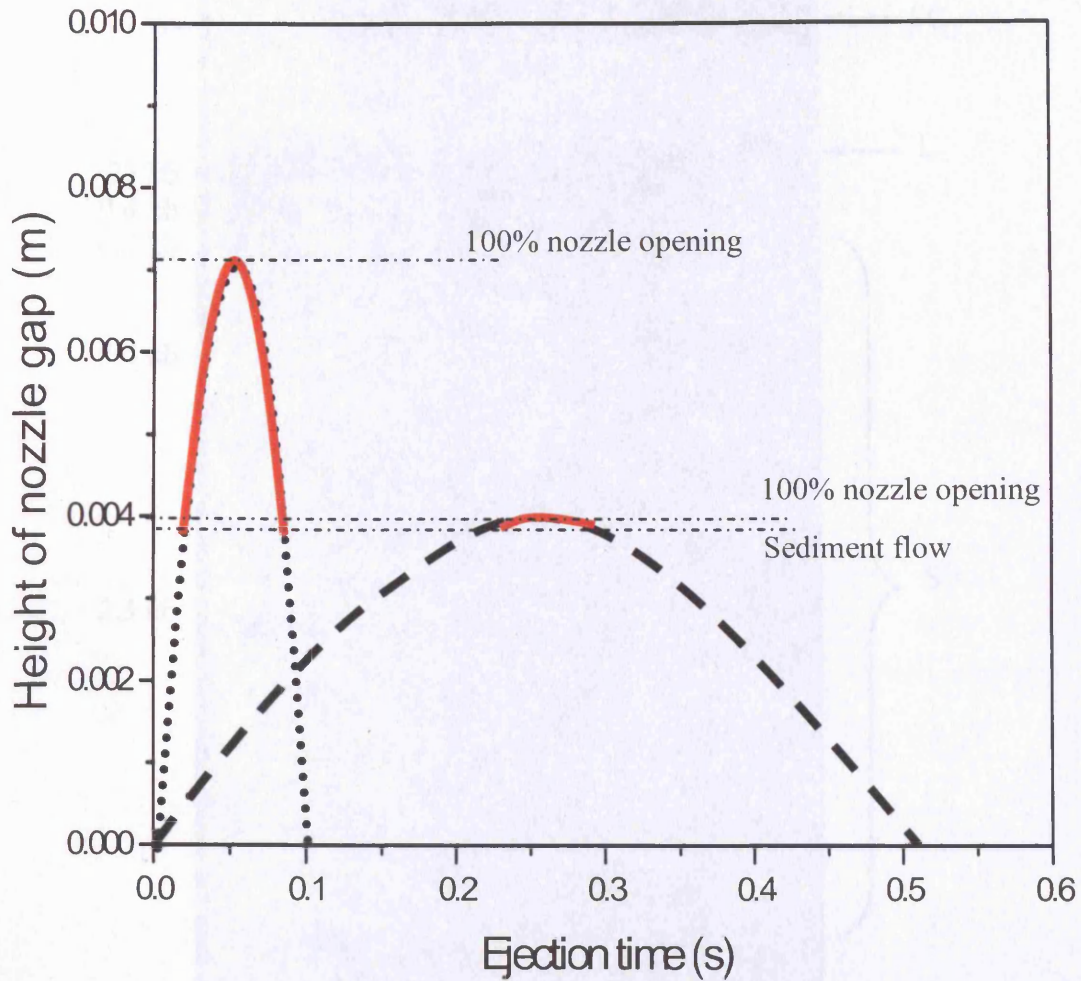
Figure 5.1   Comparison of the CSA-1 and SC-6 discharge mechanism for identical velocities at full nozzle opening. Symbols: (– –) CSA-1 discharge time; (······) SC-6 discharge time; (━) Sediment discharge.
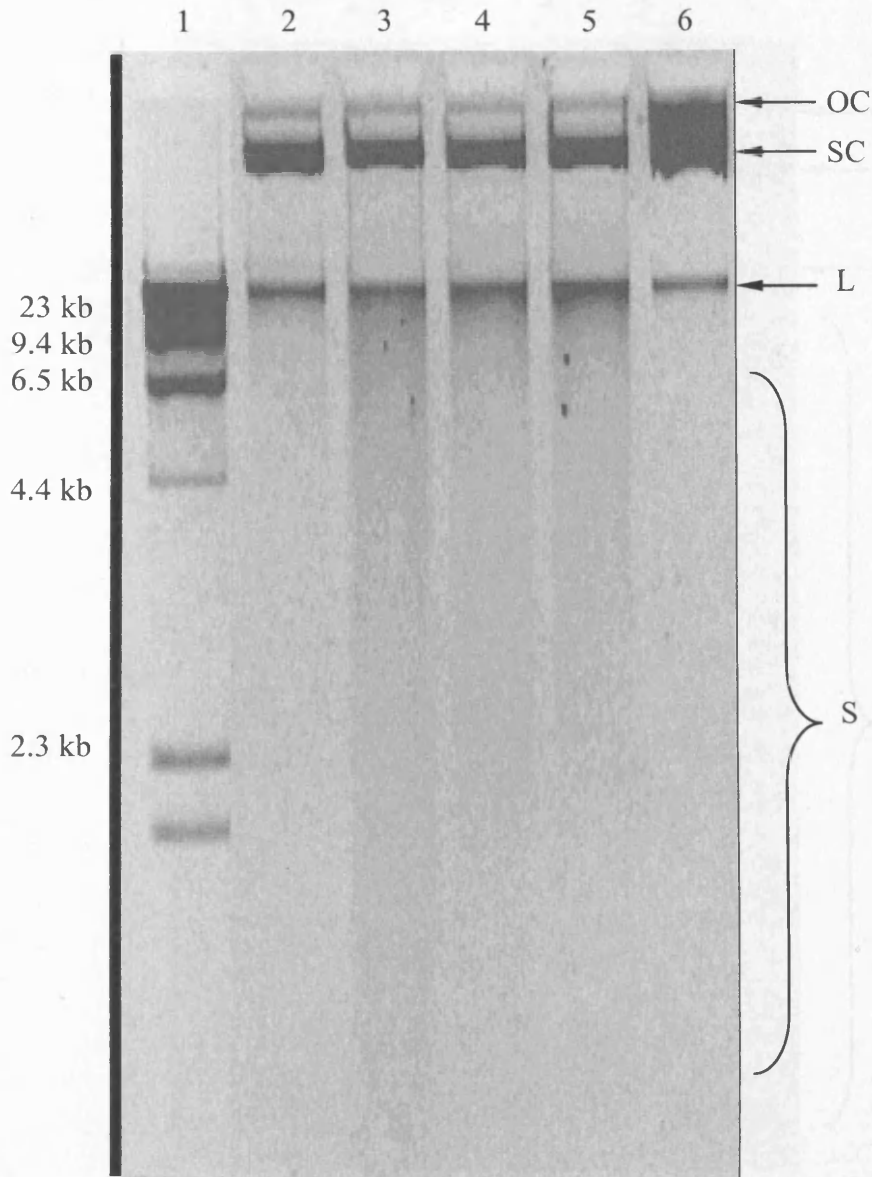
Figure 5.2   Agarose gel electrophoresis of DH5α pQR150 (20 kb) plasmid as a function of USD discharge velocity. Frozen cells (freeze thawed from -80°C) used for study. Plasmid DNA recovery from sedimented cells after various defined processing conditions: (1) λ Hind III molecular marker; (2) experimental control, no discharge of sediment; (3) USD discharge of sediment at velocity of 85 m.s^{-1} with impact onto a stainless steel stub at 90 mm perpendicular to the capillary exit; (4) USD discharge of sediment at velocity of 51 m.s^{-1} with impact onto a stainless steel stub; (5) USD discharge of sediment at velocity of 41 m.s^{-1} with impact onto a stainless steel stub; (6) 20 kb plasmid degraded at 60°C for 48 h; (OC) open circular DNA; (SC) supercoiled DNA; (L) linear DNA; (S) sheared DNA. All empty lanes were removed for clarify.
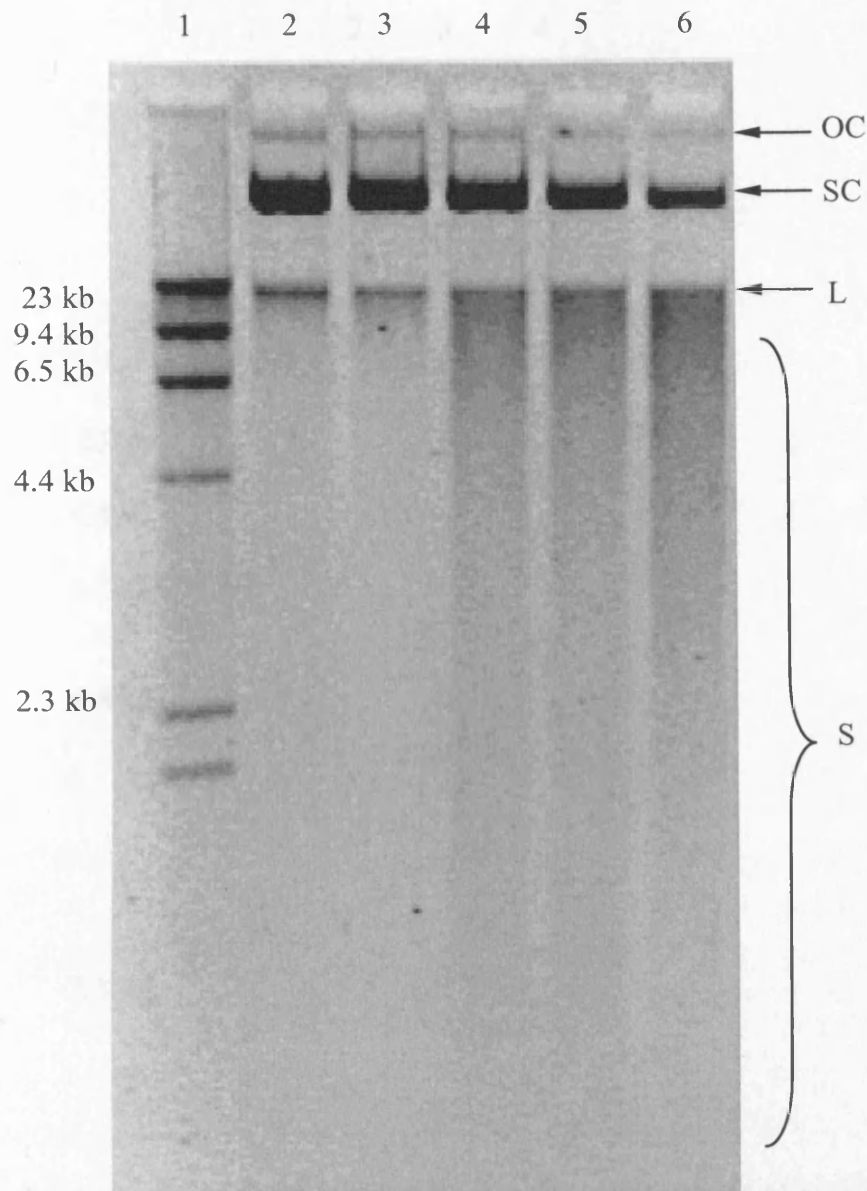
Figure 5.3 Agarose gel electrophoresis of DH5α pQR150 (20 kb) plasmid as a function of holding time after USD discharge. Frozen cells (freeze thawed from -80°C) used for study. Symbols: (1) λ Hind III molecular marker; (2) experimental control, no discharge of sediment (0 h holding time); (3) experimental control, no discharge of sediment (6 h holding time); (4) USD discharge of sediment at velocity of 85 m.s^{-1} with impact onto a stainless steel stub at 90 mm perpendicular to the capillary exit (holding time 0 h); (5) USD discharge of sediment at velocity of 85 m.s^{-1} with holding time of 2 h at room temperature of 25°C after impact; (6) USD discharge of sediment at velocity of 85 m.s^{-1} with holding time of 6 h at room temperature of 25°C after impact. All empty lanes were removed for clarify.
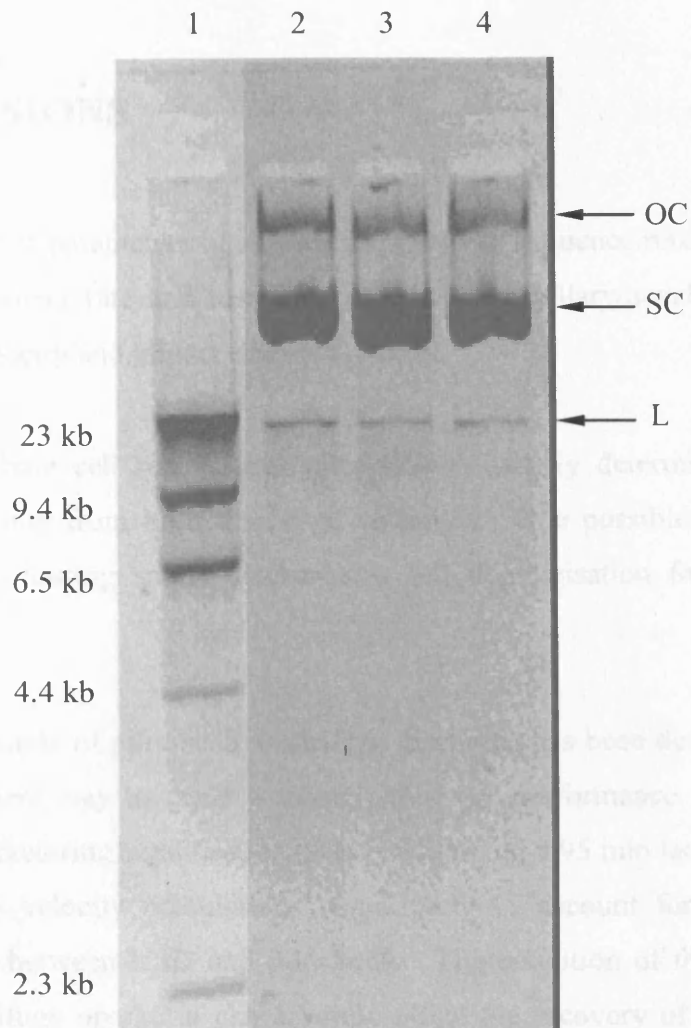
Figure 5.4   Agarose gel electrophoresis of fresh DH5α pQR150 (20 kb) plasmid as a function of USD and CSA-1 centrifuge discharge velocity.   Symbols: (1) λ Hind III molecular marker; (2) experimental control, no discharge of sediment; (3) USD discharge of sediment at velocity of 85 m.s^{-1} (holding time 0 h); (4) pilot-scale calibrated CSA-1 discharge of sediment at velocity of 80 m.s^{-1} (i.e. original velocity of 52 m.s^{-1} x K$_{(CSA-1)}$ of 1.54) (holding time 0 h).   All empty lanes were removed for clarify.

6 CONCLUSIONS

- A number of parameters have been identified to influence recovery of *E. coli* including shear rate and residence time in the capillary/nozzle, shear stress, impact velocity and impact distance.

- *E. coli* whole cell recovery at pilot-scale is largely determined by impact forces arising from high discharge velocities. One possible change in cell physiology during solids discharge is cell depolarisation followed by cell death.

- A USD mimic of pilot-scale centrifuge discharge has been devised and offers a convenient way to rapidly assess pilot-scale performance. The mimic is based on factoring a calibration factor of 1.54 and 2.95 into large-scale CSA-1 and SC-6 velocity calculations respectively to account for differences in discharge between USD and pilot-scale. The condition of the feed material and centrifuge operation can severely affect the recovery of viable material with the extent of damage dependant on cell biomechanical properties and centrifuge discharge velocity.
    - Cell biomechanical properties strongly influence the recovery of intact material. The level of cell viability after discharge may also play a significant role in determining the final yield of product. Intact cells have been characterised as having a stable intracellular environment where the product remains in the desired form.
    - Lowering the discharge velocity prior to *E. coli* solids recovery can reduce the level of damage by up to 50%.

7 RECOMMENDATIONS FOR FUTURE WORK

- The impact of cell handling on centrifuge recovery should be extended to include the effects of fermenter operating conditions e.g. the effect of media variations and harvest time. One aspect of fermentation control has already been examined by Garcia et al. (2005).

- Additional studies are required to investigate the different aspects of discharge with larger machines and to possibly incorporate this into the current USD model e.g. secondary impact experienced with the SC-6 centrifuge design.

- More work is needed to capture the interaction between product and stress conditions and the effect of cell physiology on the whole bioprocess sequence.

- The capillary device needs to be further refined in order to assess breakage at much higher velocities. Further studies are also required to characterise the viscose feed material as it initially moves through the capillary/nozzle. By constructing a transparent capillary the flow patterns and any time delays between initiating discharge and release of material can be determined and hence the discharge times can be calculated with more precision.

A1   The use of flow cytometry to study the impact of different forms of stress on *E. coli* cell physiology

A1.1 Abstract

This investigation was conducted as supervisor of an M.Eng project derived by myself and acknowledgment is due to Nelson Yeung. The objective was to extend the flow cytometry analysis in this thesis to include a study of the effect of varies stresses on changes in cell physiology. This report focuses on the use of flow cytometry to characterise cell physiology during fermentation (2 L scale) and exposure to stresses commonly experienced in unit operations, e.g. shear stress in pumps, centrifuges and homogenisers. Measurements were performed using Propidium Iodide (PI) and Bis-oxanol (BOX) stain.

The cytometer readings for the shake flask W3110 *E. coli* fermentation illustrate that during cell growth the proportion of healthy cells increased, dwarfing the proportion of dead cells present in the media. At stationary phase, healthy intact cells dominated the cell population. During the decline phase the proportion of living and dead cells were observed to decrease and increase respectively.

The physiological changes leading to cell death were different for a range of stress treatments. Heat treatment led to depolarisation followed by cell permeabilisation. Shear treatment demonstrated simultaneous depolarisation and permeabilisation. The W3110 *E. coli* cell batch (which was not induced to produce product) was suggested to be more robust than product producing W3110 *E. coli* cells from the 20 L fermentation (used in the main thesis).

A1.2 Introduction

Typically for microbes, it is considered that the ability of a microbe to reproduce itself on a nutrient agar plate constitutes the benchmark for determining how many living cells are contained in a test sample. This method does however possess a number of flaws. For example, some cells may be alive but not grow due to injury or non ideal conditions and as such would be registered as dead. Sachidanandham et al. (2005) report that some organisms are capable of forming an active but non-culturable state when exposed to stress conditions where cells remain metabolically active but cannot be detected by methods depending on cell growth. Other methods of determining viability include manual cell counting and monitoring the leakage of intracellular molecules (Hurst, 1977), e.g. intracellular protein leakage, which has been used throughout this thesis. Manual cell counting suffers from inaccuracies and can be hindered by operator fatigue with prolonged usage (Lebaron et al., 1994; Gunasekera et al., 2002). In addition, intracellular assay techniques only provide an indication of intracellular loss from a cell batch; it does not give evidence of cell physiological response to the applied stress. For example, if the average intracellular protein loss from a cell population is estimated at 10%, this could imply that all cells have lost 10% of protein or 10% of the population have lost all their intracellular protein or any combination in between. However, the measurements of individual cells could provide a solution for the problem highlighted above.

Flow cytometry has recently gained considerable attention in the field of microbiology and biotechnology including its use to investigate yeast (Hutter et al., 1979), mammalian cells (Davey et al., 1996) and *E. coli* cells (Steen et al., 1981; Hutter et al., 1979). Its use with bacterial cells is less well established because of the significantly smaller particle sizes (Hewitt et al., 1998) i.e. 1-2 μm in length compared to approximately 10 μm for mammalian cells. The technique enjoys the benefits of measuring single cell physiological properties, multi-parameter data acquisition and rapid analysis. Cells can be analysed at a rate of thousands per second as they are carried within a fast flowing fluid. As cells pass through the flow cytometer laser beam three different parameters are measured: forward scatter (FS), side scatter (SS) and fluorescence from selected dyes which provide information on particle size, particle intracellular density and cell stability respectively. By using a combination of

different cell stains a cell culture can be conveniently differentiated into sub-populations and characterised i.e. it is possible to distinguish between living and dead cells. Typically, a fully functional prokaryotic cell is characterised by active metabolic pumps embedded in the inner membrane that generate an electrochemical gradient across the cell (Chapter 1, Figure 1.8). It is suggested that with cell exposure to stress the metabolic pumps can become inactive and the membrane depolarised, eventually permeabilising before cell death (Hewitt et al., 1999). The use of selective cell dyes can be used to distinguish between different viable cell states. In the present study the relationship between stress imposed on *E. coli* cells and cell physiological changes was evaluated using flow cytometry.

A1.3 Materials and methods

A1.3.1 Batch fermentation (2 L shake flask)

Fresh W3110 *E. coli* (not expressing any periplasmic product) was used throughout this study. The cell bank was supplied by UCB Celltech (Slough, UK) and maintained as glycerol stocks (80% w/w) at −80°C. The fermentation media (pH 7) was prepared in a baffled 2 L shake flask as described in Table A1.1.

Components	Quantity
Phytone (Becton Dickinson Ltd., UK)	6.4 g
Yeast extract (Oxoid Ltd., UK)	4.0 g
Sodium chloride (VWR International, UK)	2.0 g
Deionised water	400 mL

Table A1.1 List of fermentation media components for W3110 *E. coli*.

The media was autoclaved at 121°C for 20 min and allowed to cool to room temperature before adding 400 μL of tetracycline (10 mg.mL^{-1}) and 200 μL of a thawed cell bank vial in a laminar flow hood. The flask was then incubated in a G25 shaker (New Brunswick Scientific Ltd, UK) at 200 rpm and 30°C for 17 h. Optical density measurements were recorded throughout the fermentation.

A1.3.2 Stress exposure

A1.3.2.1 Heat treatment

Fresh *E. coli* cell broth (μ = 0.0012 N.s.m^{-2}) was harvested from the 2 L shake flask fermentation at 17 h and immediately dispensed into a series of 2 mL Eppendorf tubes before immersing into a water bath of fixed temperature and time period. Heat-treated samples were immediately diluted (to a concentration of 5 x 10^3 cells.mL^{-1} in DBS) and analysed using flow cytometry.

A1.3.2.2 Capillary shear

The following section briefly describes the procedure used to study capillary shear. Further details can be found in Chapter 2, section 2.7.1.2. Fresh *E. coli* cells were concentrated, after 17 h of fermentation, in a Beckman J2-MI centrifuge with a JA10 rotor (Beckman, High Wycombe, UK) for 600 s at 10000 g. Sample volumes of 10 mL (μ = 0.005 N.s.m^{-2}) were processed three consecutive times through a capillary with diameter and length of 0.33 mm and 100 mm respectively. The samples were collected in a volumetric cylinder with a head of buffer of 100 mm depth positioned at 300 mm distance from the capillary tip in order to eliminate impact effects.

A1.3.2.3 Shear in a rotating disc device

Fresh *E. coli* sample volumes of 15 mL (μ = 0.0012 N.s.m^{-2}, 17 h fermentation) were injected into the chamber of a small-scale rotating disc device used to mimic the shear behaviour in bioprocess units such as the feed inlet of large-scale centrifuges. Further details on the design of the rotating disc device are given by Levy et al. (1999). The device was set to operate at a set speed of 11,000 and 15,000 rpm for 10 s. To avoid temperature rises during operation the device was positioned in an ice bath (4°C) at all times.

A1.3.3 Offline analysis

A1.3.3.1 Biomass measurement by optical density

Optical density (OD) measurements of the *E. coli* fermentation were performed at 600 nm using an Ultrospec 2000, Biotech spectrophotometer (Pharmacia Biotech, Cambridge, UK). The spectrophotometer was referenced with a well-spun 0 h fermentation sample obtained by centrifuging the sample for 30 min at 13000 g in a Biofuge model 13 centrifuge (Heraeus Sepatech, GmbH, Germany).

A1.3.3.2 Flow cytometry

The flow cytometry protocol is detailed in Chapter 2, section 2.8.8 and will only be summarised here. To 1 mL of diluted sample (approximately 5×10^3 cells.mL^{-1}), 5 μL of propidium iodide (PI) (200 μg.mL^{-1} in distilled water) and 5 μL of bis-oxanol (BOX) (10 mg.mL^{-1} in dimethyl sulphoxide) were added. Samples were vortexed for 10 s and left to stand for 30 s before inserting onto the cytometer platform for analysis. The sample flowrate was set to "low" with the machine analysing between 150 to 200 cells.s^{-1}. The total time taken between each experiment and analysis was < 10 min (unless otherwise stated).

A1.4 Results

A1.4.1 Fermentation monitoring

During the course of the fermentation OD$_{600}$ measurements were taken at intermittent times. Figure A1.1 shows a typical growth profile for W3110 *E. coli* with exponential growth commencing at 3 h post inoculation. Cells reach stationary phase at 15 h with a cell count of approximately 4×10^8 in the 400 mL working volume. The uptake of PI and BOX stain by *E. coli*, as shown in Figure A1.2, reveals the condition of the growing cell population. Quadrant F1 represents permeabilised cells staining positively with PI, quadrant F2 represents dead cells staining positively with both PI and BOX, quadrant F3 represents healthy cells with no staining and quadrant F4

represents depolarised cells staining positively with BOX. Analysis of the working cell bank (Figure A1.2A) shows only 34.3% of cells in full healthy state. The remaining 65.7% absorb either one or both of the dyes used and are a mixture of permeabilised cells, depolarised cells and dead cells. The cell populations evident in F1 and F4 can be considered damaged but may be recovered in the correct environment (Davey et al., 1996; Hewitt et al., 1999). Throughout the course of the fermentation the initial cell population is observed to change with the number of healthy cells increasing from 34.3% to 97.2% after 24 h (stationary phase). The cell sub-populations previously present in F1 and F4 at fermentation time 0 h is negligible by time 24 h suggesting that they have either died and shifted into F2 or recovered in the presence of the fresh energy source and accumulated in F3 or are still present but dwarfed by the larger proportion of healthy cells.

In addition to studying the growth kinetics of *E. coli*, the practice of crash cooling cells was also examined. In Figure A1.3 comparisons are made between a 24 h fermentation batch crash cooled and a 2nd batch stored at room temperature (24°C). Slight differences are evident between the two batches. The crash-cooled batch (Figure A1.3A) remains stable over the storage period showing little or no difference to the control (Figure A1.2D). However, signs of cell deterioration are evident in the batch stored at room temperature for 12 h (Figure A1.3B) with a healthy cell population of 92.2% compared to 97.5% for the crash-cooled batch. The number of depolarised cells and dead cells in Figure A1.3B is also observed to be higher than the crash-cooled batch.

A1.4.2. Effect of heat treatment

The effect of heat treatment on the survival of W3110 *E. coli* was examined. Shown in Figure A1.4 is the response of *E. coli* cells to heat treatment at 40°C. Over an exposure period of 1600 s negligible change in cell physiology is observed. However, subjecting cells to a higher temperature of 60°C, as shown in Figure A1.5, leads to a rapid decline in living cells from 99.3% before heat treatment to 11.2% after 1600 s. The dead cell population is observed to increase from 0.1% to 73.3% after 1600 s. A similar trend is observed with *E. coli* cells exposed to 80°C as illustrated in Figure

A1.6. Figure A1.7 shows a variation in the Arrhenius rate constant k (i.e. $\frac{\ln(y_2 / y_1)}{x_2 - x_1}$)

with temperature. The rate constant is observed to increase with higher exposure temperature. In Figure A1.8 a semi-log plot of k versus 1/T yields a straight line with slope $-E/R$, where E is the activation energy and R is the ideal gas constant (8.3144 J K^{-1} $gmol^{-1}$). As E increases, the sensitivity of the material in question to temperature degradation also rises.

A1.4.3 Effect of shear stresses

Figure A1.9 shows the effect of laminar capillary stress on *E. coli* physiology. Exposure of cells to a G_cT_i of 4 x 10^3 show negligible interference with cell integrity with only a few cells staining PI positive. Due to the practical limitations with generating sufficiently high capillary G_cT_i (i.e. difficult to control stability of cells with prolonged experimental time) a rotating disc device was used as a substitute to achieve the necessary G_cT_i to induce changes in cell physiology. Figure A1.10 shows the change in cell physiology as a result of shearing at 11,000 and 15,000 rpm for 10 s. There is evidence of a reduction in the number of living cells with increasing G_cT_i. The damaged cells at high G_cT_i are observed to be a mixture of ruptured and depolarised cells.
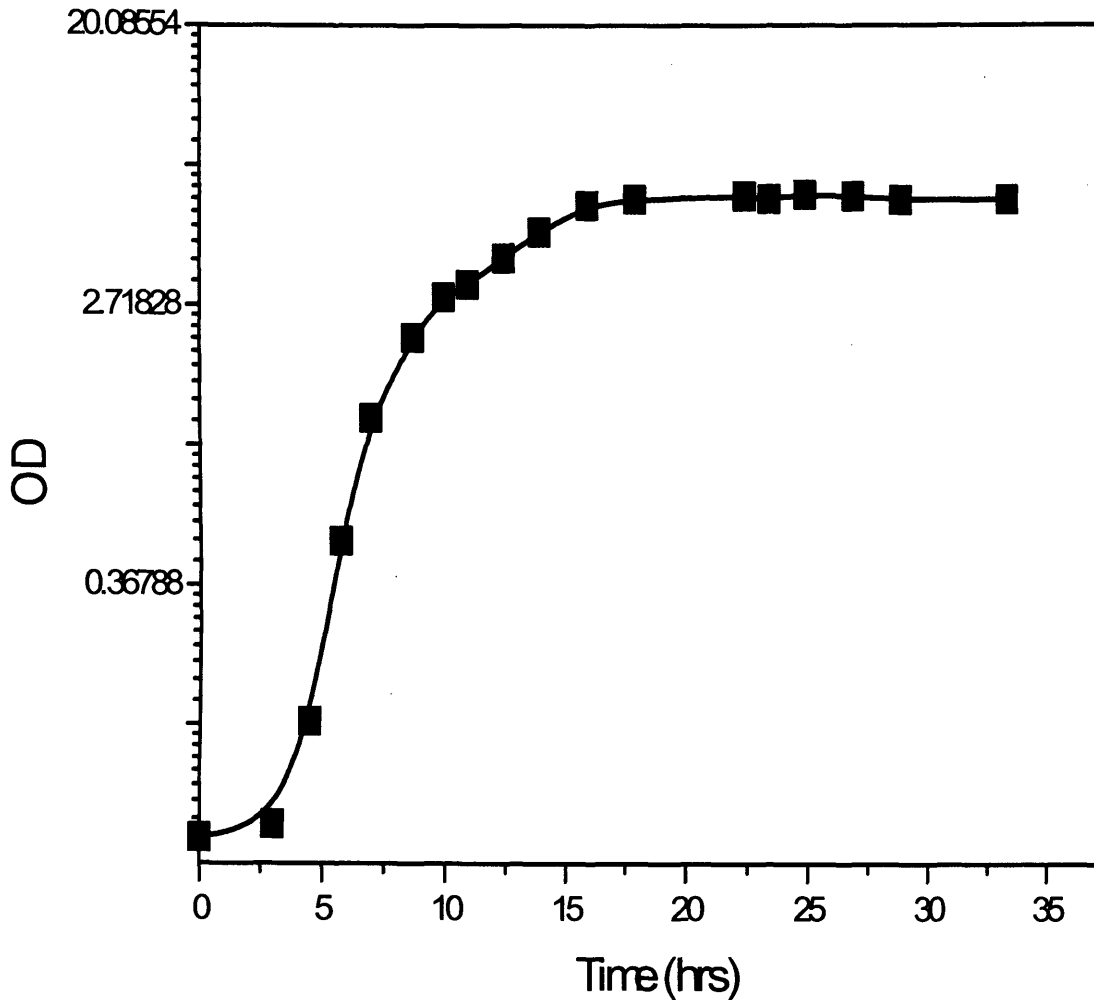
Figure A1.1   2 L shake flask fermentation profile for W3110 *E. coli* (with no product expression). The fermentation media (400 mL) was inoculated with 200 μL from the working cell bank. Samples of 1 mL were extracted at intervals of 2 to 4 h for OD_{600} measurements. The cell concentration at time 0 h is 12.25×10^5 cells.L^{-1} and at time 24 h is 10×10^8 cells.L^{-1}.
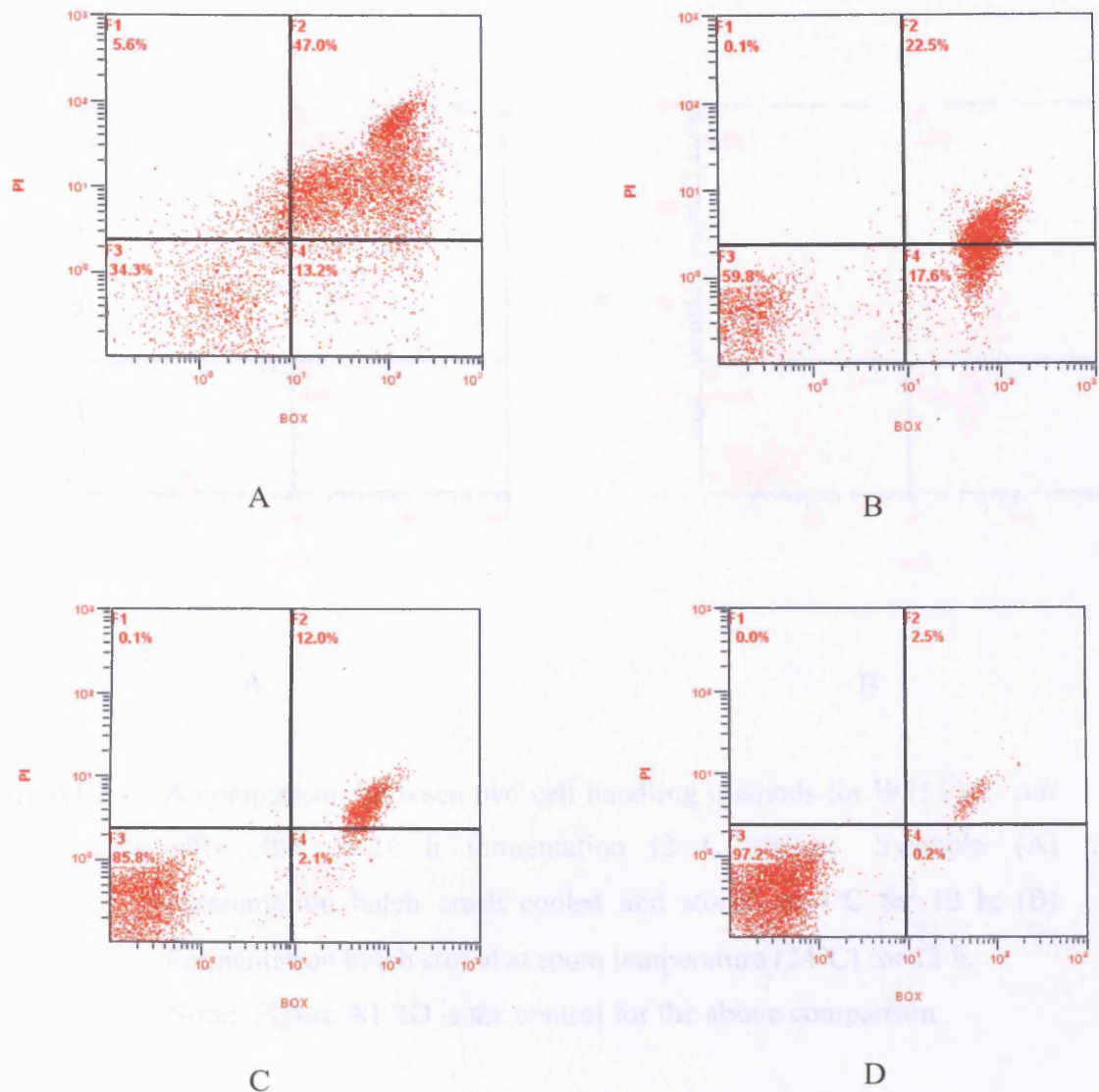
Figure A1.2   Use of flow cytometry to monitor cell viability during a 2 L batch fermentation of W3110 *E. coli*. The cell population was monitored over 24 h using two dyes, namely propidium iodide (PI) and bis-trimethine oxanol (BOX). Symbols: (A) 0 h; (B) 4 h; (C) 6 h; (D) 24 h. Quadrants: (F1) PI positive staining, cells are permeabilised; (F2) PI and BOX positive staining, cells are dead with a depolarised permeabilised cytoplasmic membrane; (F3) PI and BOX negative staining, cells are healthy and polarised; (F4) BOX positive staining, cells are depolarised.

A   B
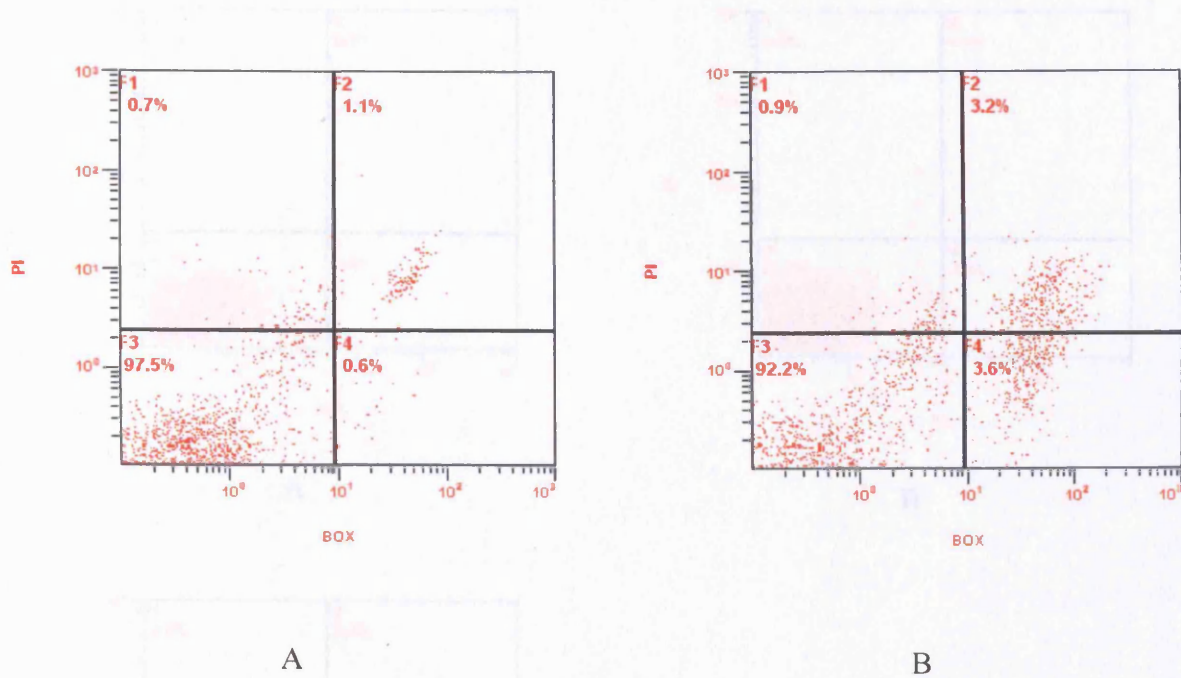
Figure A1.3   A comparison between two cell handling methods for W3110 *E. coli* cells after a 24 h fermentation (2 L scale). Symbols: (A) Fermentation batch crash cooled and stored at 4°C for 12 h; (B) Fermentation batch stored at room temperature (24°C) for 12 h.

Note: Figure A1.2D is the control for the above comparison.

Figure A1.4   Heat treatment of W3110 *E. coli* cells at 40°C with a range of exposure times. Symbols: (A) residence time 0 s; (B) residence time 800 s; (C) residence time 1600 s.
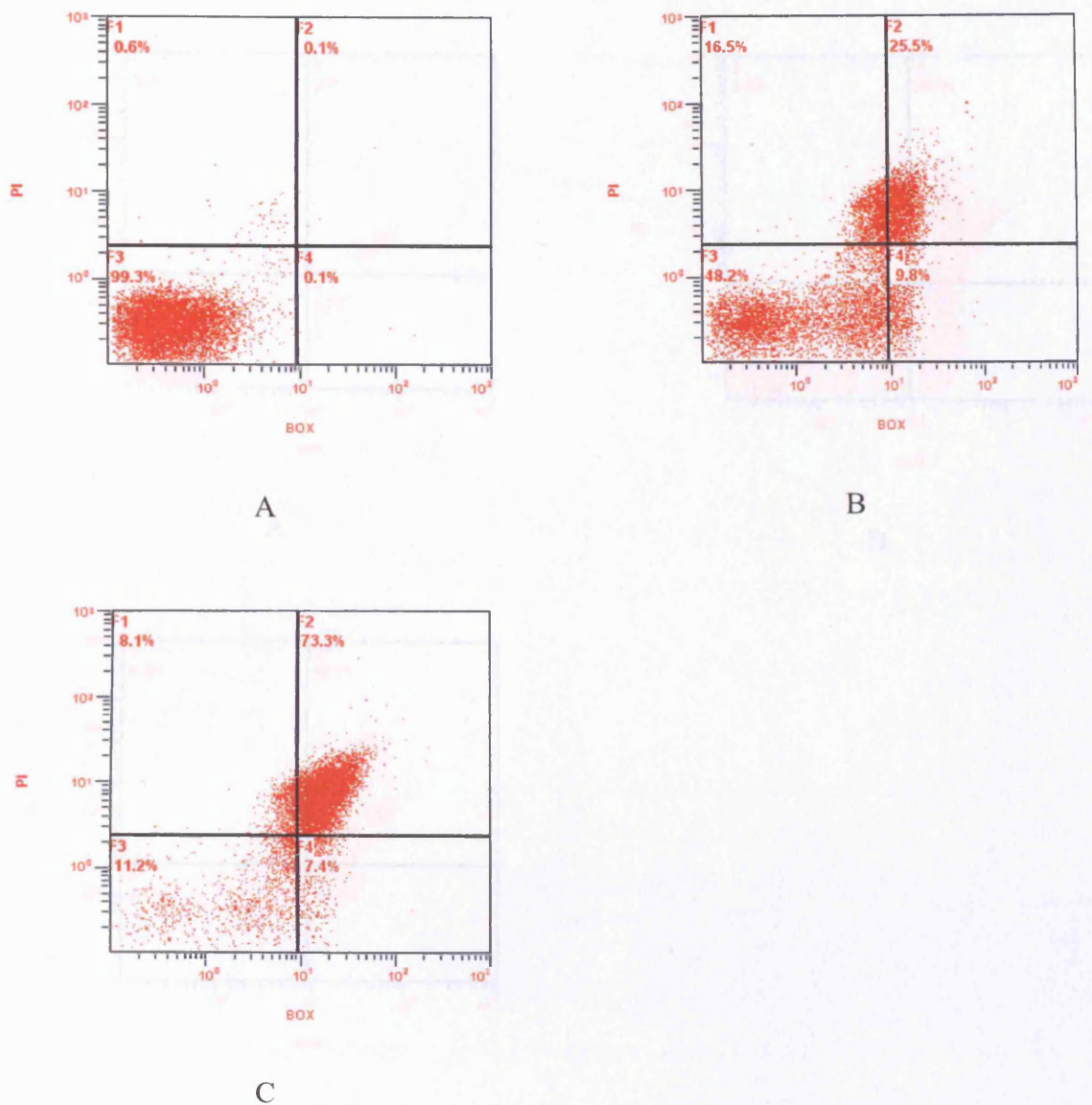
Figure A1.5   Heat treatment of W3110 *E. coli* cells at 60°C with a range of exposure times. Symbols: (A) residence time 0 s; (B) residence time 800 s; (C) residence time 1600 s.
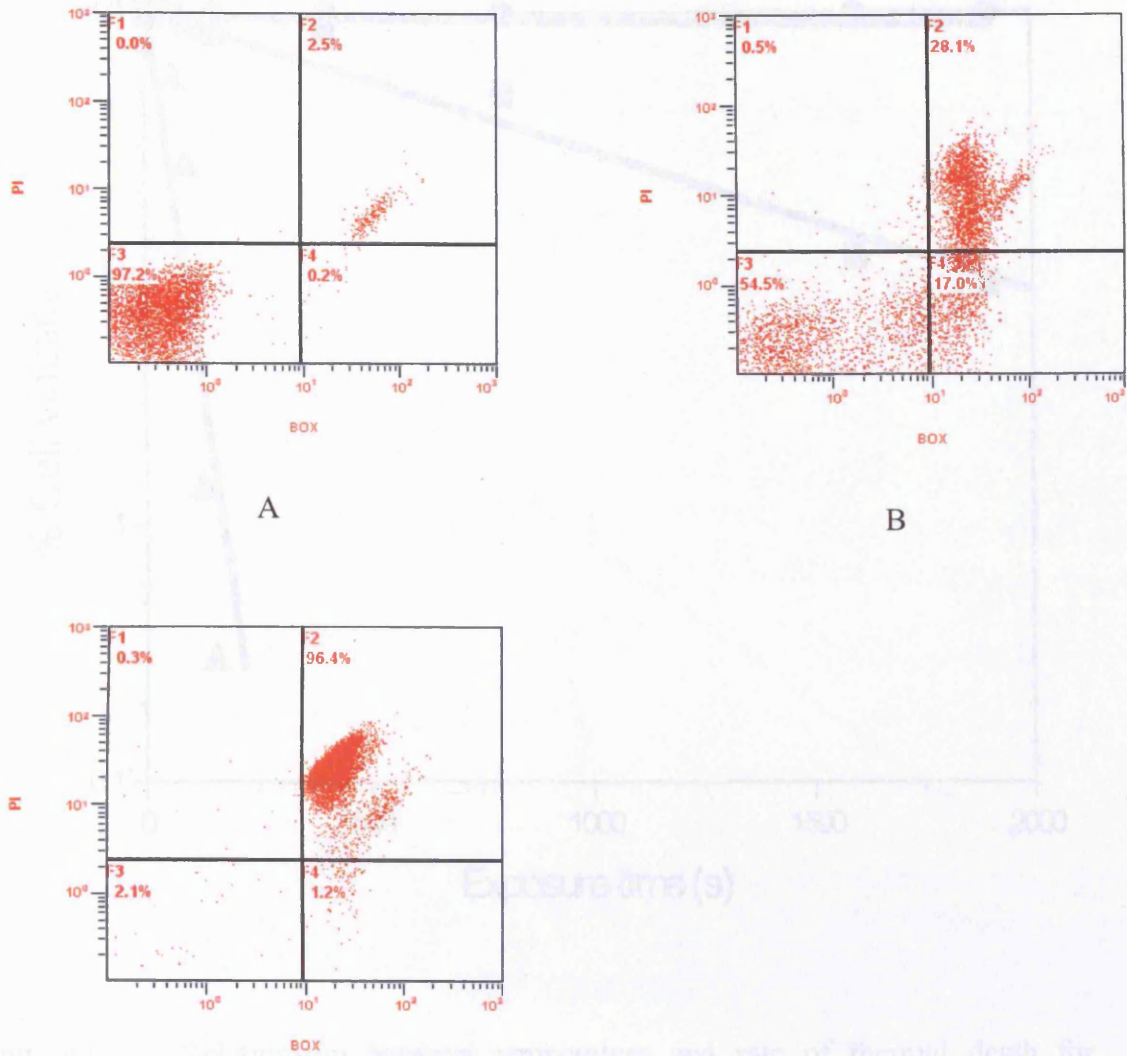
Figure A1.6   Heat treatment of W3110 *E. coli* cells at 80°C with a range of exposure times. Symbols: (A) residence time 0 s; (B) residence time 60 s; (C) residence time 150 s.
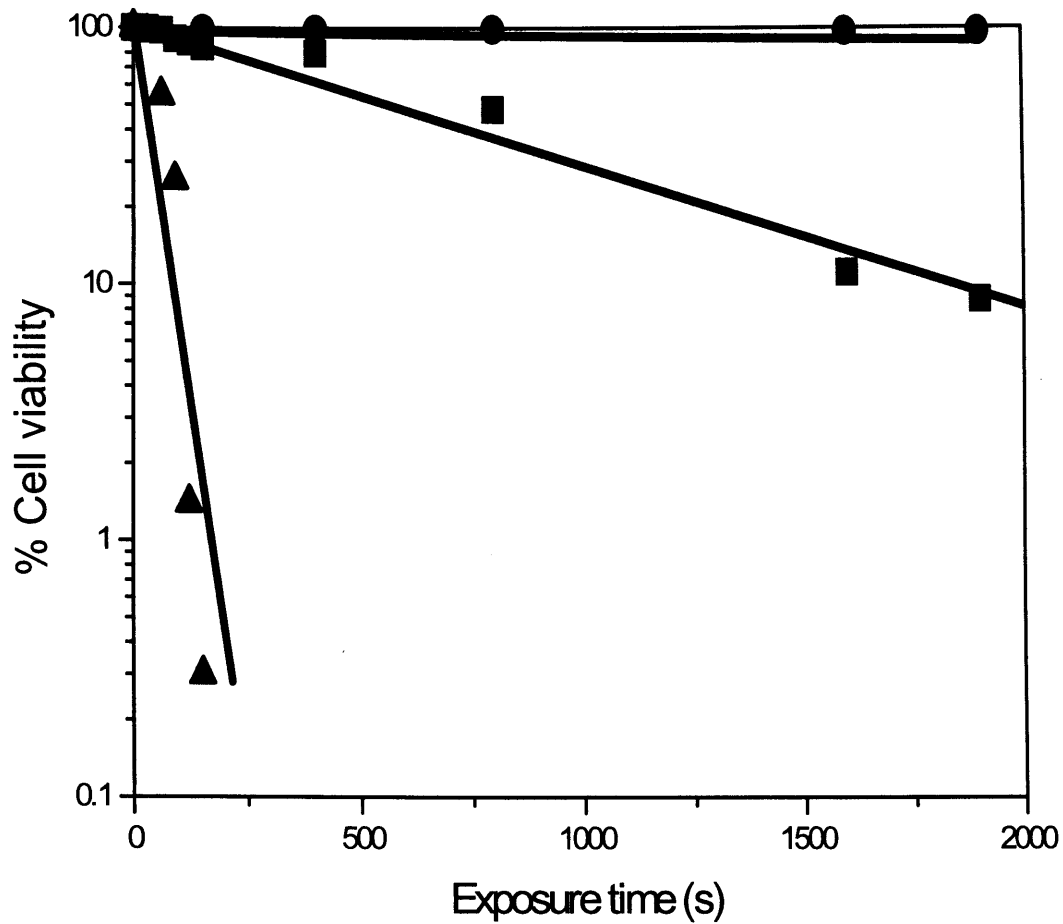
Figure A1.7   Relationship between temperature and rate of thermal death for W3110 *E. coli* cells. Symbols: (▲) heat treatment at 80°C (k = 0.039 s^{-1}); (■) heat treatment at 60°C (k = 1.27x10^{-3} s^{-1}); (●) heat treatment at 40°C (k = 1.56x10^{-5} s^{-1}).
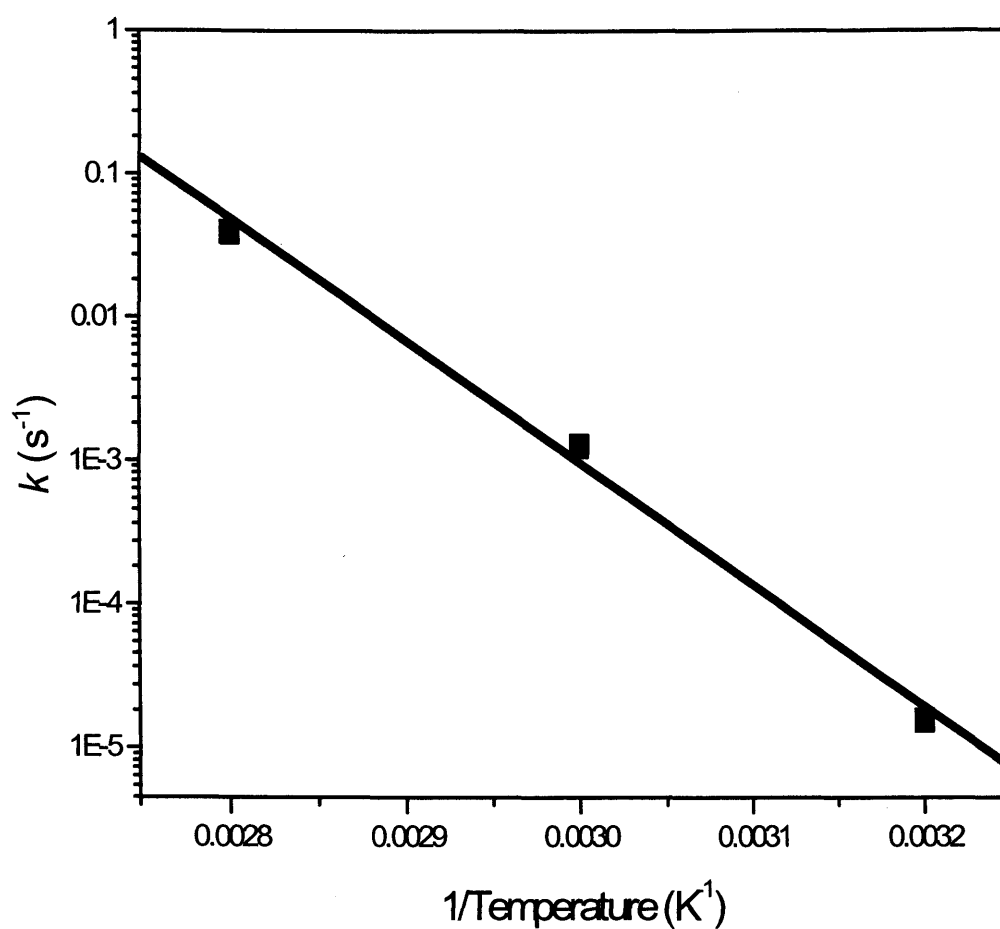
Figure A1.8   A semi-log plot of k versus 1/Temperature to determine the cell sensitivity to temperature changes. The slope is -252900 $K.min^{-1}$; therefore E is 2102 kJ $gmol^{-1}$.

A   B
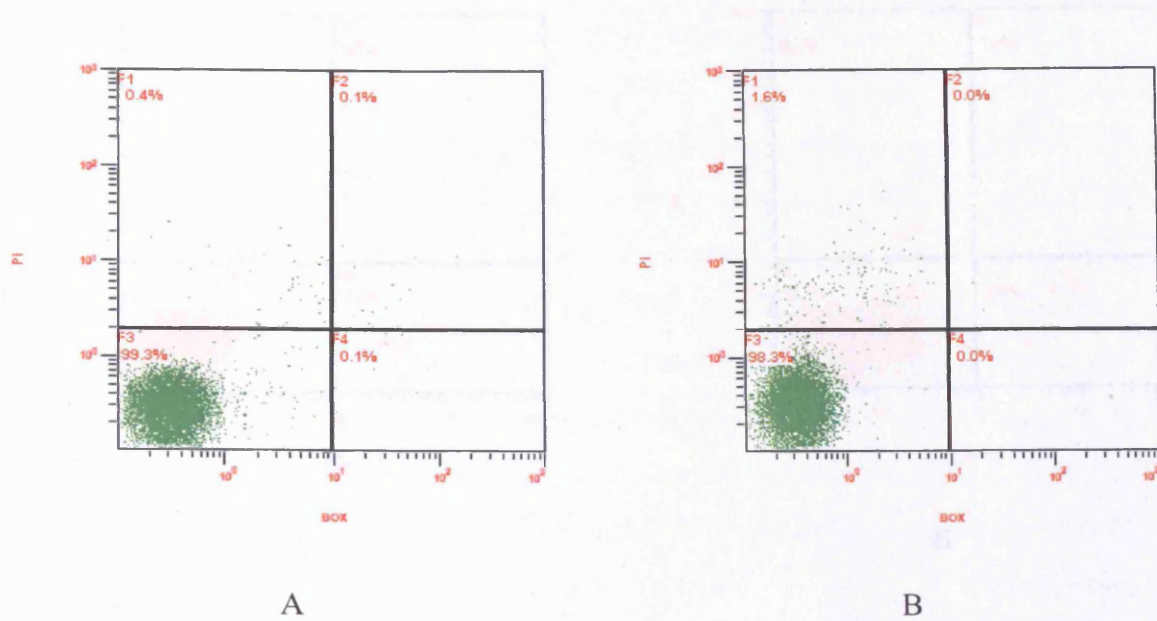
Figure A1.9   Effect of capillary G_cT_i (i.e. shear x residence time) on W3110 *E. coli* cell integrity. The temperature and viscosity were 4°C and 0.005 N.s.m^{-2} (Newtonian) with laminar flow conditions. Symbols: (A) G_cT_i of 0 (control); (B) G_cT_i of 4 x 10^3 (G_c of 633000 s^{-1}, T_i of 0.002 s (x 3 passes)). No obvious signs of cell damage were recorded under this condition.

Figure A1.10   Effect of shear exposure on W3110 *E. coli* cells in a small-scale rotating disc device. Air/liquid interfaces were minimised by filling the chamber with maximum capacity. The temperature and viscosity were 4°C and 0.0012 N.s.m^{-2} respectively. Symbols: (A) G_cT_i of 0; (B) G_cT_i of 3.3 x 10^5 (operating conditions of 11,000 rpm for 10 s); (C) G_cT_i of 4.5 x 10^5 (operating conditions of 15,000 rpm for 10 s). Conversion: shear rate in disc device (s^{-1}) = rpm x 2.988 (derived from CFD analysis).

A1.5 Discussion

Flow cytometry is a common tool used for rapid reliable screening of cell physiology for bioprocess optimisation (Lewis et al., 2004). The main advantage of this technology is that it can provide a snapshot of cell viability as a function of bioprocess environment. This study concentrates on the possible physiological changes associated with cell damage during bioprocessing. Escalating temperatures can often be associated with high shear stress or long process times, especially at large scale, if the unit operation is not properly controlled. Many authors have studied the phenomena of thermal inactivation of micro organisms (Stiles and Witter 1965; Gomez 1977; Mackey and Derrick 1987) and have identified nucleic acids, proteins and enzymes to be the main molecules damaged by the process. Grecz et al. (1977) demonstrated that temperatures above 50°C were able to induce endonucleolytic breakage in *E. coli*. Mackey et al. (1991) studied the denaturation of ribosome's in *E. coli* and concluded that ribosome melting occurred at above 60°C. For temperatures above 65°C cell wall damage may also contribute to thermal cell death (Teixeira et al., 1997). Our results suggest that temperature related cell damage consists of depolarisation followed by permeabilisation and cell death. Negligible cell damage was detected with temperatures below 40°C. However, increasing the severity of stress with either higher temperatures or longer residence time led to a greater number of dead cells which was reflected in the cells uptaking PI and BOX.

The influence of hydrodynamic forces on cells plays a significant role in determining the overall success of a bioprocess. Shear stresses have been observed to induce morphological and metabolic changes (Lange et al., 2000; Hewitt et al., 1998) in bacterial cells. Here we extend the investigation and comment on the possible side effects of these changes. Cell damage from exposure to shear was characterised by permeabilisation and depolarisation followed by cell death. The results correlate well with cell damage as measured by more traditional methods, e.g. total protein, where higher shear rates equate to greater cell damage.

A1.6 Conclusion

This work has identified several possible scenarios by which cells die from stress exposure. This work has demonstrated that exposure of cells to shear stress leads to permeabilisation and depolarisation followed by cell death. A distinct pattern of cell depolarisation followed by cell permeabilisation was observed with heat stress.

A2 DNA analysis

A2.1 Materials and methods

The DNA analysis procedure was carried out as supervisor of an MEng project and acknowledgment is due to Ben Bourne and Simyee Kong (advisor). The DNA analysis technique used is that described by Levy et al. (1999). 500 μL of clarified lysate and sheared samples were precipitated with 350 μL of isopropanol. The samples were centrifuged for 10 min at 13000 rpm in a Biofuge model 13 centrifuge (Heraeus Sepatech, GmbH, Germany) and the supernatant was decanted. The remaining pellet was washed with 70% ethanol and then re-dissolved in 50 μL TE buffer (pH 8) containing 100 $\mu g.mL^{-1}$ RNaseA. Samples were then purified using a QIAprep Spin Miniprep kit (Qiagen Ltd, West Sussex, UK) with the DNA concentrations determined using a Biomate 3 spectrophotometer at 260 nm (Thermo Spectronic, Madison, WI, USA). All samples (5 μL loading buffer and 10 μL sample) were then loaded onto a 0.8% agarose gel containing ethidium bromide and electrophoresed at 40 V and 100 mA for 9 h. Gels were scanned and analysed using the Gel Doc EQ Gel Documentation System and Quantity One analysis software (Bio-Rad Laboratories Inc, CA, USA).

A2.2 Preparation of agarose gels

To make a 0.8% gel:

- Seal the open edges of an electrophoresis tray with autoclave tape to form a mould.
- Mix 1.04 g agarose powder with 130 mL of 0.5x TBE buffer (Table A2.1) in a clean Erlenmeyer flask.
- Heat the mix in a microwave for 1 min.
- Remove and swirl the flask.
- Reheat for a further 1 min.
- Cool the solution until warm to touch (~60°C).

- Seal the edges of the mould with a small quantity of the agarose solution using a Gilson pipette.

- Position the comb into the mould.

- Add 5 μL of ethidium bromide solution to the agarose and mix gently.

- Pour the warm agarose solution into the mould avoiding any bubble formations.

- Allow the gel to set for 45 min at room temperature before removing the comb.

5x TBE Buffer	Quantity
Tris base	54.43 g
Boric acid	27.78 g
EDTA	1.85 g
Purified water	1 L

Table A2.1 Preparation of 5x TBE buffer (Prepare 1 L of 0.5x TBE buffer by adding 100 mL of 5x TBE to 900 mL water).

A3 Validation

A3.1 Introduction

A new drug cannot be manufactured without prior approval from regulatory bodies (e.g. FDA). The agency documents clearly emphasis the expectations that are required for approval. If the drug has never been marketed before, the manufacturer is required to file a new application demonstrating that the drug is safe and effective on both humans and animals. At this stage, product quality, concentration and type of impurities must be mentioned. This information is used to set the acceptance criteria after which all the other batches are required to either meet or surpass these specifications. In addition, the files must contain a detailed description of the process route used to manufacture the drug including details on installation qualification (IQ), operational qualification (OQ) and process qualification (PQ). If the report lacks confidence over quality and reproducibility of product, the FDA will not approve it.

The biopharmaceutical manufacturer is also expected to comply with good manufacturing practice (GMP) with the responsibility for maintaining product quality. Protocols and SOPs are used with operating, cleaning, maintaining and storage of equipment and staff should be properly trained to operate. These specifications fall under quality assurance (QA).

A3.2 GMP considerations

GMP regulations are required to minimise or eliminate the possibility of process errors e.g. contamination and human error such as batch mix up. This in turn protects the customer from purchasing a product which is unsafe for human consumption.

A3.2.1 Equipment validation

IQ, OQ and PQ apply to both old and new equipment and are used to ensure that all equipment and instruments meet manufacturers or preset standards for operation and performance. Movement of equipment will require re-evaluation to ensure that the move does not affect process quality.

A3.2.2 Sample management/document control

Throughout any biomanufacturing process all samples collected must be traceable in the event of a contamination or lose of product quality. Protocols must be in place for sample handling, storage and disposal. A logbook for each process step must be in place to allow one to reconstruct the analysis if necessary. With documentation comes document control. A system should be in place to review the archives of results and to ensure proper filing.

A3.2.3 Auditing

Auditing of a GMP plant falls into three categories:

- Personal: All employees do a self-check to ensure that he/she is complying with the regulations.
- Internal: An internal audit of the company practice is done by the quality control department.
- External: Company practice is assessed by an external auditor.

The results from an audit will indicate whether a company needs to modify their current practice.

A3.3 Validation of a centrifuge and its USD mimic

A3.3.1 Centrifuge validation

A3.3.1.1 Process validation

Process validation aims to ensure that a process runs according to the users specifications and that the method of operating is robust such that minimum variation occurs. The first step in completing a process validation is to define the purpose of the centrifuge e.g. to provide crude separation of liquid-solids suspensions. Operating conditions should be defined at this point e.g. flow rate and bowl speed. An acceptable criteria must be set. During the operation, samples should be taken at strategic points such as the feed inlet, discharge zone and supernatant outlet and

tested for quality using validated assay techniques. The reproducibility of the process must be demonstrated with a minimum of three runs of product and one must show that the quality falls within the acceptable range.

A3.3.1.2 Cleaning validation

A thorough cleaning process must be applied to any unit operation with the goal of eliminating contaminants and to prolong machine lifetime. Cleaning should be performed before and after processing product material. When developing a cleaning strategy, one must consider agents used, their concentrations and compatibility with equipment surfaces and product. For example, some detergents and soaps used for cleaning cannot be removed easily and therefore a different agent needs to be selected. Other factors such as residence time in the machine and surface coverage also needs consideration. Ideally a piece of equipment will have one cleaning procedure, however this will depend on the product being processed and whether the clean up occurs between batches of the same product or between batches of different product. In order to validate the cleaning program, a worse case clearance study senario is used whereby a highly concentrated feed stream is processed through the centrifuge followed by the cleaning protocol. The centrifuge is then tested extensively to ensure that the product is reduced to a predetermined acceptable limit. This can be assessed using a variety of methods including visual inspections, HPLC, and swab tests for specific contaminants. Samples should be taken at the inlet, outlet, centrifuge body and collection bowl. Staff must be sufficiently trained with following cleaning SOPs.

There should be evidence that cleaning and storage of equipment does not stimulate microbe proliferation. Equipment should always be dried before storage and preferably steam sterilised before use. Cleaning cycles should always be recorded in a log book along with any variations in quality of cleaning

A3.3.1.3 Validation of surroundings

The process area should be a clean environment with a controlled air quality. The centrifuge should have sufficient bio-containment features such as contained vessels and piping systems especially when dealing with live or genetic material. Process water and waste material should be exposed of in kill tanks.

A3.3.1.4 Assay validation

The assay techniques used to assess process efficiency must also be validated in order to prove their accuracy and reliability. The specificity and sensitivity of the analytical method must be determined. The majority of new generation assays have the ability of detecting residues at very low concentrations. If levels of contaminants or residue are not detected after cleaning, it does not necessarily mean no contaminants are present. Other assay techniques should be used in conjunction to verify results. A negative test may also be the result of poor sampling techniques.

A3.3.1.5 Quality control

To ensure protocols and SOP's are followed correctly, a supervisor should be on duty to record and document all completed tasks. Quality inspections should be carried out on a regular basis. Quality improvements should be continuous with a periodic review.

A3.3.2 USD validation

Similar to large-scale criteria, USD devices also require validation if they are incorporated into the development process. The advantage of including USD mimics is that besides only requiring small quantities of process material they could also be useful in reinforcing large-scale validation. Successful completion of this task involves filing SOP's and protocol documentation and ensuring all personnel using the equipment are properly trained. The equipment also requires IQ, OQ and PQ acknowledgement. All ancillaries associated with the model should be tested and calibrated if necessary. The model needs to be evaluated to show accurate mimicking

of its large-scale counterpart with a minimum of three trials. Process parameters such as feed type, temperature and pH should be controlled and kept in line with large scale conditions.

It is not uncommon to see many companies using extensive sampling and testing programs without ever really evaluating the effectiveness of the steps used. The technique chosen should be appropriate and reproducible. Assays used for analysis of results and cleaning inspection should be consistent with the large-scale techniques. On filing a validation report, the user has the added bonus of reducing time and effort for large-scale verification because of better understanding of the parameters that influence the process and operating limits.

A3.4 Conclusion

In conclusion, validation of equipment is performed in order to demonstrate consistency and uniformity of a process. The aim of the exercise is to show that practical data is consistent with predetermined specifications. Validation of USD tools can be very helpful in the understanding and testing of large-scale machines. The USD device has the advantage of only requiring small volumes of test material and therefore can effectively reduce time and resources for large-scale verification.

NOMENCLATURE

A	constant (-)
C	% cell breakage due to discharge from capillary or centrifuge
C_f	product concentration in feed (mg.mL^{-1})
C_h	product concentration in homogenate (mg.mL^{-1})
C_s	product concentration in test sample (mg.mL^{-1})
D_h	hydraulic diameter (m)
D_c	internal capillary diameter (m)
G_c	mass average shear rate (s^{-1})
H	height of centrifuge nozzle (m)
K_{CSA-1}	CSA-1 calibration factor (-)
K_{SC-6}	SC-6 calibration factor (-)
L_c	capillary length (m)
L	discharge nozzle length (m)
m	suspension mass (kg)
N	centrifuge rotational speed (rps)
P	centrifuge discharge pressure (pas)
ΔP	pressure drop (N.m^{-2})
Q_c	capillary suspension flowrate (m^3.s^{-1})
Q	centrifuge nozzle flowrate (m^3.s^{-1})
R_c	internal capillary radius (m)
Re	Reynolds number (-)
R_o	orifice radius (cm)
r_1	bowl inner radius (m)

r_2	radius of centrifuge inner liquid ring (m)
T_i	residence time (s)
U_c	capillary discharge velocity (m.s^{-1})
U_p	centrifuge discharge velocity (m.s^{-1})
v_{max}	maximum fluid velocity (m.s^{-1})
W	width of centrifuge nozzle (m)
X_b	jet break-up length (cm)
X_c	jet core length (cm)
X_i	Instron drive speed (m.s^{-1})

Greek Symbols

γ_w	capillary wall shear rate (s^{-1})
ρ_N	suspension density (kg.m^{-3})
μ	suspension viscosity (N.s.m^{-2})
τ	capillary shear stress (N.m^{-2})
μ_k	kinematic viscosity (m^2.s^{-1})
ε_T	total energy dissipation (J.s^{-1})
$\bar{f}$	Fanning friction factor (-)
ω	angular velocity of centrifuge bowl (rads.s^{-1})

REFERENCES

Abu-Reesh I, Kargi F. 1989. Biological responses of hybridoma cells to defined hydrodynamic shear stress. J Biotechnol 9:167-178.

Acker JP, McGann LE. 2003. Protective effect of intracellular ice during freezing. Cryobiology 46: 197-202.

Acker JP, McGann LE. 2002. Innocuous intracellular ice improves the survival of frozen cells. Cell Transplant. 11: 563-571.

Acker JP, Elliott JAW, McGann LE. 2001. Intercellular ice propagation: experimental evidence for ice growth through membrane pores. Biophys J 81: 1389-1397.

Ackermann JU, Muller S, Losche A, Bley T, Babel W. 1995. *Methylobacterium rhodesianum* cells tend to double the DNA content under growth limitations and accumulate PHB. J Biotechnol 39: 9-20.

Agerkvist I, Enfors SO. 1990. Characterisation of *E. coli* cell disintegration from a bead mill and high pressure homogenizers. Biotech Bioeng 36: 1083-1089.

Alberts B, Bray D, Lewis J, Raff M, Roberts K, Watson JD. 1994. Molecular biology of the cell 3rd ed. Garland Publishing ltd. 672-683.

Alias CB, Lopez MC, Fernandez FG, Sevilla JM, Sanchez JL, Grima E. 2004. Influence of power supply in the feasibility of *Phaeodactylum tricornutum* cultures. Biotech Bioeng 87: 723-733.

Aloi LE, Cherry RS. 1995. Cellular response to agitation characterized by energy dissipation at the impeller tip. Chem Eng Sci 51: 1523-1529.

Arnaud JP, Lacroix C, Foussereau C, Chopin L. 1993. Shear stress effects on growth and activity of *Lactobacillus delbrueckii* subsp *Bulgaricus*. J Biotechnol 29: 157-175.

Aronsson K, Ronner U, Borch E. 2004. Inactivation of *Escherichia coli*, Listeria innocua and Saccharomyces cerevisiae in relation to membrane permeabilisation and subsequent leakage of intraceullular compounds due to pulsed electric field processing. International Journal of Food Microbiology 99: 19-32.

Aunins JG, Lee AL, Volkin DB. 2000. The Biomedical Engineering Handbook, vol II. 1-16.

Al Naib SK. 1992. Jet mechanics and hydraulic structures: theory, analysis and design. Dagenham, Essex: S.K.Al Naib. 2-5

Al-Rubeai M, Singh RP, Emery AN, Zhang Z. 1995. Cell cycle and cell size dependence of susceptibility to hydrodynamic forces. Biotech Bioeng 46: 88-92.

Axelsson HAC. 1985. Centrifugation. Chapter 21 in "Comprehensive biotechnology. Vol 2, Cooney, Humphrey A.E. Pergamon Press, Oxford, UK.

Ayazi Shamlou P, Titchener-Hooker N. 1995. A physical model of high-pressure disruption of yeast cells. Chem Eng Sci 50: 1383-1391.

Ayazi Shamlou P, Titchener-Hooker N. 1993. Turbulent aggregation and breakup of particles in stirred vessels, in processing of solid-liquid suspensions. Chap 1: 1-26. Butterworth Heinemann.

Bell DJ, Dunnill P. 1982. Shear disruption of soya protein precipitate particles and the effect of aging in a stirred tank. Biotech Bioeng 24: 1271-1285.

Bell DJ, Hoare M, Dunnill P. 1983. The formation of protein precipitates and their centrifugal recovery. Adv Biochem Eng/Biotech 26: 1-72.

Belter PA, Cussler EL, Hu WS. 1988. Centrifugation. In: Bioseparation: downstream processing for biotechnology. New York: John Wiley and Sons : 47-73.

Better M, Chang CP, Robinson RR, Horwitz AH. 1988. *Escherichia coli* secretion of an active chimeric antibody fragment. Science 240: 1041-1043

Bibby K, Davis J, Jones C, IMS Global Consulting. 2003. Biopharmaceuticals-Moving to centre stage. BioPeople North American Biotechnology Industry and Suppliers Guide 3-11.

Bobrowicz G. 1999. The compliance costs of hasty process development. Biopharm 12 (Aug): 35-38.

Born C, Zhang Z, Al-Rubeai M, Thomas CR. 1992. Estimation of disruption of animal cells by laminar shear stress. Biotech Bioeng 40: 1004-1010.

Boulding N, Yim SSS, Keshavarz-Moore E, Shamlou PA, Berry M. 2002. Ultra scale-down to predict filtering centrifugation of secreted antibody fragments from fungal broth. Biotech Bioeng 79: 381-388.

Bowering LC. 2000. An engineering study of the design, integration and control of antibody fragment production processes. University of London Thesis.

Bonnerjea J, Jackson J, Hoare M, Dunnill P. 1988. Affinity flocculation of yeast cell debris by carbohydrate-specific compounds. Enzyme Microb Technol 10: 357-360.

Boss MA, Kenten JH, Wood CR, Emtage JS. 1984. Assembly of functional antibodies from immunoglobulin heavy and light chains synthesised in *E. coli*. Nucleic Acid Research 12: 3791-3806

Bowen WR, Gan Q. 1992. Properties of Microfiltration membranes: The effects of adsorption and shear on the recovery of an enzyme. Biotech Bioeng 40: 491-497.

Boychyn M, Yim SSS, Bulmer M, More J, Bracewell DG, Hoare M. 2004. Performance prediction of industrial centrifuges using scale-down models. Bioprocess Biosyst Eng 26: 385-391.

Boychyn M, Yim SSS, Shamlou PA., Bulmer M, More J, Hoare M. 2001. Characterization of flow intensity in continuous centrifuges for the development of laboratory mimics. Chem Eng Sci 56: 4759-4770.

Boychyn M, Doyle W, Bulmer M, More J, Hoare M. 2000. Laboratory scale down of protein purification processes involving fractional precipitation and centrifugal recovery. Biotech Bioeng 69: 1-10.

Brekke OH, Sandlie I. 2003. Therapeutic antibodies for human disease at the dawn of the 21st century. Nat Rev Drug Discovery 2: 52-62.

Bradford MM. 1976. A rapid and sensitive method for the quantitation of microgram quantities of protein utilizing the principle of protein-dye binding. Analytical Biochemistry 72: 248-254.

Braun V. 1975. Covalent lipoprotein from the outer membrane of *E. coli*. Biochem Biophys Acta (BBA) 415: 335-377.

Bridges BA, Ashwood-Smith MJ, Munson RJ. 1969. Susceptibility of mild thermal and of ionizing radiation damage to the same recovery mechanisms in *E. coli*. Biochem Biophys Res Commun. 35: 193-196.

Brookman J. 1974. Mechanism of cell disruption in a high-pressure homogeniser. Biotech Bioeng 16: 371-383.

Brunner KH, Hemfort H. 1988. Downstream processes: Equipment and techniques, Centrifugal separation in biotechnological processes, Advances in biotechnological processes. Vol 8, Mizrahi A, Alan R. Liss inc, New York: 1-50.

Brunton JH, Rochester MC. Erosion of solid surfaces by the impact of liquid drops. In erosion-treatise on material science and technology, C.M. Preceed 185-248.

Buchner J, Rudolf R. 1991. Renaturation, purification and characterisation of recombinant Fab fragments produced in *Escherichia coli*. Biotechnology 9: 157-162.

Burks EA, Iverson BL. 1995. Rapid high yield recovery of a recombinant digoxin binding single chain Fv from *E. coli*. Biotech Prog 11: 112-114.

Byrne EP, Fitzpatrick JJ, Pampel LW, Titchener-Hooker NJ. 2002. Influence of shear on particle size and fractal dimension of whey protein precipitates: implications for scale-up and centrifugal clarification efficiency. Chem Eng Sci 57: 3767-3779.

Cabilly S, Riggs AD, Pande H, Shively JE, Holmes WE, Rey M, Perry J, Wetzel R, Heyneker HL. 1984. Generation of antibody activity from immunoglobulin polypeptide chains produced in *E. coli*. Proc National Academy of Science 81: 3273-3277.

Carlson A, Signs M, Liermann L, Boor R, Jem KJ. 1995. Mechanical disruption of *E. coli* for plasmid recovery. Biotech Bioeng 48: 303-315.

Carter P, Kelley RF, Rodrigues ML, Snedcor B, Covarrubias M, Velligan MD, Wong WHT, Rowland AM, Kotts CE, Carver ME, Yang M, Bourell JH, Shepare HM, Henner D. 1992. High level *E. coli* expression and production of a bivalent humanised antibody fragment. Biotechnology 10: 163-167.

Chabb HE, Chamow MS. 2001. Therapeutic antibody expression technology. Current Opinions in Biotechnology 12: 188-194.

Chalmers JJ, Bavarian F. 1991. Microscopic visualisation of insect cell-bubble interactions II: The bubble film and bubble rupture. Biotechnol Prog 7: 151-158.

Chan G, Booth AJ, Mannweiler K, Hoare M. 2006. Ultra scale-down studies of the effect of flow and impact conditions during *E. coli* processing. Biotech Bioeng (submitted).

Chandra S, Avendisian CT. 1991. On the collision of a droplet with a solid surface. Proc R Soc Lond A 432, 13.

Chester KA, Hawkes RE. 1995. Clinical issues in antibody design. Trends in Biotechnology 13: 294-300.

Cherry RS, Hulle CT. 1992. Cell death in the thin films of bursting bubbles. Biotechnol Prog 8: 11-18.

Cherry RS, Know KJ. 1990. Transient shear stresses on a suspension cell in turbulence. Biotech Bioeng 36: 563-571.

Cherry RS, Papoutsakis ET. 1988. Physical mechanisms of cell damage in micro-carrier cell culture bioreactors. Biotech Bioeng 32: 1001-1014.

Cherry RS, Papoutsakis ET. 1986. Hydrodynamic effects of cells in agitated tissue culture reactors. Bioprocess Eng 1: 29-41.

Chisti Y. 1999. Shear sensitivity. In: Flickinger MC, Drew SW, editors. Encyclopedia of bioprocess technology: Fermentation, biocatalysis, and bioseparations. New York Wiley 5: 2379-2406.

Chisti Y. 2000. Animal-cell damage in sparged bioreactors. Trends in Biotechnol 18: 420-432.

Clarkson AI, Lefevre P, Titchener-Hooker NJ. 1993. A study of the process interactions between cell debris clarification stages in the recovery of yeast intracellular products. Biotech Prog 9: 464-467.

Collins S, Attouche C, Yau C, Jones M, Lovitt R. 1996. Institution of chemical engineers research event, University of Leeds, UK: 52-54.

Ciccolini LAS, Shamlou PA, Titchener-Hooker N. 2002. A mass balance study to assess the extent of contaminant removal achieved in the operations for the primary recovery of plasmid DNA from *E. coli* cells. Biotech Bioeng 77: 796-805.

Ciccolini LAS, Ayazi Shamlou P, Titchener-Hooker NJ, Ward JM, Dunnill P. 1998. Time course of SDS-alkaline lysis of recombinant bacterial cells for plasmid release. Biotech Bioeng 60: 768-770.

Croughan MS, Hamel JF, Wang DIC. 1987. Hydrodynamic effects on animal cells grown in microcarrier cultures. Biotech Bioeng 29: 130-141.

Croughan MS, Sayre ES, Wang DIC. 1989. Viscous reduction of turbulent damage in animal cell cultures. Biotech Bioeng 33: 862-972.

Curly J, Smiley L. 2003. Chromatography for plasmid DNA manufacture-tutorial: Novel adsorbent technology for cGMP production of plasmid DNA. Gen Eng News 23:42.

Dangl JL, Parks DR, Oi VT, Herzenberg LA. 1982. Rapid isolation of cloned isotype switch variants using fluorescence activated cell sorting. Cytometry 2: 395-401.

Datar R, Rosen CG. 1987. Centrifugal separation in the recovery of intracellular protein from *E. coli*. J Chem Eng 34: 49-56.

Datar R. 1986. Economics of primary separation steps in relation to fermentation and genetic engineering. Process Biochemistry, Feb: 19-25.

Davey HM, Douglas BK. 1996. Flow cytometry and cell sorting of heterogeneous microbial populations: the importance of single-cell analyses. Microbiological reviews 60: 641-696.

Davies TW, Metcalfe RA, Jackson MK. 1980. The anatomy and impact characteristics of large scale water jets. Fifth international symposium on jet cutting technology 15-21.

Deere D, Shen J, Vesey G, Bell P, Bissinger P, Veal D. 1998. Flow cytometry and cell sorting for yeast viability assessment and cell selection. Yeast 14: 147-160.

Demain AL. 2000. Microbial biotechnology. Trends in Biotechnol 18: 26-31.

Dooley BS, Warncke AE, Gharib M, Tryggvason G. 1997. Vortex ring generation due to the coalescence of a water drop at a free surface. Exps Fluids 22: 369.

Doulah M, Brookman J. 1975. A hydrodynamic mechanism for the disintegration of *Saccharomyces cerevisiae* in an industrial homogeniser. Biotech Bioeng 17: 845-858.

Doran PM. 1993. Design of reactors for plant cells and organs. Advanced Biochemical Engineering Biotechnology 48: 117-168.

Doran PM. 2000. Bioprocess engineering principles. Academic Press Limited.

Dunlop EH, Namdev PK, Rosenberg MZ. 1994. Effect of fluid shear forces on plant cell suspensions. Chem Eng Sci 49: 2263-2276.

Durland RH, Eastman EM. 1998. Manufacturing and quality control of plasmid-based gene expression systems. Advanced Drug Delivery Review 30: 33-48.

Edwards N, Beeton S, Bull AT, Merchuk JC. 1989. A novel device for the assessment of shear effects on suspended microbial cultures. Appl Microbiol Biotechnol 30: 190-195.

Engler C, Robinson C. 1981. Disruption of Candida utilis cells in high-pressure flow devices. Biotech Bioeng 23: 765-780.

Follows M, Hetherington PJ, Dunnill P, Lilly MD. 1971. Release of enzymes from bakers yeast by disruption in an industrial homogenizer. Biotech Bioeng 13: 549-560.

Fox RW, McDonald AT. 1994. Introduction to fluid mechanics (4th ed). John Wiley and Sons, Inc 330-333.

Frangos JA, Mc Entire LV, Eskin SG. 1988. Shear stress induced stimulation of mammalian cell metabolism. Biotech Bioeng 32: 1053-1060.

Garcia-Arrazola R, Siu SC, Chan G, Buchanan I, Doyle B, Titchener-Hooker N, Baganz F. 2005. Evaluation of a pH-stat feeding strategy on the production and recovery of Fab' fragments from *E. coli*. Biochem Eng Journal 23: 221-230.

Garcia-Briones MA, Chalmers JJ. 1994. Flow parameters associated with hydrodynamic cell injury. Biotech Bioeng 44: 1089-1098.

Gierczycki AT, Ayazi Shamlou P. 1996. Aggregation of monosized particles in turbulently agitated suspensions- A simplified approach. Chemical and Biochemical Engineering Quarterly 10: 125-128.

Gomez RF. 1977. Nucleic acid damage in thermal inactivation of vegetative microorganisms. Adv Biochem Eng 5: 49-67.

Gray PP, Dunnill P, Lilly MD. 1973. The clarification of mechanically disrupted yeast suspensions by rotary vacuum pre-coat filtration. Biotech Bioeng 15: 309-320.

Gray PP, Dunnill P, Lilly MD. 1972. The continuous-flow isolation of enzymes. In Ferment Technol Today, G. Terui ed., Soc of Ferment Technol, Tokyo 347-351.

Grecz N, Bhatarakamol S. 1977. Apurinic acid endonuclease implicated in DNA breakage in *E. coli* subjected to mild heat. Biochem Biophys Res Commun 77: 1183-1188.

Groep ME, Gregory ME, Kershenbaum LS, Bogle IDL. 2000. Performance modelling and simulation of biochemical process sequences with interacting unit operations. Biotech Bioeng 67: 300-310.

Gunasekera TS, Sorensen A, Attfield PV, Sorensen SJ, Veal DA. 2002. Inducible gene expression by non-culturable bacteria in milk after pasteurisation. Appl Environ Microbiol 68: 1988-1993.

Haller KK, Ventikos Y, Poulikakos D, Monkewitz P. 2002. Computational study of high-speed liquid droplet impact. J Appl Phys 92: 2821-2828.

Harnby N, Edwards MF, Nienow AW. 1992. Mixing in the process industries, 2nd ed. Butterworth-Heinemann Ltd, Oxford, UK. Biochem Biophys Res Com 60: 140-145.

Handa A, Emery AN, Spier RE. 1987. On the evaluation of gas-liquid interfacial effects on hybridoma viability in bubble column bioreactors. Dev Biol Stand 66: 241-253.

Hashish M, Reichman JM. 1980. Analysis of waterjet cutting at high traverse rates. Fifth international symposium on jet cutting technology 57-74.

Hatz H, Burgdorf K, Holtje JV. 1990. Isolation and separation of the glycan strands from murein of *Escherichia coli* by reversed-phase high-performance liquid chromatography. Analytical Biochem 190: 120-128.

Hearle DC, Aguilera-Soriano G, Titchener-Hooker NJ, Wiksell E. 1994. Quantifying the fouling effects of a biological process stream on chromatographic supports. Proc IChemE Res Event 174-176.

Hewitt CJ, Nebe-Von Caron G, Nienow AW, McFarlane CM. 1999. Use of Multi-staining flow cytometry to characterise the physiological state of *Escherichia coli* W3110 in high cell density fed-batch cultures. Biotech Bioeng 63: 705-711.

Hewitt CJ, Boon LA, McFarlane CM, Nienow AW. 1998. The use of flow cytometry to study the impact of fluid mechanical stress on *Escherichia coli* W3110 during continous cultivation in an agitated bioreactor. Biotech Bioeng 59: 612-620.

Higgins JJ, Lewis DJ, Daly WH, Mosqueira FG, Dunnill P, Lilly MD. 1978. Investigation of the unit operations involved in the continuous flow isolation of β-galactosidase. Biotech Bioeng 20: 159-182.

Hrycak P, Lee D, Gauntner J, Livingood J. 1969. Experimental flow characteristics of a single turbulent jet impinging on a flat plate. Lewis research center, NASA, Cleveland, Ohio 720-03.

Hudson PJ. 1998. Recombinant antibody fragments. Current Opinion in Biotechnology 9: 395-402.

Hudson PJ. 1999. Recombinant antibody constructs in cancer therapy. Current Opinion in Immunology 11: 548-557.

Hull AS, Middelberg APJ. 1993. Evidence that septated *E. coli* disrupt preferentially during high-pressure homogenisation. Food Bioprod Processing, Trans Inst Chem Eng, Part C 71:264-266.

Humphreys DP. 2003. Production of antibodies and antibody fragments in *E. coli* and a comparison of their functions, uses and modification. CURR Opin Drug Discovery Dev 6: 188-196

Humphrey DP, Heywood SP, King LM, Bowering LC, Turner JP, Lane SE. 2004. Engineering of *E. coli* to improve the purification of periplasmic Fab fragments: changing the p*I* of the chromosomally encoded PhoS/PstS protein. Protein Expression and Purification 37: 109-118

Hurst A. 1984. Reversible heat damage. In repairable lesions in microorganisms ed. Hurst A, Nasim A. Academic press, London, UK. 303-316.

Hurst A, Hughes A, Beare-Rogers JL, Collins-Thompson DL. 1973. Physiological studies on the recovery of salt tolerance by *Staphylococcus aureus* after sublethal heating. J Bacteriol 116: 901-907.

Hurst A. 1977. Bacterial injury: A review. Can J Microbiol 23: 936-977.

Hutter KL, Eipel HE. 1979. Microbial determinations by flow cytometry. J Gen Microbiol 113: 369-375.

Jaouen P, Vandanjon L, Quemeneur F. 1999. The shear stress of microalgal cell suspensions (*Tetraselmis suecica*) in tangential flow filtration systems: the role of pumps. Bioresource Technol 68: 149-154.

Jin K, Thomas ORT, Dunnill P. 1994. Monitoring recombinant inclusion body recovery in an industrial disc stack centrifuge. Biotech Bioeng 44: 455-460.

Johnston W, Cord-Ruwisch R, Cooney MJ. 2002. Industrial control of recombinant *E. coli* fed-batch culture: new perspectives on traditional controlled variables, Bioprocess Biosyst Eng 25: 111–120.

Karlsson JOM, Cravalho EG, Toner M. 1993. Intracellular ice formation: causes and consequences. Cryo-lett 14: 323-334.

Kawase Y, Moo-Young M. 1990. Mathematical models for design of bioreactors: Applications of Kolmogoroff's theory of isotropic turbulence. Chem Eng Sci 43: 19-41.

Keshavarz-Moore E, Hoare M, Dunnill P. 1990. Disruption of baker's yeast in a high-pressure homogeniser: New evidence on mechanism. Enzyme Microb Technol 12: 764-770.

Kretzmer G, Schugerl K. 1991. Response of mammalian cells to shear stress. Applied Microbiol Biotechnol 34: 613-616.

Kula MR, Schuette H, Vogles G, Frank A. 1990. Cell disintegration for the purification of intracellular proteins. Food Biotechnol 4: 169-183.

Kula MR, Schutte H. 1987. Purification of proteins and the disruption of microbial cells. Biotechnol Prog 3: 31-42.

Lander R, Manger W, Lee A. 2000. Gaulin homogeniser: A mechanistic study. Biotechnol Prog 16: 80-85.

Lange H, Taillandier P, Riba JP. 2001. Effect of high shear stress on microbial viability. J Chem Technol Biotechnol 76: 501-505.

Lebaron P, Troussellier M, Got P. 1994. Accuracy of epiflourescence microscopy counts for direct estimates of bacterial numbers. J Microbial Methods 19: 89-94.

Lee SY. 1996. High cell-density culture of *E. coli*. Trends in Biotechnol 14: 98-105.

Lencki RW, Tecante A, Choplin L. 1993. Effect of shear on the inactivation kinetics of the enzyme dextransucrase. Biotech Bioeng 42: 1061-1067.

Lesser MB, Field JE. 1983. The geometric wave theory of liquid impact, sixth conference on erosion by liquid and solid impact, Cavendish laboratory, Madingley road, Cambridge, CB3 OHE, UK.

Levesque MJ, Sprague EA, Schwartz CJ, Nerem RM. 1989. The influence of shear stress on cultured vascular endothelial cells: the stress response of an anchorage dependent mammalian cell. Biotechnol Prog 5: 1-8.

Levy MS, Lotfian P, Kennedy RO, Lo-Yim MY, Shamlou PA. 2000. Quantitation of supercoiled circular content in plasmid DNA solutions using a fluorescence-based method. Nucleic Acids Research 28: 12 E57.

Levy MS, Kennedy RD, Shamlou PA, Dunnill P. 2000. Biochemical engineering approaches to the challenges of producing pure plasmid DNA. Trends in Biotechnology 18: 296-305.

Levy MS, Collins IJ, Yim SS, War JM, Titchener-Hooker N, Shamlou P, Dunnill P. 1999. Effect of shear on plasmid DNA in solution. Bioprocess Eng 20: 7-13.

Levy MS, Ciccolini LAS, Yim SS, Tsai JT, Titchener-Hooker N, Shamlou PA, Dunnill P. 1999. The effects of material properties and fluid flow intensity on plasmid DNA recovery during cell lysis. Chem Eng Sci 54: 3171-3178.

Leung WWF. 1998. Industrial centrifugation technology. McGraw-Hill. pp306.

Lewis G, Taylor IW, Nienow AW, Hewitt CJ. 2004. The application of multi-parameter flow cytometry to the study of recombinant *Escherichia coli* batch fermentation processes. J Ind Microbiol Biotechnol 31: 311-322.

Lightfoot EN, Moscariello JS. 2004. Bioseparations. Biotech Bioeng 87: 259-273.

Lozina-Lozinsky LK. 1965. Survival of some insects and cells following intracellular ice formation. Fed Proceed 15: S206-S211.

Lutkemeyer D, Ameskamp N, Tebbe H, Wittler J, Lehmann J. 1999. Estimation of cell damage in bench and pilot-scale affinity expanded-bed chromatography for the purification of monoclonal antibodies. Biotech Bioeng 65: 114-119.

Maa YF, Hsu CC. 1996. Effect of high shear on proteins. Biotech Bioeng 51: 458-465.

Mackey BM, Miles CA, Parsons SE, Seymour DA. 1991. Thermal denaturation of whole cells and cell components of *E. coli* examined by differential scanning calorimetry. Journal of Gerneral Microbiology 137: 2361-2374.

Mackey BM, Derrick CM. 1987. Changes in the heat resistance of Salmonella typhimurium during heating at rising temperatures. Letters in Applied Microbiology 4: 13-16.

Maguire LA, Zhang H, Shamlou PA. 2003. Preparation of small unilamellar vesicles (SUV) and biophysical characterization of their complexes with poly-L-lysine-condensed plasmid DNA. Biotechnol Appl Biochem 37: 73-81.

Mannweiler K, Hoare M. 1992. The scale-down of an industrial disc stack centrifuge. Bioprocess Eng 8: 19-25.

Mannweiler K, Titchener-Hooker NJ, Hoare M. 1989. Biochemical engineering improvements in the centrifugal recovery of biological particles. IChemE-Symposium on Adv Biochem Eng 105-117.

Mark M. 1994. Biopharmaceutical R&D success rates and development times. A new analysis provides benchmarks for the future. Biotechnology 12: 674-679.

Marquet M, Horn NA, Meek JA. 1995. Process development for the manufacture of plasmid DNA vectors for use in gene therapy. Biopharm 8:26.

Martineau P, Jones P, Winter G. 1998. Expression of an antibody fragment at high levels in the bacterial cytoplasm. Journal of Molecular Biology 280: 117-127.

Maybury JP, Mannweiler K, Titchener-Hooker NJ, Hoare M, Dunnill P. 1998. The performance of a scaled down industrial disc stack centrifuge with a reduced feed material requirement. Bioprocess Eng 18: 191-199.

Maybury JP, Hoare M, Dunnill P. 1999. The use of laboratory centrifugation studies to predict performance of industrial machines: studies of shear-insensitive and shear-sensitive materials. Biotech Bioeng 67: 265-273.

Mazur P. 1984. Freezing of living cells: mechanisms and implications. Am J Physiol 247: C125-C147.

McQueen A, Bailey JE. 1989. Influence of serum level, cell line, flow type and viscosity on flow-induced lysis of suspended mammalian cells. Biotechnol Lett 11: 531-536.

McQueen A, Meilhoc E, Bailey JE. 1987. Flow effects on the viability and lysis of suspended mammalian cells. Biotechnol Lett 9: 831-836.

Meister BJ, Scheele GF. 1969. Prediction of jet length in immiscible liquid systems. AIChE J 15: 689.

Miller J, Rogowski M, Kelly W. 2002. Using a CFD model to understand the fluid dynamics promoting *E. coli* breakage in a high-pressure homogeniser. Biotech Prog 18: 1060-1067.

Moreira JL, Paula MA, Aunins JG, Carrondon MJT. 1995. Hydrodynamic effects on BHK cells grown as suspended natural aggregates. Biotech Bioeng 46: 351-360.

Mosqueira FG, Higgins JJ, Dunnill P, Lilly MD. 1981. Characteristics of mechanically disrupted bakers yeast in relation to its separation in industrial centrifuges. Biotech Bioeng 23: 335-343.

Muldrew K, Acker JP, Wan R. 2000. Investigations into quantitative post hypertonic lysis theory using cultured fibroblasts. Cryobiology 41: 337.

Murrell NJ. 1998. An engineering study of the recovery of shear sensitive biological materials by high speed disk stack centrifugation. University of London Thesis.

Nanninga N. 1998. Morphogenesis of *Escherichia coli*. Microbiology and Molecular Biology Reviews 62: 110-129.

Neal G, Christies J, Keshavarz-Moore E, Shamlou PA. 2003. An ultra scale-down approach for the prediction of full-scale recovery of ovine polycolonal immunoglobulins used in the manufacture of snake venom-specific Fab' fragment. Biotech Bioeng 81: 149-157.

Neal G, Francis R, Keshavarz-Moore E, Shamlou PA. 2004. Separation of IgG precipitate from contaminating proteins using Microfiltration. Biotech and Applied Biochem 39: 241-248

Nebeker EB. 1983. Standoff distance improvement using percussive jets, Scientific Associates, Inc. Santa Monica, California for US department of energy under contract DEAC01-79ET14280, p28-44.

Nebe-von-Caron G, Stephens PJ, Hewitt CJ, Powell JR, Badley RA. 2000. Analysis of bacterial function by multi-colour and single cell sorting. J Microsc Methods 42: 97-114.

Nebe-von Caron G, Bradley RA. 1995. Viability assessment of bacteria in mixed populations using flow cytometry. J Microscopy 179: 55-66.

Neppiras EA, Hughes DE. 1964. Some experiments on the disintegration of yeast by high intensity ultrasound. Biotechnol Bioeng 6: 247-270.

Nikaido H, Vaara M. 1985. Molecular basis of bacterial outer membrane permeability. Microbiol Rev 49: 1-32.

Obara T, Bourne NK, Field JE. 1995. Liquid-jet impact on liquid and solid surfaces. WEAR 186-187: 388-394.

Oh SKW, Nienow AW, Al-Rubeai M, Emery AN. 1989. The effects of agitation intensity with and without continuous sparging on the growth and antibody production of hybridoma cells. J Biotechnol 12: 45-62.

Olive GE. 1959. Ps in metals caused by collision with liquid drops and soft metal spheres. Journal of Research of National Bureau of Standards 62: 229-246.

Papoutsakis ET. 1991. Fluid-mechanical damage of animal cells in bioreactors. Trends in Biotech 9: 427-437.

Pellon JR, Ulmer KM, Gomez RF. 1980. Heat damage to the folded chromosome of *E. coli* K-12. Applied and Environmental Microbiology 40: 358-364.

Peterson JF, McIntire LV, Papoutsakis ET. 1988. Shear sensitivity of cultured hybridoma cells (CRL-8018) depends on mode growth, culture age and metabolic concentration. J Biotechnol 7: 229-246.

PhRMA. www.phrma.org

Prather KJ, Sagar S, Murphy J, Chartrain M. 2003. Industrial scale production of plasmid DNA for vaccine and gene therapy: plasmid design, production and purification. Enzyme and Microbial Technology 33: 865-883.

Prazeres DMF, Ferreira GNM. 2004. Design of flowsheets for the recovery and purification of plasmids for gene therapy and DNA vaccination. Chem Eng and Processing 43 : 615-630.

Prescott LM, Harley JP, Klein DA. 1999. Microbiology (4th edition). WCB McGraw-Hill, p55.

Ramamurthy V, Thacker SP, Kothari RM. 1992. Optimised protocol for the pilot-scale preparation of fungal cellulase. J Indust Microbiol 9: 121-125.

Reichman JM, Cheung JB. 1980. Research and development of a high–pressure waterjet device for geothermal exploration and drilling. Fifth international symposium on jet cutting technology 181-200.

Reichert JM. 2000. New biopharmaceuticals in the USA: trends in development and marketing approvals 1995-1999. Trends in Biotechnol 18: 364-369.

Richards JR, Lenhoff AM, Beris AN. 1994. Dynamic break-up of liquid-liquid jets. Phys Fluids 6: 8.

Rodrigues ML, Snedecor B, Chen C, Wong WLT, Garg S, Blank GS, Maneval D, Carter P. 1993. Engineering Fab fragments for efficient F(ab)$_2$ formation in *E. coli* and for improved *in vivo* stability. Journal of Immunology 151: 6954-6961.

Roque ACA, Lowe CR, Taipa MA. 2004. Antibodies and genetically engineered related molecules: Production and Purification. Biotechnology Progress 20: 639-654.

Ruthven DM. 1997. Encyclopaedia of separation technology. Vol 1. John Wiley and Son, Inc. P282.

Sachidanandham R, Gin KYH, Poh CL. 2005. Monitoring of active but non-culturable bacterial cells by flow cytometry. Biotech Bioeng 89: 24-31.

Salte H, Tustian AD, Willoughby N, Hoare M, Titchener-Hooker N. 2005. A novel ultra scale-down approach for predicting the separation performance of high cell density cultures (in preparation).

Save SS, Pandit AB, Joshi JB. 1994. Microbial cell disruption: Role of cavitation. J Chem Eng 55: B67-B72.

Schlichting H. 1968. Boundary layer theory. McGraw-Hill, 6th ed. pp686.

Schutte H, Kula MR. 1990. Pilot and process scale techniques for cell disruption. Biotechnol Appl Biochem 12: 599-620.

Segal DM, Weiner GJ, Weiner LM. 1999. Bispecific antibodies in cancer therapy. Current Opinion in Immunology 11: 558 562.

Seifert VM, Hunte C. 2002. High level production of functional antibody Fab fragments in an oxidising bacterial cytoplasm. J Mol Biol 315 (1): 1-8.

Shaffer M. 1992. Drugs approved in 1991. FDA talk paper (jan 15, 1992), Food and Drug administration, U.S. department of health and human services.

Shah DN, Kothari RM. 1991. Fermentative production of injectable –grade calcium gluconate. Biotechnol Prog 7: 67-69.

Shamlou PA, Stavrinides S, Titchener-Hooker N, Hoare M. 1994. Growth-independent breakage frequency of protein precipitates in turbulently agitated bioreactors. Chem Eng Sci 49: 2647-2656.

Shamlou PA, Siddiqi SF, Titchener-Hooker NJ. 1995. A physical model of high-pressure disruption of bakers yeast cells. Chem Eng Sci 50: 1383-1391.

Shamlou PA, Gierczycki AT, Titchener-Hooker N. 1996. Breakage of flocs in liquid suspension agitated by vibrating and rotating mixers. Chem Eng Sci 62: 23-34.

Shapiro HM. 1995. Practical flow cytometry, 3rd ed. Wiley-Liss, NY.

Shavlovsky DS. 1972. Hydrodynamics of High pressure fine continuous jets. First International symposium on jet cutting technology, A6-81.

Shibui T, Munakata K, Matsumoto R, Ohta K, Matsushima R, Morimoto Y, Nagahari K. 1993. High-level production and secretion of a mouse chimeric Fab fragment with specificity to human carcino embryonic antigen in *E. coli*. Applied Microbiology and Biotechnology 38: 770-775.

Siddiqi SF, Titchener-Hooker NJ, Shamlou PA. 1997. High pressure disruption of yeast cells: The use of scale down operations for the prediction of protein release and cell debris size distribution. Biotech Bioeng 55: 642-649.

Siddiqi SF, Bulmer M, Shamlou P, Titchener-Hooker NJ. 1995. The effects of fermentation conditions on yeast cell debris particle size distribution during high-pressure homogenisation. Bioprocess Eng 14: 1-8.

Smith FT, Li L, Wu GX. 2003. Air cushioning with a lubrication/inviscid balance. J Fluid Mech 482: 291-318.

Stathopoulos NA, Hellums JD. 1985. Shear stress effects on human embryonic kidney cells. In vitro. Biotech Bioeng 27: 1021-1026.

Steen HB, Boye E. 1981. *Escherichia coli* growth studied by dual parameter flow cytophotometry. J Bacteriol 145: 1091-1094.

Steponkus PL, Wolfe J, Dowgert MF. 1981. Stresses induced by contraction and expansion during a freeze-thaw cycle: a membrane perspective, in G.J.Morris, A Clarke (eds), Effects of low temperatures on biological membranes, Academic Press, Toronto, 307-322.

Stiles ME, Witter LD. 1965. Thermal inactivation, heat injury and recovery of Staphylococcus aureus. Journal of Dairy Science 48: 677-681.

Summers D. 1995. Waterjet Technology, E&FN SPON pp82.

Suppes G, Egan S, Casillan AJ, Chan KW, Seckar B. 2003. Impact of high pressure freezing on DH5α *E. coli* and red blood cells. Cryobiology 47: 93-101.

Surrey MR, Davies RJ. 1996. Pilot-scale liquid culture and harvesting of an entomopathogenic nematode. Heterorhabditis bacteriophora. J Invertebr Pathol 67: 92-99.

Teeters MA, Conrardy SE, Thomas BL, Root TW, Lightfoot EN. 2003. Adsorptive membrane chromatography for purification of plasmid DNA. J Chromatography A 989: 165-173.

Teixeira P, Castro H, Mohacsi-Farkas C, Kirby R. 1997. Identification of sites of injury in Lactobacillus bulgaricus during heat stress. Journal of Applied Microbiology 83: 219-226.

Theodossiou I, Collins IJ, Ward JM, Thomas ORT, Dunnill P. 1997. The processing of a plasmid-based gene from *E. coli*. Primary recovery by filtration. Bioproc Eng 16: 175-183.

Titchener-Hooker N, Zhou Y, Hoare M, Dunnill P. 2001. Biopharmaceutical process development: Part II, Methods of reducing development time. Biopharm Europe (Sept) 68-74.

Titchener-Hooker NJ, McIntosh RV. 1993. A study of the effect of low frequency conditioning on the size distribution properties and centrifugal recovery of human albumin precipitates. Bioprocess Eng 8: 215-222.

Vandanjon L, Rossignol N, Jaouen P, Robert JM, Quemeneur F. 1999. Effects of shear on two microalgae species. Contribution of pumps and valves in tangential flow filtration systems. Biotech Bioeng 63: 1-9.

Varga EG, Titchener-Hooker NJ, Dunnill P. 2001. Prediction of the pilot-scale recovery of a recombinant yeast enzyme using integrated models. Biotech Bioeng 74: 96-107.

Vickers GW, Harrison PW, Houlson R. 1980. Extending the range of cavitation cleaning jets. Fifth international symposium on jet cutting technology, 403- 412.

Virkar PD, Narendranathan NJ, Hoare M, Dunnill P. 1981. Studies of the effects of shear on globular proteins: Extension to high shear fields and to pumps. Biotech Bioeng 23: 425-429.

Virkar PD, Hoare M, Chan MYY, Dunnill P. 1982. Kinetics of the acid precipitation of soya protein in a continuous-flow tubular reactor. Biotech Bioeng 24: 871-887.

Vogel JH, Kroner KH. 1999. Controlled shear filtration: A novel technique for animal cell separation. Biotech Bioeng 63: 663-674.

Wang DIC, Sinskey TJ. 1968. Effect of centrifugation on the viability of burkitt lymphoma cells. Biotech Bioeng 10: 641-649.

Wan Y, Vassan S, Raja G, Hale G, Cui Z. 2005. Separation of monoclonal antibody alemtuzumab monomer and dimmers using ultrafiltration. Biotech Bioeng 90: 422-432.

Walsh G. 2003. Biopharmaceutical benchmarks-2003. Nature Biotechnol 21: 865-870.

Wang Z, Yuan Z, Hengge UR. 2004. Processing of plasmid DNA with ColE1-like replication origin. Plasmid 51: 149-161.

Wase DAJ, Patel YR. 1985. Variations in volumes of microbial cells with change in the agitation rates of chemostat cultures. J Gen Microbiol 131: 725-736.

Weaver JC, Harrison GI, Bliss JG, Mourant JR, Powell KT. 1988. Electroporation: High frequency of occurrence of a transient high-permeability state in erythrocytes and intact cells. FEBS Letter 229: 30-34.

Welty JR, Wicks CE, Wilson RE. 1984. Fundamentals of momentum, heat, and mass transfer. 3rd ed. John Wiley and Sons. 202-209.

Weiss DA, Yarin A. 1999. Single drop impact onto liquid films: neck distortion, jetting, tiny bubble entrainment, and crown formation. J Fluid Mech 385: 229-254.

Wild J, Walter WA, Gross CA, Altman E. 1993. Accumulation of secretory protein precursors in *Escherichia coli* induces the heat shock response. J Bacteriol 175: 3992-3997.

Willems A, Leoen J, Schoonoghe S, Grooten J, Mertens N. 2003. Optimizing expression and purification from cell culture medium of tri-specific recombinant antibody derivatives. J Chromatography 786: 161-176.

Willoughby N, Martin P, Titchener-Hooker N. 2004. Extreme scale-down of expanded bed adsorption: Purification of an antibody fragment directly from recombinant *E. coli* culture. Biotech Bioeng 87: 641-647.

Woodcock E, Grigg GW. 1972. Repair of thermally-induced DNA breakage in *E. coli*. Nature New Biol 237: 76-79.

Wortman AT, Bissonnette GK. 1988. Metabolic processes involved in repair of *E. coli* cells damaged by exposure to acid mine water. Applied and Environmental Microbiology. 54: 1901-1906.

Wu J, King G, Daugulis AJ, Faulkner P, Bone DH, Goosen MFA. 1990. Adaptation of insect cells to suspension culture. J Ferment Bioeng 70: 90-93.

Yanaida K. 1974. Flow characteristics of water jets. Second international symposium on jet cutting technology, A2-19.

Yanaida. K, Ohashi A. 1978. Flow characteristics of water jets. Fourth international symposium on jet cutting technology, A3-39.

Yanaida K, Ohashi A. 1980. Flow characteristics of water jets in air. Fifth International Symposium on jet cutting technology, A3: 33.

Yarin AL, Weiss DA. 1995. Impact of drops on a solid surface: self-similar capillary waves, and splashing as a new type of kinematic discontinuity. J Fluid Mech 283: 141.

Yim SS, Shamlou PA. 2000. The engineering effects of fluid flow on freely suspended biological macro-materials and macromolecules. Advances in Biochem Eng/Biotech 67: 83-121.

Zhang Z, Al-Rubeai M, Thomas CR. 1993. Estimation of disruption of animal cells by turbulent capillary flow. Biotech Bioeng 42: 987-993.

Zhou YH, Titchener-Hooker NJ. 1999. Visualizing integrated bioprocess designs through "windows of operation". Biotech Bioeng 65: 550-557.